

**WestminsterResearch**

<http://www.westminster.ac.uk/research/westminsterresearch>

**Miniaturised and reconfigurable planar filters for ultra-wideband applications**

**Khondker M.F. Rabbi**

Faculty of Science and Technology

This is an electronic version of a PhD thesis awarded by the University of Westminster. © The Author, 2014.

This is an exact reproduction of the paper copy held by the University of Westminster library.

---

The WestminsterResearch online digital archive at the University of Westminster aims to make the research output of the University available to a wider audience. Copyright and Moral Rights remain with the authors and/or copyright owners.

Users are permitted to download and/or print one copy for non-commercial private study or research. Further distribution and any use of material from within this archive for profit-making enterprises or for commercial gain is strictly forbidden.

---

Whilst further distribution of specific materials from within this archive is forbidden, you may freely distribute the URL of WestminsterResearch: (<http://westminsterresearch.wmin.ac.uk/>).

In case of abuse or copyright appearing without permission e-mail [repository@westminster.ac.uk](mailto:repository@westminster.ac.uk)

**MINIATURISED AND RECONFIGURABLE PLANAR FILTERS  
FOR ULTRA-WIDEBAND APPLICATIONS**

**KHONDKER M. F. RABBI**

A thesis submitted in partial fulfilment of the  
requirements of the University of Westminster for  
degree of Doctor of Philosophy

February 2014

## ABSTRACT

An increasing demand for electromagnetic spectrum has resulted from the emergence of feature-rich and faster throughputs wireless applications. This necessitates the developments of dynamic reconfigurable or multifunctional systems to better exploit the existing spectrum.

Future wireless devices will be expected to communicate over several bands with various other devices in order to fine tune the services they provide to the user. Each band may require a separate RF transceiver and such modern wireless multi-band multi-mode communication systems call for high performance, highly integrated compact modules. Since the Federal Communications Commission (FCC) released the unlicensed frequency band 3.1-10.6 GHz for ultra-wideband (UWB) commercial communications, the development race for commercialising UWB technology has seen a dramatic increase around the world.

The aim of this research is to develop reconfigurable planar microwave filters for ultra-wideband applications. The project investigates some key design issues of reconfigurable filters, which are being observed constantly in the latest development and realisation of microwave filters. Both analytical and numerical methods are performed to construct a realistic and functional design. Two different types of frequency reconfigurability are investigated in this thesis: discrete (e.g. PIN diode, Optical switch) and continuous (e.g. varactor diode). Using the equivalent circuits and considering the direct coupled filter structure in most cases, several topologies with attractive features are developed for future communication systems. The proposed works may be broadly categorised into three sections as follows.

The first section explores a square ring shape close loop resonator along with an open-circuited stub in the symmetry plane. To realise a reconfigurable frequency states within the same spectrum, an innovative approach is developed for this case. An optical or

photoconductive switch, comprised of a silicon die activated using near infrared light is investigated as a substitute of PIN diode and performances are evaluated to compare the feasibilities. In addition, an in-band interference rejection technique via externally coupled T-shape resonator is shown. However, it is observed that both structures achieve significant size reductions by utilising the inner part of the resonators.

To improve the filter selectivity, a convenient design approach generating a pair of transmission zeros between both passband edges and a single zero in the stop band for harmonic suppression is discussed in the second section. Moreover, the development of notched rejection bands are studied and several novel methods to create a single and multiple notched bands employing the square ring shape structure are proposed. On inspection, it is found that the notch structure can be implemented without deteriorating the filter performances. The discussions are supplemented with detailed design examples which are accompanied by theoretical, simulated and experimental results in order to illustrate the filter development process and showcase practical filter performance.

The third section reveals a novel highly compact planar dual-mode resonator with sharp rejections characteristics for UWB applications. A bandwidth reconfiguring technique is demonstrated by splitting its even-mode resonance. Filter structure with the dual-mode resonator is shown to have a relatively wide tuning range, significantly low insertion loss and a constant selectivity along with frequency variations in comparison to similar published works. Finally, the earlier dual-mode structure are modified to realise a dual wideband behaviour. A detail analysis with comprehensive design procedures is outlined and a solution for controlling the frequency bandwidths independently according to the application interest is provided. In line with the previous section, experimental verification is presented to support and supplement the discussions.

# TABLE OF CONTENTS

<b>1.0 INTRODUCTION</b>	<b>1</b>
1.1 Overview of Recent Research	4
1.2 Objectives of Research and Review of the Thesis	11
1.3 References	15
<b>2.0 MICROSTRIP LINE DISCONTINUITY AND FILTER THEOR</b>	<b>21</b>
2.1 The Microstrip Line	21
2.2 Microstrip Discontinuities	27
2.3 Microstrip Coupled Lines	31
2.4 Filter Design Theories	34
2.6 References	38
<b>3.0 COMPACT RECONFIGURABLE UWB BANDPASS FILTERS</b>	<b>39</b>
3.1 Analysis and Equivalent Circuit	41
3.2 UWB Bandpass Filters with Reconfigurable Notched Band	60
3.3 References	68
<b>4.0 HIGHLY SELECTIVE RECONFIGURABLE UWB FILTERS</b>	<b>71</b>
4.1 Analysis of the Proposed Filter Resonator	73
4.2 Single and Multi-Notched Band Technique	91
4.3 References	100
<b>5.0 MINIATURISED UWB FILTERS WITH RECONFIGURABLE BANDWIDTH AND FREQUENCY</b>	<b>102</b>
5.1 Proposed Filter Structure	104
5.2 CPW-fed Reconfigurable Filter	117
5.3 References	123
<b>6.0 DUAL MODE DUAL WIDEBAND BANPASS FILTER WITH INDEPENDENTLY CONTROLLED FREQUENCY BANDWIDTH</b>	<b>126</b>
6.1 Characteristics of the Proposed Filter	127
6.2 Dual Band Inverter	132
6.3 Design Procedure of the Reconfigurable Dual Wideband BPF	137
6.4 References	144
<b>7.0 CONCLUSION AND FUTURE WORK</b>	<b>147</b>
7.1 Research Contributions	148
7.2 Future Work	149

## LIST OF ACRONYMS

UWB	Ultra-wideband
ABCD	Transfer matrix
BPF	Bandpass filter
CAD	Computer-Aided Design
dB	Decibel
DGS	Defected ground structures
DSS	Dumbbell-shaped slot
EBG	Electromagnetic bandgap
EM	Electromagnetic
FBW	Fractional bandwidth
GHz	Gigahertz
MM	Millimetre
IEEE	Institute of Electrical and Electronics Engineers
IF	Intermediate frequency
LCP	Liquid Crystal Polymers
LTCC	Low-Temperature Cofired Ceramics
MEMS	Microelectromechanic Systems
MIC	Microwave Integrated Circuits
MMIC	Monolithic Microwave Integrated Circuits
RF	Radio frequency
BST	Barium Strontium Titanate
SIR	Stepped impedance resonator
TEM	Transverse electromagnetic propagation mode
TZ	Transmission zero
UIR	Uniform impedance resonator
WLAN	Wireless local area network
WiMAX	Worldwide Interoperability for Microwave Access

## LIST OF FIGURES

### Chapter 1

**Fig. 1-1** (a) A typical filter bank consists of a number of fixed filters, and (b) A reconfigurable or tunable filter as an alternate of multiple fixed filters

**Fig. 1-2** Reconfigurable UWB filter with banpass to a bandstop transformation

**Fig. 1-3** UWB BPF filter with switchable notch frequency

### Chapter 2

**Fig. 2-1** Side on view of excited microstrip line with corresponding electric (solid lines) and magnetic (dashed lines) fields

**Fig. 2-2** Microstrip characteristic impedance as a function of  $W/h$

**Fig. 2-3** Effective dielectric constant of the microstrip line as a fuction of  $W/h$  for different dielectric constants

**Fig. 2-4** Microstrip discontinuities: (a) step, (b) open-end, (c) gap, and (d) bend

**Fig. 2-5** Side on view of field distribution of microstrip coupled lines of (a) even mode (b) odd mode excitation

**Fig. 2-6** Lumped element circuit model of coupled transmission lines

**Fig. 2-7** Frequency behaviour of four basic types of filter

**Fig. 2-8** Lowpass filter with degree of  $n$

**Fig. 2-9** Lowpass to Bandpass element transformation

### Chapter 3

**Fig. 3-1** Equivalent transmission line model of the proposed filter

**Fig. 3-2** Equivalent circuits of (a) Quarter wavelength ( $\lambda_g/4$ ) and Half wavelength ( $\lambda_g/2$ )

**Fig. 3-3** Calculated filter frequency response

**Fig. 3-4** Transmission line network of the bandstop filter

**Fig. 3-5** (a) Layout of the proposed UWB filter (dimensions in millimetres), (b) Equivalent transmission line model

- Fig. 3-6** Bandwidth of the proposed filter is influenced by (a) changing impedance of  $Z_b$ , changing impedance of  $Z_a$
- Fig. 3-7** (a) Equivalent circuit of optical switch, and (b) corresponding response in the 'ON' state using  $50 \Omega$  transmission line.
- Fig. 3-8** Equivalent circuit of PIN diode, (a) in Reverse bias or 'OFF', (b) in Forward bias or 'ON', and (c) corresponding response in 'ON' state using  $50 \Omega$  transmission line
- Fig. 3-9** (a) Photograph of fabricated filter with optical switch, (b) Simulated response of filter with the gap in the bridged and open states, (c) Measured response of the fabricated filter with the optical switch in the ON and OFF states, and (d) Measured group delay of bandpass filter in the ON state
- Fig. 3-10** (a) Photograph of fabricated filter with PIN diode, (b) Simulated response of filter with the gap in the bridged and open states, (c) Measured response of the fabricated filter with the PIN diode in the ON and OFF states, and (d) Measured group delay of bandpass filter in ON state
- Fig. 3-11** (a) Layout of the proposed UWB filter with reconfigurable notch structure, (b) EM simulated response of the proposed UWB filter without reconfigurable notch structure
- Fig. 3-12** Layout of the switchable notch structure
- Fig. 3-13** Transmission response of the reconfigurable notch structure
- Fig. 3-14** (a) Simulated s-parameter response of filter in the ON states (b) Measured s-parameter response of the fabricated filter in the ON states, (c) Measured s-parameter response of the fabricated filter in the OFF states
- Fig 3-15** Simulated S-parameter responses [insertion loss ( $S_{21}$ )] of the proposed notch frequency with varying (a) length ( $L_{AB}$ ) of section A, B and (b) width of section C
- Fig 3-16** Measured Group delay response using PIN diode OFF

## Chapter 4

- Fig. 4-1** (a) Initial configuration of the UWB bandpass filter with shunt short-circuited stubs, (b) Replacing short-circuited stubs with two sections of open-circuited stubs for generating transmission zeros
- Fig. 4-2** Comparison between conventional and modified BPF
- Fig. 4-3** Transmission line model of short to open-circuited stub configuration

- Fig. 4-4** (a) Schematic layout (dimensions in mm) and (b) Equivalent circuit of the proposed UWB bandpass filter
- Fig. 4-5** Circuit model response of proposed filter
- Fig. 4-6** (a) Series transmission line is replaced by open stub T-shaped and (b) Transmission response of conventional and modified filter with T-shaped structure
- Fig. 4-7** Equivalent transmission line model of the proposed filter
- Fig. 4-8** (a) Schematic of the proposed reconfigurable UWB bandpass filter and (b) Circuit schematic for the filter prototype
- Fig. 4-9** (a) Conventional and (b) Modified Bandpass transmission response
- Fig. 4-10** Equivalent circuit of the notch structure
- Fig. 4-11** Simulated and measured response of the fabricated filter with the pin switch (a) Bandpass filter with a notched band at 3.5 GHz in the PIN1 ON state and PIN2 OFF state, (b) Bandpass filter with full passband in the PIN1 OFF state and PIN2 OFF state
- Fig. 4-12** Coupling coefficient ( $k$ ) with respect to vary the section ( $\theta_8 + \theta_9$ ) position
- Fig. 4-13** Bandstop filter in the PIN1 OFF state and PIN2 ON state
- Fig. 4-14** Photograph of the fabricated filter
- Fig. 4-15** Notch structure (a) Notch equivalent circuit, (b) Notch layout
- Fig. 4-16** Simulated response of the reconfigurable notch structure (a) With switch ON (b) With switch OFF
- Fig. 4-17** Simulated and measured results (a) with pin diode and (b) with optical switch
- Fig. 4-18** (a) Coupling co-efficient ( $k$ ) between coupled transmission lines vs gap, and (b) A photograph of the fabricated filter
- Fig. 4-19** (a) Geometry and equivalent circuit of the multi-notched structure and (b)UWB filter integrates with multi-notched structure
- Fig. 4-20** UWB bandpass filter with dual notch using composite right/left handed resonator
- Fig. 4-21** UWB bandpass filter with triple notch using composite right/left handed resonator and a quarter wavelength short-circuited coupled resonator (a) Simulation, (b) Measured

## Chapter 5

- Fig. 5-1** Layout of the proposed bandpass filter with a reconfigurable notched band structure
- Fig. 5-2** (a) Equivalent filter transmission line model, (b) Equivalent odd-mode and even-mode circuit
- Fig. 5-3** Odd-mode resonance without the grounded  $L_7$  effect
- Fig. 5-4** Even-mode resonance with the grounded  $L_7$  effect
- Fig. 5-5** Modified Dual-Mode Resonator with Improved Upper Stopband using bandstop structure (a) Pole response, (b) Transmission response
- Fig. 5-6** Improved filter lower selectivity via I/O coupling
- Fig. 5-7** (a) Simulated  $|S_{21}|$ -parameter with lower and upper skirt, (b) Simulated and measured S-parameters of the proposed filter, and (c) Effect in the main transmission line by varying width of the SIR resonator
- Fig. 5-8** (a) Filter layout with loading varactor diode, (b) Simulated  $|S_{21}|$  of the proposed resonator under weak coupling with varied  $L_7$
- Fig. 5-9** (a) Simulated S-parameter ( $|S_{21}|$ ) of the proposed filter under different loading capacitance, (b) Simulated S-parameter ( $|S_{11}|$ ) of the proposed filter under different loading capacitance
- Fig. 5-10** (a) Simulated and measured S-parameter ( $|S_{21}|$ ) of the proposed filter under different biasing voltages, (b) Simulated and measured S-parameter ( $|S_{11}|$ ) of the proposed filter under different biasing voltages
- Fig. 5-11** Photograph of the proposed filter
- Fig. 5-12** Cross section of a doubly metalized line
- Fig. 5-13** (a) Top side (CPW feeding lines), (b) Back side (filter resonators) layout of reconfigurable filter with CPW feeding lines, and (c) Layout of the proposed UWB bandpass filter with optical switch model (dimensions in mm), and (d) Equivalent circuit of the proposed filter
- Fig. 5-14** Transmission response (a) no connection between CPW ports, (b) a single CPW port is connected through ground, and (c) both CPW ports are connected through ground
- Fig. 5-15** (a) 3-D filter layout generated by EM sonnet software and transmission response of the reconfigurable filter with optical switch model in the (b) ON, and (c) OFF states

## Chapter 6

**Fig. 6-1** Schematic layout of the proposed filter

**Fig. 6-2** The normalised resonator length against  $\theta_2$  for various impedance ratios  $R_z$  to visualize the effect of the stepped impedance on the length of the resonator

**Fig. 6-3** Simulated values of the degenerate modes' frequencies against the length of  $L_5$  when  $(L_1 + L_2 + L_3 + L_4)$  are fixed

**Fig. 6-4** Schematic layout with open stubs and source-load coupling

**Fig. 6-5** (a) Model of resonator mid-section and equivalent lumped element circuit of direct-coupled dual-mode resonator, (b) Comparison of driving point impedance of direct coupled dual-mode resonator mid-section and that of equivalent circuit (c) transfer impedance of direct coupled dual-mode resonator mid-section and that of equivalent circuit

**Fig. 6-6** Dual-band resonator with open-circuited stub

**Fig. 6-7** Layout of the proposed dual-wideband bandpass filter with a reconfigurable frequency states

**Fig. 6-8** Simulated and measured response of the fabricated filter with the pin switch (a) Both Channels are on with at centre frequency at 4.9 and 9.6 GHz in the PIN1 ON state and PIN2 ON state [STATE-1], (b) One Channels is on at centre frequency at 9.6 and one is off at 4.9 GHz in the PIN1 OFF state and PIN2 ON state [STATE-2]

**Fig. 6-9** Simulated and measured response of the fabricated filter with the pin switch (a) One Channels is on at centre frequency at 4.9 and one is off at 9.6 GHz in the PIN1 ON state and PIN2 OFF state [STATE-3], (b) Both Channels are off with at centre frequency at 4.9 and 9.6 GHz in the PIN1 OFF state and PIN2 OFF state [STATE-4]

**Fig. 6-10** Photograph of the fabricated filter

## **ACKNOWLEDGEMENTS**

First and foremost, I would like to express my sincere gratitude and acknowledgement to Dr. Djuradj Budimir for his for his valuable guidance, advice and timely care extended to me during my research period. His imminent way of thinking has supported me to explore my research abilities and encouraged in implementing the ideas with absolute satisfaction. I am able to successfully complete this research work and deliver this thesis because of his immense patience and constructive feedbacks.

I would like to acknowledge the help and assistance of Dr. Andrzej Tarczynski for his continuous support throughout this work, especially for keeping me motivated and giving me guidance when I hit in the dead ends. I also would like to show my appreciation to staffs of Department of Electronic, Network and Computer Engineering, University of Westminster for their supports in various capacities during these years.

Finally, I would like to dedicate this work to my parents and wife for their continuous encouragements and giving me time to finish this thesis as well as express my heartfelt appreciations to them for inculcating the importance of long life learning in me.

## AUTHOR'S DECLARATION

I declare that all the material contained in this thesis is my own work.

# List of Publications

## Journals

K. Rabbi and D. Budimir, "Highly Selective Reconfigurable Filters for UWB Systems", IEE Microwave Wireless Component Letters, vol. 24, no.9, pp.146-148, 2014.

K. Rabbi and D. Budimir, "Compact UWB Bandpass Filter with Reconfigurable Notched", IET Electronics Letters , vol. 49, no. 11, 2013.

K. Rabbi, L. Athukorala and D. Budimir, "Highly Linear Microstrip Wideband Bandpass Filter with Switchable Notched band for Wireless Applications", Microwave and Optical Technology Letters, vol. 55, pp.1331-1335, 2013.

K. Rabbi, L. Athukorala and D. Budimir, "High-Linearity Reconfigurable Microstrip Bandpass Filters with Tunable Notch", Microwave and Optical Technology Letters, vol. 55, pp.-418-421, 2012.

K. Rabbi and D. Budimir, "Miniaturized Dual-Mode Dual Wideband Bandpass Filters with Independently Controlled Frequency Bandwidths", IEEE Transactions on Microwave Theory and Techniques (Revision)

## Conferences

K. Rabbi and D. Budimir, "Miniaturized Dual-mode Microstrip Bandpass Filter with a Reconfigurable Notched Band for UWB Applications" IEEE MTT-S International Microwave Symposium Dig. (IMS), pp. 1-3, USA, 2-7 June 2013.

K. Rabbi and D. Budimir, "Miniaturised Sharp Rejection Bandpass Filter with Reconfigurable Bandwidth for UWB Applications", 43<sup>rd</sup> European Microwave Conference (EuMC), pp. 1023-1026, 6-11, Nuremberg, Germany, October 2013.

K. Rabbi, L. Athukorala and D. Budimir, "High-Linearity Reconfigurable Microstrip UWB Bandpass Filters", 41<sup>st</sup> European Microwave Integrated Circuits Conference (EuMIC), pp. 172-175, Manchester, UK, October 2011.

K. Rabbi and D. Budimir, "Optically Reconfigurable CPW Filters for UWB Applications", IEEE Antennas and Propagation Society (AP-S/URSI), USA, pp. 1-2, 8-14 July 2012.

K. Rabbi and D. Budimir, "Simulation of Reconfigurable WLAN Notch for UWB Filters", IEEE Antennas and Propagation Society (AP-S/URSI), USA, pp. 3178-3180, 3-8 July 2011.

Rabbi, K., Athukorala, L., Panagamuwa, C., Vardaxoglou, John C. and Philippakis, M. and Budimir, D., "Optically Reconfigurable Microstrip UWB Bandpass Filters", IEEE LAPC, pp. 617-620, 8-9 November 2010.

---

# 1.0 INTRODUCTION

---

With the advancement of modern wireless communication applications, the finite frequency spectrum has to accommodate additional systems and thus it is becoming increasingly congested. Hence, RF signal must be confined to the assigned spectrum ranges. As a key component to restrict signals, filters are required with stringent requirements such as high performance, low cost, compact size, and light weight. Generally, a microwave filter performs a frequency band limiting operation in the frequency domain which passes desirable signals and attenuates unwanted signals of other frequencies. Regardless of their applications, filter shape signals in amplitude and phase with respect to the frequency in a prescribed aspect to generate a compliant output. This feature makes filters useful in wireless communication systems and four main classes filter available based on their function of operations: low pass, high pass, band pass and band stop or notched band in some cases filter.

More commonly, filters can be implemented with two different types of elements in accordance to the wavelength requirement such as lumped elements (inductor, capacitor, and resistor) or distributed elements (microstrip, waveguide, or any other transmission line medium). To realise lumped elements with adequate accuracy especially at microwave frequencies is extremely difficult due to its inherent parasitic effects. Planar distributed filters can be integrated into an IC but the size of a distributed filter is directly proportional its operating wavelength, this approach may only applicable on a limited version of filters, where the operating frequencies agrees filters to fit into an IC. In addition, the unloaded quality factor of a distributed resonator is directly proportional to its physical size. Hence, distributed IC filters incur severe losses which may affect the overall system performance.

Due to the reason above, planar strip line technology such as microstrip have become immensely popular for distributed filters. Although waveguide components can handle higher power than the planar transmission line and have low losses but it is not the first choice in the communication systems that requires mobility because of their bulk size and

heavy weight. Moreover, fabrication processes of the waveguide components are more expensive than that for strip transmission lines.

Although most microwave filters are built-up with distributed components and characterised by the conventional electromagnetic theory, the analysis of the filter structures in practical using the proposed theory is very complex and tedious tasks as the theory is the mathematical formulation of the propagation of electromagnetic waves and it is concerned with interrelated electric and magnetic fields as well as the time varying effects between two fields. As a result, lumped elements can be chosen for modelling and demonstrating the behaviour of the intended filters.

Over the recent years, advances in modern wireless communication systems are pushing for multi-frequency band and multi-functional operation. This trend has led to the development of different kinds of reconfigurable or tunable filters. However, reconfigurable or multiband filters are still the subject of intense research due to limitations such as the number of bands attainable, bandwidth or centre frequency tuning range, selectivity according to passband changes, and linearity in addition to the issues pertaining to fixed filters.

A typical filter bank is illustrated in Figure 1-1 as an example of multiband systems which consists of a number of fixed filters and each filter is directed for each band; this type of system arrangement is not only occupied large space but also requires high loss multi-throw switches. To overcome these drawbacks, reconfigurable or tunable filters are emerged as an alternate solution which can be tuned or reconfigured according to application specifications. These kinds of filters would be directed at supporting multiple wireless functions using common hardware hence decreasing the overall system complexity and potentially improving its performance and functionality.

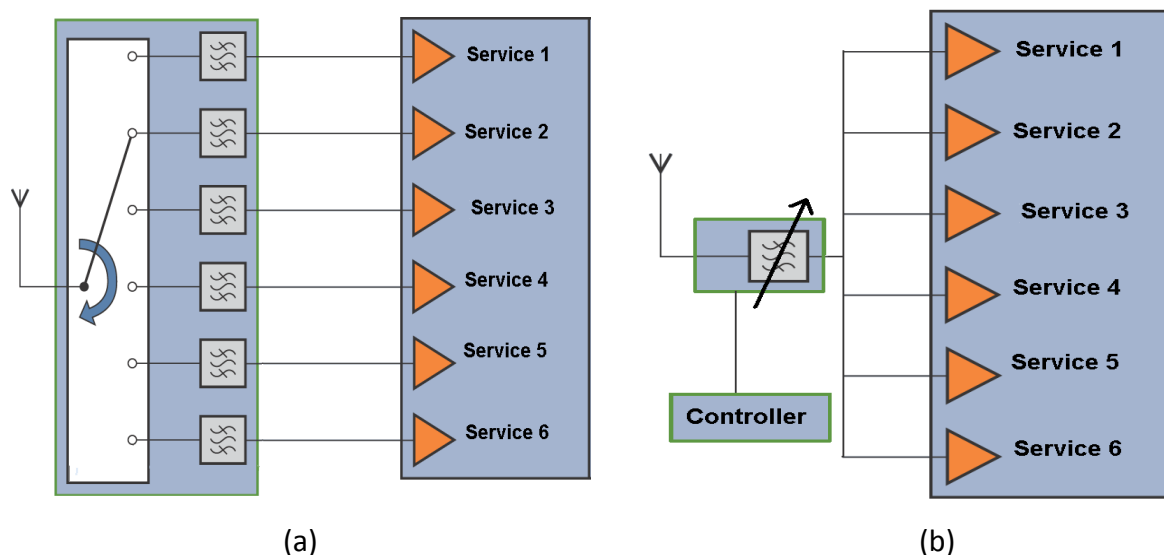


Fig. 1-1 (a) A typical filter bank consists of a number of fixed filters, and (b) A reconfigurable or tunable filter as an alternate of multiple fixed filters.

Since the Federal Communications Commission (FCC) of the United States released the unlicensed frequency band 3.1-10.6 GHz for ultra-wideband (UWB) commercial communications, the development race for commercialising UWB technology is heating up in Europe and all over the world [1]. Moreover, research on UWB devices has greatly accelerated but characterisation of UWB filter such as miniaturisation, high selectivity, flat group delay, in-band frequency rejection notch, and low insertion loss over the frequency range have always been a challenging task.

This research addresses some of the fundamental challenges experiencing in microwave filters. For instance, concerns such as filter size, loss, selectivity and reconfigurability are central to the theme of the thesis. The rest of this chapter details the aims and objectives of this investigation. This is followed by an overview of some significant contributions and developments from past research work particularly in the area of planar microwave filters not only to give a survey of the type of solutions available but also to serve as a basis for comparison. For better accessibility, an outline of the thesis is illustrated next with a summary of each chapter.

## 1.1 Overview of Recent Research

A brief overview of some of the recent developments to distributed planar resonators especially on UWB filters, relevant to the set objectives of this investigation is outlined in this section. Also over the past few decades, electronically switchable and reconfigurable microwave devices such as filters are in great demand for existing wireless communication systems, and recent research into reconfigurable filters using different methodologies and structure have been quoted in this discussion.

### 1.1.1 UWB Bandpass Filters

UWB devices has greatly accelerated and there are a number of different approaches have been reported for the filter realisation. For example, multi-mode resonator (MMR) [2]-[3] has been widely used to achieve ultra-wideband passband characteristics. The main drawback of MMR-based technique is that it suffers a narrow upper stopband performance due to high order harmonics which arises just after the first passband. In [4] demonstrates a UWB filter using stepped-impedance stub-loaded resonator (SISLR). The proposed SISLR is observed to have advantage of supporting more degrees of freedom to adjust the resonant frequencies, but, the stop band edges prompt low attenuation to escalate the possibility of signal error rating.

Quasi-lumped element prototype is another technique which has been adopted to build UWB bandpass filters [5]-[7]. In [5], a high-pass filter characteristic was realised as part of developing UWB filters by employing microstrip-coplanar waveguide (CPW) structure. Moreover, to construct a UWB bandpass filters, [6] and [7] used lumped element bandpass filter prototype with multilayer liquid-crystal-polymer (LCP) arrangement where the former utilised open and short stubs and the latter used stepped impedance resonators (SIR). Despite their efforts to introduce a new technique, the resulting filters have a large size and complicated in design causing fabricating problems.

Microwave bandpass filters commonly employ a ring resonator with the benefit of compact circuit size, split mode, and sharp rejection skirts [8]-[10]. In compare with patch resonator,

ring structure facilitates low conductor loss and high power handling capability [11-12]. A square ring resonator using two tuning stubs, orthogonal feeders, and dual mode effects demonstrated a wide passband, high selectivity, and an increased stopband bandwidth [13]. Interdigital coupled feed lines were employed to acquire quintuple resonance in a passband [14]. In [15], a bandpass filter with two ring resonators achieves 80% fractional bandwidth. But the proposed ring resonator structures in [14]-[15] require direct-tapped feeding arrangement between two ports, which causing poor rejection performance in a frequency range below the desired passband.

Furthermore, to achieve better selectivity, much effort has been made by generating transmission zeros, for example, in [16] reported five short-circuited stub for the evolutions of UWB filter with pairs of transmission zeros but the filter experienced poor out-of-band performance as well as large size. In [17] addressed the quintuple-mode UWB bandpass filter with sharp roll-off and super-wide upper stopband. Although the aperture-backed structure can boost the coupling degree of the I/O lines, the fabrication procedure would become complexity.

### 1.1.2 Reconfigurable Planar Filters

There is growing demand in the wireless communications industry for reconfigurable microwave filters as it makes microwave transceivers adaptable to multiple bands of operation employing a single filter. Reconfigurable/Tunable filters can substitute the necessity of shifting between several filters to get more than a single filter response by offering switching elements embedded into a filter structure. Reconfigurable filters can be realised in a variety of ways and it can be classified into two different categories, namely, filters with discrete switching or tuning and filters with continuous tuning. Filter topologies showing a discrete switching usually use PIN diodes, MEMS switches, or Optical switches. In contrast, filter structures using varactor diodes, ferroelectric/magnetic materials, or MEMS capacitors are widely used to obtain continuous tuning.

Several design techniques are developed to produce reconfigurable discrete states on a filter response, which are drawing attention for low cost implementation [18]-[20]. Recently, the

filter in [18] adopts the frequency selective characteristic of a cascade of unit electromagnetic gap (EBG) structures that can be reconfigured using MEMS switches to exhibit either a bandpass or bandstop response with a 3-dB fractional bandwidth (FBW) of 72% and a mid-band insertion loss 1.96 dB. The drawbacks associated with MEMS switches include the need for bias lines and their limited power handling capability as well as poor switching speed. In [19] presents a bandpass-to-bandstop filter (17% FBW at 2.45 GHz) with a closed ring resonators whose switchability achieves from the perturbation effect on degenerate modes. When the perturbation varactor is at series resonance, its reactance dies out and a bandstop characteristic is formed, conversely bandpass filter response is attained by turning the perturbation varactor to be capacitive. Another technique shows in [20] where a bandpass to a bandstop transformation attains for ultra wideband applications using four PIN diodes as shown in Fig. 1-2. Although the design is innovative but incurs high insertion loss (>2 dB) and cost because of using four PIN diodes.

Tuning centre frequency in discrete steps with PIN diode technology has been achieving particular attention over continuous tuning element varactor diode due to its low RF losses and signal distortion, especially in broad bandwidth case where large tuning is required. In addition, a PIN diode offers high power handling capability, quick switching speed as well as providing  $Q > 50$  below 10 GHz with reduced cost, easier packaging and a lower bias voltage. A filter illustrated in [21], which can generate broad and narrow bandwidths by adapting inter-resonator couplings. The filter in [22] proposes a topology where frequency can be shifted in four steps ranging from 290 MHz to 600 MHz with 22.1% to 25.3% FBW using ten PIN diodes. Due to provide a large tuning steps, a proportionate number of switching elements i.e. ten diodes in this case and bias circuits are needed, resulting escalate the circuit complexity and parasitic effects.

A reconfigurable bandpass filter is designed in [23] to interchange the centre frequency and bandwidth between WiFi and UMTS standards with low loss and power consumption using two PIN diodes. A tunable side coupled resonator filter with three centre frequency ( $f_0$ ) states (9,10 and 11 GHz) that two possible bandwidths ranging from 7.7% to 14.7% for each state can be observed in [24]. A reconfigurable bandwidth which is varied from 4.45% to 10.5% with a 2:1 tunable passband ratio ( $f_0 = 9\text{GHz}$ ) utilising a dual mode square resonator

can be seen in [25]. Another dual mode filter is shown in [26] where the propose filter achieves asymmetrical filter response by tuning its centre frequency and transmission zeros position using a modified square resonator. The proposed asymmetrical response is obtained by manipulating the size of the dual mode resonator while the overall effect of the mode-splitting perturbation is kept constant. A single switch reconfigurable filter using a dual mode triangular patch resonator is developed to achieve a tunable passband ratio 1.9:1. However, the filter is restricted by the finite tuning ratio [27] at 10 GHz ( $f_0$ ) with a 3-dB FBW of 4.5% in the narrowband case and 8.6% in the wideband state. Additionally, a switchable dual-band BPFs ( $f_0$  at 0.96 GHz and 1.6 GHz) with four states is proposed by loading six PIN blocks in [28], and a dual-band BPFs with only one channel at a time in [29].

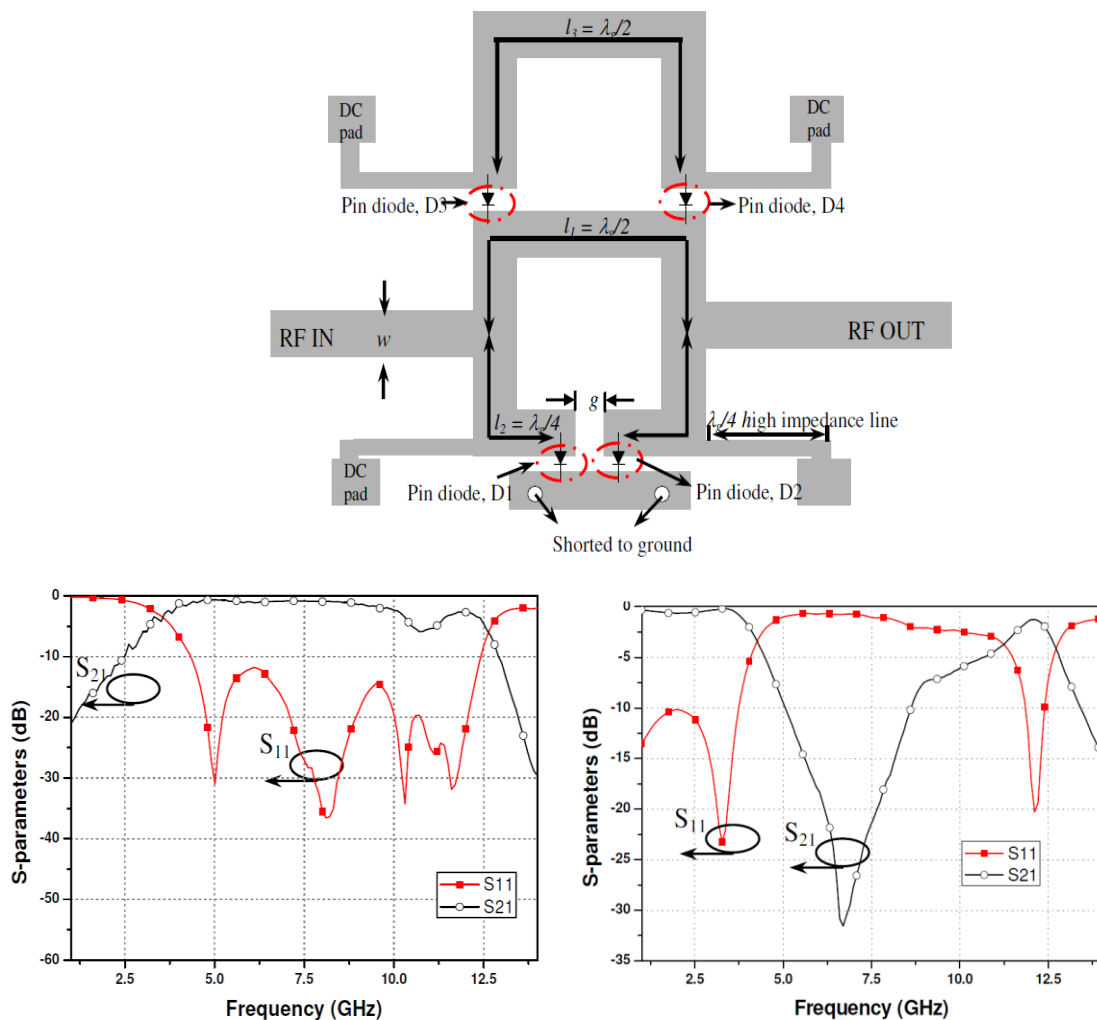


Fig. 1-2 Reconfigurable UWB filter with bandpass to a bandstop transformation [20]

Moreover, optical switches are incorporated to this shift method as a substitute of PIN diode. The advantages of this approach are high switching speed, immune to

electromagnetic interferences, and no external bias circuitry is required. A centre frequency switchable filter using a pair of optically operated silicon switches is presented in [30] where the design was produced by modifying a single pole parallel-coupled line filter and the maximum frequency switching range is approximately 380 MHz with 1.86% variations. A frequency tunable antenna using pairs of optically illuminated switches is proposed in [31]. The centre frequency is shifted by 40% (from 2.26 GHz to 3.15 GHz) when both switches are activated. Also, optically controlled resonators [32] and phase-shifter [33] have been presented recently.

On the other hand, many filters with continuous tuning have been investigated in the past where centre frequency is the most common filter parameter to reconfigure [34]-[37]. The reason for choosing centre frequency tunability is that it can be attained conveniently by using reactive elements whose reactance values can be altered continuously by varying bias voltages. Tunable combline filters were first shown in [34] where a relatively high tuning range of 53% has been reported, with mid-band insertion loss in excess of around 5 dB. The bandwidth variation was restricted to around 12%. In [38], a tunable third order filter is using thin-film Barium Strontium Titanate (BST) is reported where the achievable bandwidth of 400 MHz with 16% tuning range and passband insertion loss ranging between 3 and 5 dB. Generally, varactor diode is being found the most popular controllable tuning element among other switching types, namely, Barium Strontium Titanate (BST) [38],[39], piezoelectric [40]. However, the use of varactor diodes has many disadvantages including high insertion loss and unacceptable distortion (IIP3 around 6 dBm ~ 24 dBm) [41].

On inspection of the research literature, it is clear that most of the proposed methods of bandwidth and frequency reconfigurability are for narrowband applications. Because a proportionate number of switches and bias circuit are required to achieve a large number of tuning or switching steps. This escalates circuit complexity and detrimental parasitic effects can become an issue. Also, variation in bandwidth as centre frequency is tuned is a common problem as the resonator coupling coefficients may vary with the tuning frequency. Furthermore, most of the reported filters offering reconfigurable feature either has larger size, high insertion loss or the control range is not wide enough to satisfy the major services and standard. These issues form the main focus of this research project.

### 1.1.3 UWB Bandpass Filters with Notched-Band

The increasing deployment of wireless networking technology as well as other wireless technologies in the same spectrum is rapidly increasing radio frequency interference, threatening the data throughput performance. This is particularly true for UWB which covers a very wide frequency band and is overlapped with WiMAX (3.5 GHz) in the lower band and with WLAN (5.8 GHz) in the upper band. An ideal solution in such circumstances is a bandpass filter with a rejection notched band that can be switched or fixed within the passband. Hence, some of the suggested UWB bandpass filters in the previous section are constructed with one or more rejection bands. However, designing UWB bandpass filters with notched band structures is found not to be straight forward and the challenges are include strong harmonic response, decrease in frequency-utilising efficiency, large circuit size, or high fabrication cost.

For filters adopting multi-mode resonators (MMRs) with parallel coupled structure, the rejection band is implemented by embedding a slotted quarter wavelength open-circuited stub within the MMRs [42]. UWB bandpass filter in microstrip technology based on open-short transmission line is shown a notched band using two quarter wavelength open-circuited stub and the proposed notch frequency can be reconfigured by turning the PIN diode on/off states as in Fig. 1-3 [43]. However, the notch provides relatively narrowband tuning and it is not possible to completely block the entire passband. Also, UWB bandpass filters consist of multi-mode resonators which are aligned with coupled feeding ports and produced a single or multiple rejection bands via folding transmission line length [44]-[45].

In [46], compact defected ground structures are used to create the notch. A third-order suspended strip line (SSL) filter is included to achieve the band rejection. Unfortunately, this configuration consumes a large size. UWB filter based on coplanar wave guide (CPW) technology is demonstrated a technique in which a rejection band frequency is allocated by placing slotted dual quarter wavelength open-circuited stubs in the ground plane [47].

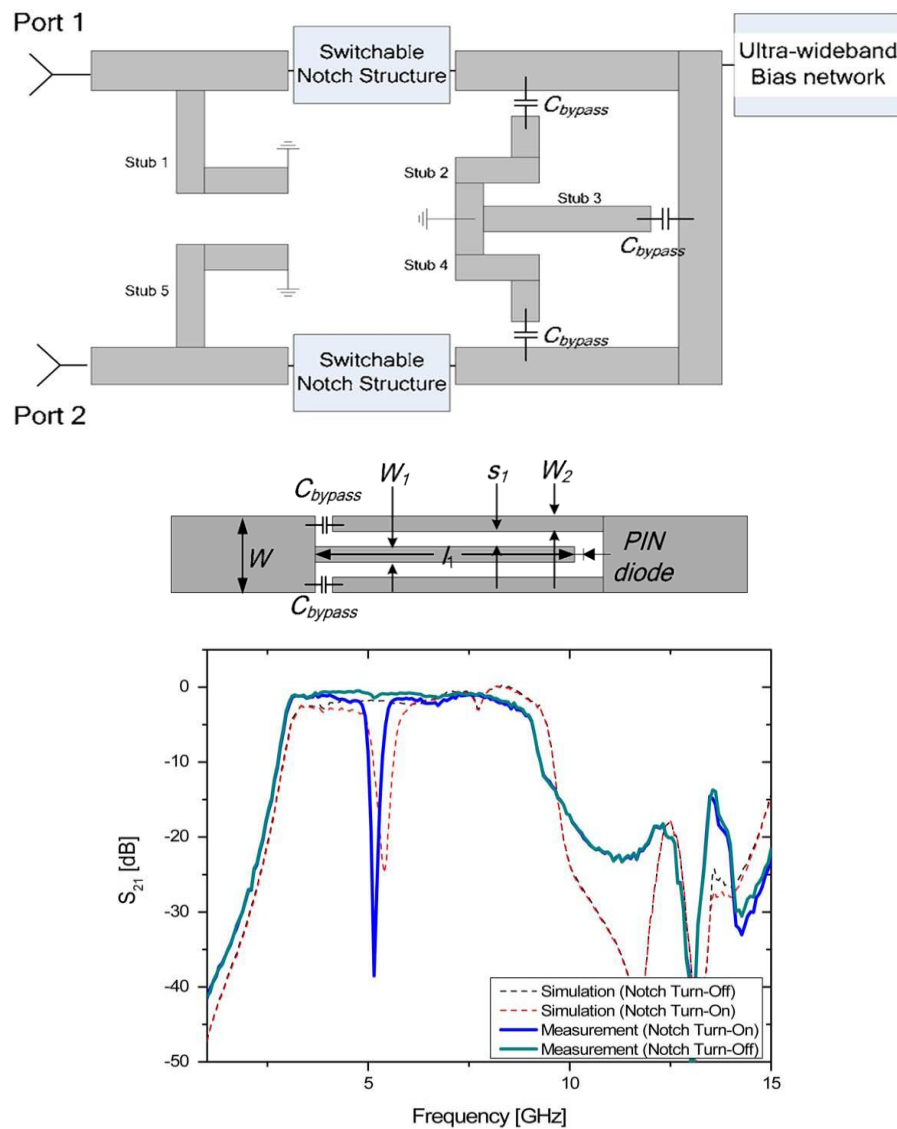


Fig. 1-3 UWB BPF filter with switchable notch frequency [43]

UWB filter with multiple notched bands using multilayer nonuniform periodical structure has been proposed in [48], where filter with single, double, and triple notch bands are implemented on the liquid crystal polymer (LCP) substrate. Although the design techniques are effective but the design methodologies are very complex and not suitable for existing microwave integrated circuits.

UWB filter with multiple notch bands frequency using asymmetric coupling strip is achieved by diverting signals into two paths, which makes it possible to create multiple transmission zeros [49]. The two desired rejection bands were generated using simplified composite right/left-handed resonator, which is coupled capacitively to the filter resonator. UWB filter based on MMR are constructed with notch frequency using SIR structure coupled with filter

resonator through coupling gap [50]. However, these techniques seriously increase the circuit size of the filter.

## 1.2 Objectives of Research and Review of the Thesis

### 1.2.1 Objectives of Research

The primary purpose of the proposed research is concerned with analysis and development of wideband reconfigurable filters using microstrip technology for ultra-wideband bandpass (UWB) applications include several key challenges related to bandpass filters such as selectivity, harmonic suppression, miniaturisation, and in-band rejection. Also, the feasibility of switches (i.e. optical switch, PIN diode, and varactor diode) are investigated so as to highlight their potential on reconfiguring resonators. These objectives have been taken up in the following steps.

The main focus of the project is the development of a novel miniaturised resonator structure which has the ability to suppress spurious harmonics, can be reconfigured electronically or optically in various states such as switching frequency (e.g. bandpass to bandstop), notched band or bandwidth, and also be able to attain high selectivity, low insertion loss. Due to this regard, several resonators structures has been chosen for investigation including circular or square ring, and open loop based configurations. Quarter or half wave length stub type resonators are given particular attention due to achieve wideband response in a convenient way and to avoid fabrication complexities. Common ground section and folded resonator by bending inward is employed to attain compactness. The proposed structure may be modelled by an equivalent circuit, which can be useful to analyse inherent features such as sharpening the selectivity or improving wide stopband by employing transmission zero.

In the next stage of this work, the developed structure is studied to realise reconfigurable frequency states which can switch form a bandpass to a bandstop response for the lower UWB band (3.1-5.2 GHz) applications. The resonator equivalent circuit may be used as a basis for developing a filter design procedure as well as to be realized with relative ease. An

optical or photoconductive switch, comprised of a silicon die activated using near infrared light is investigated as an alternative of PIN diode switch. The equivalent circuit parameters of both switches may be extracted using electromagnetic simulator and linearity validation studies can be performed to compare feasibilities.

To extend the analysis further, several other issues pertaining to filters such as improving passband selectivity or suppressing harmonics by introducing transmission zeros are considered for developing a commercially viable resonator structure. Due to the possibility of the interference of signals generated by some other wireless services like as WiMax, wireless local area networks (WLAN) or WiFi systems with the UWB signals. UWB bandpass filters should be designed with the notched band structure so that it could suppress in-band interferences. Theoretical analysis may be derived in order to establish the behaviour of notch structure, which also provides a solution to be controlled notched band electronically without effecting the filter response. Moreover, the development of bandpass filters with multi notched band is taken account part of this investigation.

The investigation then focuses on constructing a novel structure to implement dual wideband behaviour by using a single resonator. The proposed structure also develops a solution by which frequency bandwidths can be controlled independently according to applications interest. Additionally, stepped impedance based techniques are utilised in order to further reduce the resonator footprint and the dual-mode feature is incorporated varying filter bandwidth. Finally, another new compact CPW fed reconfigurable UWB bandpass filter using DML lines concept is discussed as a substitute of direct coupled feeding line, which has high selectivity filtering characteristics and relatively small size.

### 1.2.2 Review of the Thesis

This section summarizes the contents of the subsequent chapters to provide the reader with a quick glance at the material covered, where the conclusions are presented in chapter seven.

Chapter two of the thesis outlines background theory relevant to the research work undertaken. The characterization of microstrip lines and their associated discontinuities properties are discussed. Coupled line theory is also illustrated here as coupled lines are employed later in generating transmission zeros. A highlight of lowpass to bandpass filters design procedure is presented since these synthesis formulas are convenient for microwave bandpass filter implementation.

Chapter three of the report presents the ring shape microstrip structure based on stub type resonators for miniaturisation of UWB filter. The background theory and a simplified design procedure relevant to the work is discussed. Also, the filter with reconfiguring technique using PIN diode and Optical switch is developed where the proposed design behaves as a bandpass filter with a passband between 3.1 GHz to 5.0 GHz while in the other mode, it behaves as a bandstop filter in the same band. Furthermore, the ring shape microstrip structure with switchable band rejection option is considered to eliminate undesired signal frequencies and an embedded T-shape structure is analysed for this purpose. avoids enlarging the size problem of the filter structure.

Chapter four of the dissertation focuses on the developing of miniaturised high selectivity UWB bandpass filters using open loop resonator with deep attenuations at lower and upper bands. A technique is introduced to attain filter with second harmonic suppression. This methodology is shown to be very effective for the improvement of the stopband of the filter. Moreover, several novel approaches are developed for reconfiguring filter states such as bandpass to bandstop frequency states within the same bandwidth, switchable single or multiple notch frequencies. Various configurations are studied and samples are fabricated in order to validate the design concept.

Chapter five of the report firstly explores a highly compact dual-mode ring resonator configuration for the design of planar RF and microwave bandpass filters. The structure based on stepped impedance resonator (SIR) is analysed and the existence of two unique modes of resonance is substantiated. A design approach for microwave bandpass filter with bandwidth reconfigurability is developed using dual mode feature. The presented approach aims to achieve relatively wide tuning range with low in-band insertion loss and without affecting the filter selectivity while the fractional bandwidth varies. Finally, a CPW-fed reconfigurable filter is examined as a substitute of direct coupled feeding line structure in order to achieve further miniaturisation.

Chapter six of the report presents a novel structure to implement dual-wideband behaviour using single ring resonator, in which a dual band inverter is adopted without enlarging circuit size. The second half of the chapter investigates bandpass filters with independently controlled frequency bandwidths. Comparisons of simulated and measured results of the designed filters are presented to verify the arguments.

Chapter seven of the thesis concludes some remarks from the research and provides suggestion for possible future work.

## 1.3 References

- [1-1] FCC, Revision of Part 15 the Commission's Rules Regarding Ultra-Wide-Band Transmission System, First Note and Order Federal Communication Commission, ET-Docket 98-153, Oct. 2002.
- [1-2] L. Zhu, S. Sun, and W. Menzel, "Ultra-wideband (UWB) bandpass filter using multiple-mode resonator," *IEEE Microwave Wireless Components Letters*, vol. 15, no. 11, pp. 796-798, Nov. 2005.
- [1-3] J. Gao, L. Zhu, W. Menzel, and F. Bögelsack, "Short-circuited CPW multiple-mode resonator for ultra-wideband (UWB) bandpass filter," *IEEE Microw. Wireless Components Letters*, vol. 16, no. 3, pp. 104-106, Mar. 2006.
- [1-4] Q.X. Chu, X.K. Tian, Design of UWB bandpass filter using stepped-impedance stub-loaded resonator, *IEEE Microwave Wireless Components Letters*, vol. 20, no.9, pp. 501-503, Sep. 2010.
- [1-5] T. Kuo, S. Lin, and C. Chen, "Compact ultra-wideband bandpass filters using composite microstrip-coplanar-waveguide structure," *IEEE Transactions on Microwave Theory and Techniques*, vol. 54, no. 10, pp. 3772-3778, Oct. 2006.
- [1-6] Z. Hao and J. Hong, " Ultra-wideband bandpass filters using multilayer liquid-crystal-polymer technology," *IEEE Transactions on Microwave Theory and Techniques*, vol. 56, no. 9, pp. 2095-2100, Oct. 2008.
- [1-7] Z. Hao and J. Hong, " Ultra-wideband bandpass filters using embedded stepped impedance resonators on multilayer liquid crystal polymer substrate," *IEEE Microwave Wireless Components Letters*, vol. 18, no. 9, pp. 581-583, Sep. 2008.
- [1-8] K. Chang, *Microwave Ring Circuits and Antennas*. New York, Wiley,1996.

[1-9] P. Troughton, "Measurement techniques in microstrip," *Electronics Letters*, vol. 5, no. 2, pp. 25–26, Jan. 1969.

[1-10] I. Wolff, "Microstrip bandpass filters using degenerate modes of a microstrip ring resonators," *Electronics Letters*, vol. 8, no. 12, pp. 163–164, Jun. 1972.

[1-11] J. S. Hong and S. Li, "Theory and experiment of dual-mode microstrip triangular patch resonators and filters," *IEEE Transactions on Microwave Theory and Techniques*, vol. 52, no. 4, pp. 1237–1243, Apr. 2004.

[1-12] J. S. Hong and M. J. Lancaster, "Capacitively loaded microstrip loop resonator," *Electronics Letters*, vol. 30, no. 18, pp. 1494–1495, Sep. 1994.

[1-13] L.-H. Hsieh and K. Chang, "Compact, low insertion-loss, sharp-rejection, and wide-band microstrip bandpass filters," *IEEE Transactions on Microwave Theory and Techniques*, vol. 51, no. 4, pp. 1241–1246, Apr. 2003.

[1-14] S. Sun and L. Zhu, "Wideband microstrip ring resonator bandpass filters under multiple resonances," *IEEE Transactions on Microwave Theory and Techniques*, vol. 55, no. 10, pp. 2176–2182, Oct. 2007.

[1-15] W. Liu, Z. Ma, C. P. Chen, G. Zheng, and T. Anada, "A novel UWB filter using a new type of microstrip double-ring resonators," in *Asia–Pacific Microwave Conference*, pp. 33–36, Dec. 2006.

[1-16] H. Shaman and J. Hong, "A novel ultra-wideband (UWB) bandpass filter (BPF) with pairs of transmission zeroes," *IEEE Microwave Wireless Components. Letters*, vol. 17, no. 2, pp. 121–132, Feb. 2007.

[1-17] X.H. Wu, Q.X. Chu, X.K. Tian, X. Quyang, "UWB Quintuple-mode, Bandpass filter with sharp roll-off and super-wide upper stopband", *IEEE Microwave Wireless Components Letters*, vol. 21, no. 12, 661–663, Dec. 2011.

- [1-18] M. F. Karim, A. Q. Liu, A. Alphones, and A. B. Yu, "A novel reconfigurable filter using periodic structures," IEEE MTT-S International Microwave Symposium. Digest, San Francisco, CA USA, pp. 943–946, Jun. 2006.
- [1-19] Y.-M. Chen, S.-F. Chang, C.-Y. Chou, and K.-H. Liu, "A reconfigurable bandpass-bandstop filter based on varactor-loaded closed-ring resonators," IEEE Microwave Magazine, vol. 10, no.1, pp. 138–140, Feb. 2009.
- [1-20] M.F. Karim, Y.X Guo, Z.N. Chan and L.C. Ong, "Miniaturized reconfigurable and switchable filter from UWB to 2.4 GHz WLAN using PIN diodes", IEEE MTT-S International Microwave Symposium. Digest, Boston USA, pp. 509-512, Jun. 2009.
- [1-21] Lugo, C., Jr. and Papapolymerou, J. , "Electronic Switchable Bandpass Filter Using PIN Diodes for Wireless Low Cost System-on-a-package Applications," IEE Microwave Antennas and Propagation, Vol. 151, No.6, pp. 497 – 502, Dec. 2004.
- [1-22] Koochakzadeh, M. and Abbaspour-Tamijani, A., "Switchable Bandpass Filter for 0.3-0.6 GHz," IEEE MTT-S International Microwave Symposium, San Francisco, CA USA, pp. 557 – 560, Jun. 2007.
- [1-23] Brito-Brito, Z., Llamas-Garro, I., Navarro-Muñoz, G., Perruisseau-Carrier, J. and Pradell, L., "UMTS-WiFi Switchable Bandpass Filter," 39th European Microwave Conference, pp. 125-128, Rome, Italy, Oct. 2009.
- [1-24] Lugo, C., Jr. and Papapolymerou, J., "Six-state reconfigurable filter structure for antenna based systems," IEEE Transactions on Antennas and Propagation, Vol. 54, No. 2, pp. 479 – 483, Feb. 2006.
- [1-25] Lugo, C., Jr., Hadrick, J. and Papapolymerou, J., " Dual Mode Reconfigurable Filter for 3D System on Package (SOP) Integration," 55th Electronic Components and Technology Conference, pp. 532 – 535, Jun. 2005.

[1-26] Lugo, C., Jr. and Papapolymerou, J.," Dual-Mode Reconfigurable Filter With Asymmetrical Transmission Zeros and Center Frequency Control, IEEE Microwave and Wireless Components Letters, Vol. 16, No. 9, pp. 499 - 501, Sep. 2006.

[1-27] C. Lugo and J. Papapolymerou, "Single switch reconfigurable bandpass filter with variable bandwidth using a dual-mode triangular patch resonator," IEEE MTT-S International Microwave Symposium. Digest, pp. 779–782, June 2005.

[1-28] Dai G.L., Xia M.Y., "Design of compact dual-band switchable bandpass filter", Electronics Letters, vol. 45, no. 10, pp. 506–507, May 2009.

[1-29] Mahe F., Tanne G., Rius E., Person C., Toutain S., Biron F., Billonet L., Jarry B., and Guillion P. , "Electronically switchable dual-band microstrip interdigital bandpass filter for multi standard communication applications," European Microwave Conference, pp. 1-4, Oct. 2000.

[1-30] A. Chauraya, J. Kelly, R. D. Seager, and J. C. Vardaxoglou, "Frequency switchable microstrip filter for microwave frequencies," European Microwave Conference, vol. 1, pp. 5-7, Oct. 2005.

[1-31] C. J. Panagamuwa, A. Chauraya, and J. C. Vardaxoglou, "Frequency and beam reconfigurable antenna using photoconducting switches," IEEE Transactions on Antennas and Propagation, vol. 54, pp. 449-454, Feb. 2006.

[1-32] G. Zouganelis and D. Budimir, "Silicon gap-loaded microstrip slit-tetragonal resonator under IR-irradiation," Microwave and Optical Technology Letters. vol. 49, pp. 699-702, Mar. 2007.

[1-33] M. El Khaldi, F. Podevin, and A. Vilcot, "Optically controlled phase-shifter based on gaps on microstrip line," Microwave Photonics, pp. 263-266, Sep. 2003.

- [1-34] I. C. Hunter and J. D. Rhodes, "Electronically tunable microwave bandpass filters," *IEEE Transactions on Microwave Theory and Techniques*, vol. 30, no. 9, pp.1353–1360, Sep. 1980.
- [1-35] J. Uher and W. J. R. Hoefer, "Tunable microwave and millimeter-wave band-pass filters," *IEEE Transactions on Microwave Theory and Techniques*, vol. 39, pp. 643–653, Apr. 1991.
- [1-36] Germán Torregrosa-Penalva, Gustavo López-Risueño, and José I. Alonso, "A simple method to design wide-band electronically tunable combline filters," *IEEE Transactions on Microwave Theory and Techniques*, vol. 50, no. 1, pp. 172–177, Jan. 2002.
- [1-37] Young-Hoon Chun and Jia-sheng Hong, "Electronically Reconfigurable Dual-Mode Microstrip Open-Loop Resonator Filter," *IEEE Microwave and Wireless Components Letters*, Vol. 18, No.7, pp. 449–451, Jul. 2008.
- [1-38] Jayesh Nath, Dipankar Ghosh, Jon-Paul Maria, Angus I. Kingon, Wael Fathelbab, Paul D. Franzon and Michael B. Steer, "An Electronically Tunable Microstrip Bandpass Using Thin-Film Barium-Strontium-Titanate (BST) Varactors," *IEEE Transactions On Microwave Theory and Techniques*, Vol. 53, No. 9, pp. 2707 – 2712, Sep. 2005.
- [1-39] Young-Hoon Chun, Jia-Sheng Hong, Peng Bao, Timothy J. Jackson, Michael J. Lancaster, "Tunable Bandstop filter Using BST Varactor Chips," *European Microwave Conference*, Oct. 2007.
- [1-40] Mahmoud Al-Ahmad, Richard Matz, and Peter Russer, "Wide Piezoelectric Tuning of LTCC Bandpass Filters," *IEEE MTT-S International Microwave Symposium. Digest*, pp. 1275 - 1278, Jun. 2005.
- [1-41] B. E. Carey-Smith and P. A. Warr, "Distortion mechanisms in varactor diode-tuned microwave filters", *IEEE Transactions on Microwave Theory and Techniques*, vol. 54, no. 9, pp. 3492-3500, Sep. 2006.

- [1-42] C. Wang, C. Lee, and C. Hsu, "Band-notched UWB bandpass filter design using tri-section SIR," Asia Pacific Microwave Conference, pp. 1-4, Dec. 2008.
- [1-43] Young-Hoon Chun., Shaman H., Jia-Sheng Hong, "Switchable embedded band notch structure for UWB bandpass filter", IEEE Microwave Wireless Components Letters, vol.18, no. 9, pp. 590–592, Sep. 2008.
- [1-44] Sai Wai. Wong, Lei Zhu, "Implementation of compact UWB bandpass filter with a notch-band", IEEE Microwave Wireless Components Letters, vol. 18, no. 1, pp. 10–12, Jan. 2008.
- [1-45] C. Kim and K. Chang, "Ultra-wideband (UWB) ring resonator bandpass filter with a notch band," IEEE Microwave Wireless Components Letters, vol. 21, no. 1, pp. 206–208, Apr. 2011.
- [1-46] W. Menzel and P. Feil, "Ultra-wideband (UWB) filter with WLAN notch", European Microwave Conference, Munich, Germany, pp.595–598, Sep. 2006.
- [1-47] S. Mao, Y. Chueh, C. Chen, and M. Hsieh, "Compact ultra-wideband conductor-backed coplanar waveguide bandpass filter with a dual band-notched resonator," IEEE Microwave Wireless Components Letters, vol. 19, no. 3, pp. 149–151, Mar. 2009.
- [1-48] Z.C. Hao, J.S. Hong, "Ultra-wideband bandpass filter with multiple notch bands using nonuniform periodical slotted ground structure", IEEE Transactions on Microwave Theory and Techniques, vol. 57, no. 12, pp. 3080–3088, Dec. 2009.
- [1-49] K. Song, Q. Xue, "Compact ultra-wideband (UWB) bandpass filter with Multiple notch bands", IEEE Microwave Wireless Components Letters, vol. 20, no. 8, pp. 447–449, Aug. 2010.
- [1-50] Q. Chu, and X. Tian, "Design of a compact UWB filter with notched band," Asia Pacific Microwave Conference, pp. 37-40, Dec. 2010.

---

## 2.0 MICROSTRIP LINE DISCONTINUITY AND FILTER THEORY

---

Microstrip line is one of the most popular types of planar transmission lines, primarily because it can be fabricated by photolithographic processes and is easily integrated with other active and passive microwave devices. In addition, the characterization of discontinuity reactance is essential in the case of microstrip lines. Most of the discontinuities contribute to parasitic reactance. Discontinuities in microstrip lines involve an abrupt change in dimensions of the conductor, giving rise to a change in the electric and the magnetic field distributions. Firstly, this chapter presents a brief background and design equations for microstrip lines, discontinuities useful for design of filters. Later, the basic filter theory behind the work undertaken in this research is illustrated.

### 2.1 The Microstrip Line

Microstrip transmission lines consist of a conductor printed on top of thin, grounded dielectric substrate as it is illustrated in Fig. 2-1. The property of the conductor associates with the dielectric filling dictate the signal transmission characteristics of the line.

Due to the exposed characteristics of the microstrip line, the electromagnetic fields subsist not only within the dielectric but also enhance into the air above. The relative permittivity of

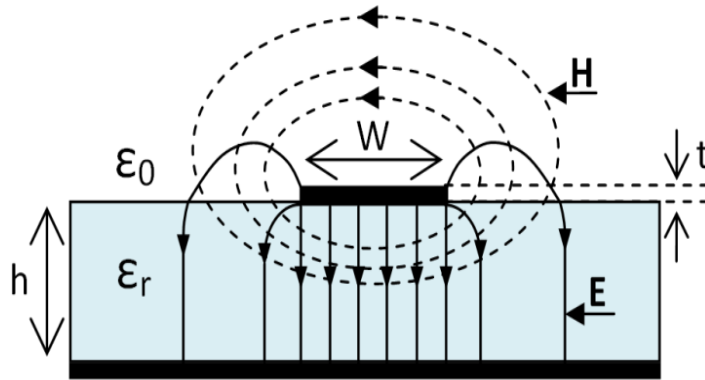


Fig. 2-1: Side on view of excited microstrip line with corresponding electric (solid lines) and magnetic (dashed lines) fields.

the material  $\epsilon_r$  is almost always greater than unity resulting the fields in air propagate faster than the fields within the dielectric hence microstrip lines, cannot support a pure transverse electromagnetic wave.

The comparably weak longitudinal field elements allow a quasi-static approximation to be applied in characterizing the line up to a few giga hertz [1]. This method considers the propagation of a pure TEM mode which greatly cut down the related calculations. Once the capacitance per unit length with and without the dielectric,  $C_d$  and  $C_0$  respectively are decided, the effective relative dielectric constant,  $\epsilon_{eff}$ , the characteristic impedance in the free space,  $Z_0$ , phase constant,  $\beta$ , angular frequency  $\omega$  and phase velocity,  $V_p$ , may be computed using (2.1) - (2.4) respectively, where  $c$  is the speed of light in free space.

$$\epsilon_{eff} = \frac{C_d}{C_0} \quad (2.1)$$

$$Z_0 = \frac{1}{c\sqrt{C_0 C_d}} \quad (\Omega) \quad (2.2)$$

$$\beta = \frac{\omega}{c} \left( \frac{C_d}{C_0} \right) \quad (radian / m) \quad (2.3)$$

$$V_p = c \sqrt{\frac{C_0}{C_d}} \quad (m/s) \quad (2.4)$$

The closed form expression that provide accuracy better than one percent are given as follows,

For narrow microstrip lines,  $\frac{W}{h} \leq 1$

$$\epsilon_{eff} = \frac{\epsilon_r + 1}{2} + \frac{\epsilon_r - 1}{2} \left[ \left(1 + 12 \frac{h}{W}\right)^{-0.5} + 0.04 \left(1 - \frac{W}{h}\right)^2 \right] \quad (2.5)$$

$$\text{Characteristic impedance } Z_{narrow} = \frac{\eta}{2\pi \sqrt{\epsilon_{re}}} \ln\left(\frac{8h}{W} + 0.25 \frac{W}{h}\right) \quad (2.6)$$

For wide microstrip lines,  $\frac{W}{h} \geq 1$

$$\epsilon_{re} = \frac{\epsilon_r + 1}{2} + \frac{\epsilon_r - 1}{2} \left(1 + 12 \frac{h}{W}\right)^{-0.5} \quad (2.7)$$

$$\text{Characteristic impedance } Z_{wide} = \frac{\eta}{\sqrt{\epsilon_{re}}} \left[ \frac{W}{h} + 1.393 + 0.677 \ln\left(\frac{W}{h} + 1.444\right) \right]^{-1} \quad (2.8)$$

where  $\eta=120\pi$  ohms is the wave impedance in the free space.

### 2.1.1 Synthesis Formulas

Approximate expressions for  $W/h$  in terms of characteristic impedance  $Z_c$  and relative permittivity  $\epsilon_r$ , are derived by [2] as follows

For  $\frac{W}{h} \leq 2$

$$\frac{W}{h} = \frac{8 \exp(A)}{\exp(2A) - 2} \quad (2.9)$$

with

$$A = \frac{Z_c}{60} \left\{ \frac{\epsilon_r + 1}{2} \right\}^{0.5} + \frac{\epsilon_r - 1}{\epsilon_r + 1} \left\{ 0.23 + \frac{0.11}{\epsilon_r} \right\} \quad (2.10)$$

For  $\frac{W}{h} \geq 2$

$$\frac{W}{h} = \frac{2}{\pi} \left\{ (B-1) - \ln(2B-1) + \frac{\epsilon_r - 1}{2\epsilon_r} [\ln(B-1) + 0.39 - \frac{0.61}{\epsilon_r}] \right\} \quad (2.11)$$

with

$$B = \frac{60\pi^2}{Z_c \sqrt{\epsilon_r}} \quad (2.12)$$

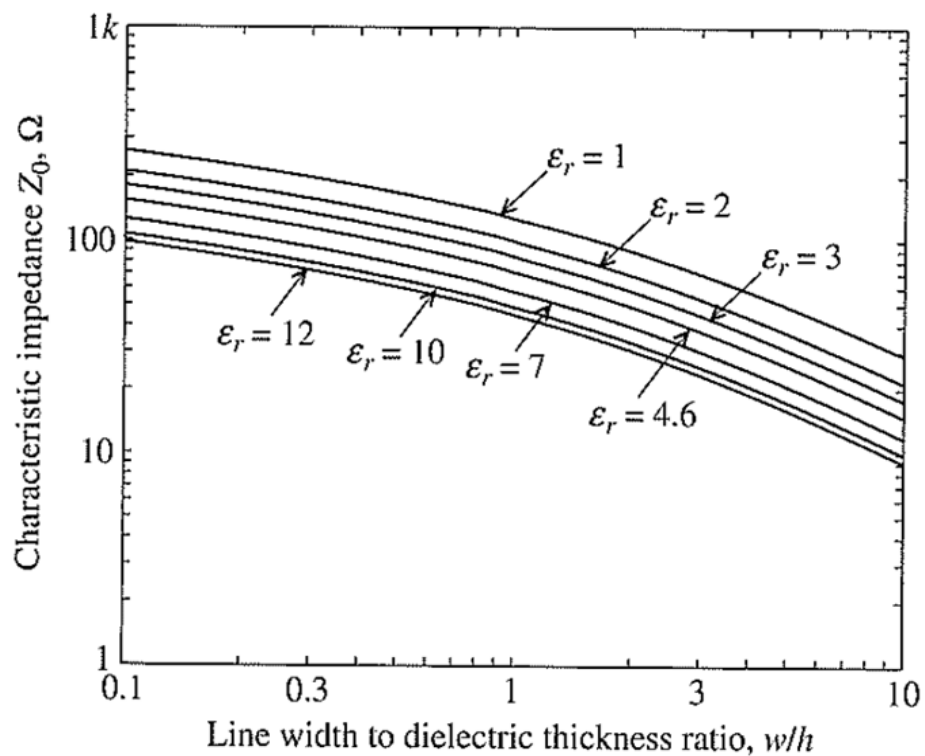


Fig. 2-2 Microstrip characteristic impedance as a function of  $W/h$  [3]

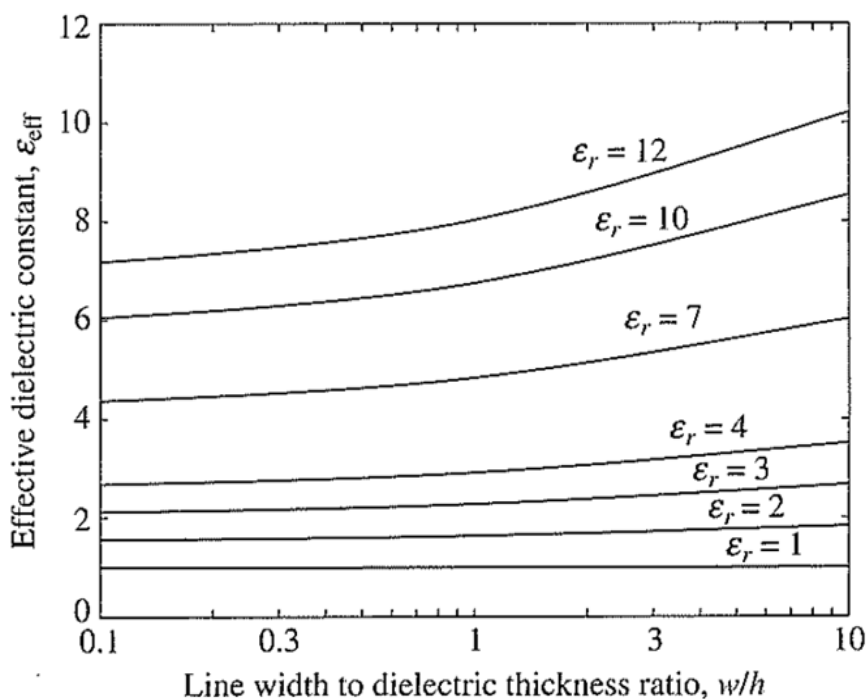


Fig. 2-3 Effective dielectric constant of the microstrip line as a function of  $W/h$  for different dielectric constants [3]

Full wave electromagnetic analysis methods have become the standard nowadays due to the widespread availability of powerful computers as well as full wave electromagnetic software packages. These techniques solve Maxwell's equations, employing advanced numerical methods, for the corresponding line parameters by utilising the given boundary conditions. While taking into consideration all longitudinal field components as well, these calculations are usually performed over a number of frequencies and therefore are capable to account for dispersive effects of the line. All in all, the full wave analysis techniques are able to provide significantly more accurate results by exploiting modern computing power.

Microstrip lines have relatively high loss arising from conductor loss, dielectric loss and radiation loss. Conductors dissipate power as heat due to the finite conductance of the metal trace. Dielectric loss is due to the heating effect caused by the movement of atoms within the substrate as a result of the applied field. In addition, since the microstrip is a semi open structure, any radiation is either free to propagate away or to induce currents on the metallic vicinity, causing the radiation or the commonly named housing loss. Out of these three loss mechanisms, the conductor and dielectric loss are the most significant.

Conductor loss is generally the most dominant contributor to the overall loss and is exacerbated at high frequencies due to the skin effect [4]. At RF and microwave frequencies, current is no longer uniformly distributed across the cross section of the signal trace. Due to eddy currents induced within the trace, signal current vanishes in the centre of the conductor and concentrates near the trace edges. This effectively reduces the cross-sectional area of the trace at high frequencies, increases the trace resistance and therefore also the attenuation constant of the line. Even though the attenuation constant may be determined with accuracy given the exact knowledge of the trace geometry as well as the field distribution [5], the computation is complicated. On the other hand, methods such as the perturbation method [1] and Wheeler's incremental inductance formula [5], given by (2.13), may be used to determine conductor attenuation constant,  $\alpha_c$ , approximately, where  $x$  is the distance into the conductor trace,  $W$  is the trace width and the surface resistance,  $R_s$ , is given by (2.14).

$$\alpha_c = \frac{R_s}{2Z_0\sqrt{\mu_0/\epsilon}} \frac{dZ_0}{dx} \quad (\text{dB/unit length}) \quad (2.13)$$

$$R_s = \sqrt{\frac{\omega\mu_0}{2\sigma}} \quad (\Omega) \quad (2.14)$$

With the widespread availability of full wave electromagnetic software, it is possible to extract the attenuation constants from a matched line, one at a time, from simulations using equation (2.15). For example, when the conductor attenuation constant is to be determined, the condition that the loss tangent of the dielectric substrate,  $\tan \delta = 0$ , is imposed and to determine the dielectric attenuation constant, the metal conductivity,  $\sigma$ , is assumed to be infinite. The overall attenuation constant may be found by the summation of these attenuation constants. The net attenuation is required to determine the unloaded quality factors of distributed resonators as described in the next section.

$$\alpha_{c/d} = \frac{-\ln |S_{21}|}{z} \quad (\text{dB/unit length}) \quad (2.15)$$

## 2.2 Microstrip Discontinuities

Microstrip discontinuities generally incurred in the layout of the practical filters include steps, open-ends, gaps, bends, and junctions as in Fig. 2-4. Discontinuities create parasitic reactances, which effect the transmission line field distributions. The altered electric field distribution can be represented by an equivalent capacitance, and the changed magnetic field distribution can be expressed in terms of an equivalent inductance. The equivalent circuit model of the discontinuity region can be modelled accurately by extrapolating the effective dimensions and taken into account in the filter design with full-wave electromagnetic (EM) simulations.

### 2.2.1 Steps in Width

The junction of two lines having different widths forms this type of discontinuity. The equivalent circuit consists of a shunt capacitance  $C$  in the plane of junction and series inductors  $L_1$  and  $L_2$  on either side of it as shown in Fig. 2-4(a). For a symmetrical step, the capacitance and inductance may be approximated by using the following formulas [2]

$$\frac{C}{\sqrt{W_1 W_2}} (pF / m) = (4.386 \ln \epsilon_r + 2.33) \frac{W_2}{W_1} - 5.472 \ln \epsilon_r - 3.17 \quad (2.16)$$

$$\frac{L}{H} (nH / m) = 40.5 \left( \frac{W_2}{W_1} - 1.0 \right) - 32.57 \ln \frac{W_2}{W_1} + 0.2 \left( \frac{W_2}{W_1} - 1 \right)^2 \quad (2.17)$$

$$L_1 (nH) = \frac{L_{w1}}{L_{w1} + L_{w2}} L \quad \text{and} \quad L_2 (nH) = \frac{L_{w2}}{L_{w1} + L_{w2}} L$$

$$\text{with } L_{wi} (nH) = Z_c \sqrt{\epsilon_r} / c \quad (2.18)$$

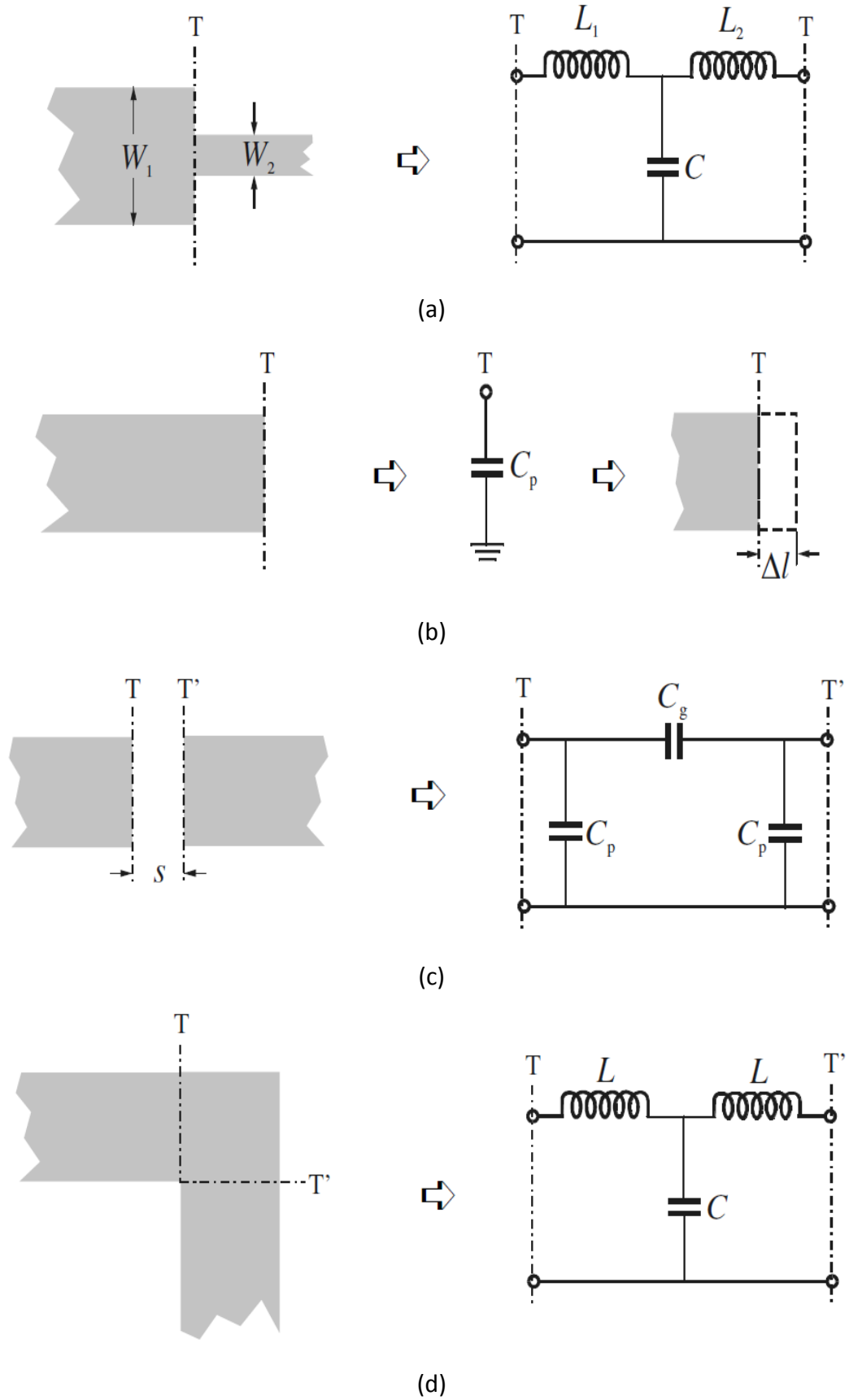


Fig. 2-4 Microstrip discontinuities: (a) step, (b) open-end, (c) gap, and (d) bend [4]

### 2.2.2 Open-ends

The closed form expression for apparent increase  $\Delta l$  in line length due to the open-end capacitance as in Fig. 2-4(b) is given below [2]

$$\frac{\Delta l}{h} = 0.412 \left\{ \frac{\epsilon_{re} + 0.3}{\epsilon_{re} - 0.258} \right\} \left( \frac{W/h + 0.264}{W/h + 0.8} \right) \quad (2.19)$$

Where  $\epsilon_{re}$  is the effective dielectric constant. For  $W/h \geq 0.2$  and  $2 \leq \epsilon_r \leq 50$ , yields results which are within 4 percent of the numerical results.

The open-circuit capacitance  $C_p$  may be obtained from the value of  $\Delta l/h$  by using the following equation

$$\frac{C_p}{W} = \frac{\Delta l}{h} \frac{1}{W/h} \frac{\sqrt{\epsilon_{re}}}{cZ_o} \quad (2.20)$$

Where  $c$  is the velocity of light in free space and  $\epsilon_{re}$  is the effective dielectric constant corresponding to the impedance  $Z_o$ .

### 2.2.3 Gaps

Corresponding susceptances as demonstrated in Fig. 2-4(c) can be obtained from the equivalent circuit capacitances  $C_g$  and  $C_p$ . If the two transmission lines are identical, then a plane of circuit symmetry exists and it can be analysed using odd/even mode analysis. The incident wave along the transmission lines are opposite (equal magnitude but  $180^\circ$  out of phase) in the odd mode namely anti-symmetrical and equal (equal magnitude and equal phase) in the even mode so-called symmetrical. These are expressed in terms of  $C_{even}$  and  $C_{odd}$  as follows [2]

$$C_p = \frac{1}{2} C_{even} \quad (2.21)$$

$$C_g = \frac{1}{2} (C_{odd} - \frac{1}{2} C_{even}) \quad (2.22)$$

Where  $C_{even}$  and  $C_{odd}$  are the equivalent circuit parameters for the gap when it is excited symmetrically and anti-symmetrically by creating virtually open and ground plane at the plane of circuit symmetry, respectively.

The closed form expressions for  $C_{even}$  ( $C_e$ ) and  $C_{odd}$  ( $C_o$ ) for  $\epsilon_r=9.6$  and  $0.5 \leq W/h \leq 2$  are

$$C_o / W(\text{pF} / \text{m}) = s / W m_o \exp(K_o)$$

$$C_e / W(\text{pF} / \text{m}) = s / W m_e \exp(K_e)$$

where

$$m_o = W/h(0.267 \ln W/h - 0.3853), K_o = 4.26 - 0.631 \ln W/h \text{ (for } 0.1 \leq s/W \leq 1.0)$$

$$m_e = 0.8675, K_{e0} = 2.043(W/h)0.12 \text{ (for } 0.1 \leq s/W \leq 0.3)$$

The values of  $C_e$  and  $C_o$  for other values of  $\epsilon_r$  in the range  $2.5 \leq \epsilon_r \leq 15$  can be calculated by using the following scaling relations

$$C_e(\epsilon_r) = C_e(9.6) (\epsilon_r/9.6)^{0.9} \quad (2.22)$$

$$C_o(\epsilon_r) = C_o(9.6) (\epsilon_r/9.6)^{0.8} \quad (2.23)$$

## 2.2.4 Bends

Microstrip right-angle band may be designed by an equivalent T-network as illustrated in Fig. 2-4(d). The closed form equations are given in [4] as follows

$$\begin{aligned} \frac{C}{W1}(\text{pF} / \text{m}) &= \left[ \left\{ \frac{(4\epsilon_r + 12.5)W/h - (1.83\epsilon_r - 2.25)}{\sqrt{W/h}} + \frac{0.02\epsilon_r}{W/h} \right\} \right] \text{ for } W/h \leq 1 \quad (2.24) \\ &= (9.5\epsilon_r + 1.25)W/h + 5.2\epsilon_r + 7.0 \quad \text{for } W/h \geq 1 \end{aligned}$$

$$\frac{L}{h}(nH / \text{m}) = \left[ 100 \left\{ 4\sqrt{\frac{W}{h}} - 4.21 \right\} \right] \quad (2.25)$$

## 2.3 Microstrip Coupled Lines

When a pair of parallel microstrip lines are placed in close proximity, microwave signal may be coupled from one line to another. The cross section of a coupled microstrip line with the corresponding electromagnetic fields in the even and odd mode is shown in Fig. 2-5.

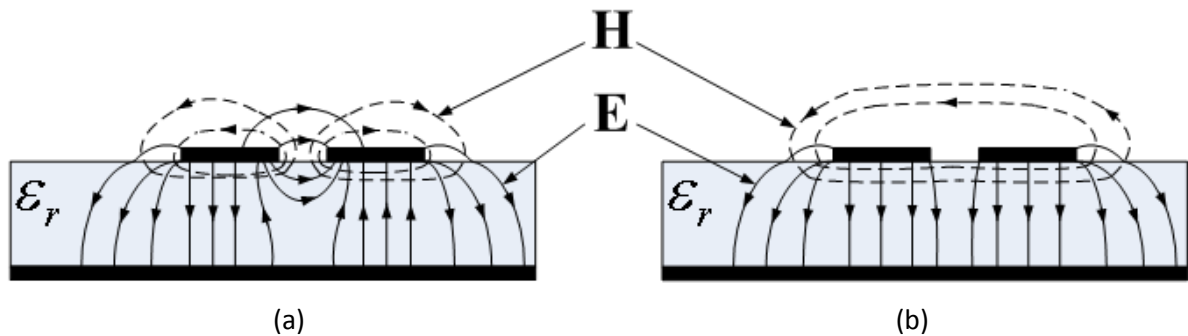


Fig. 2-5: Side on view of field distribution of microstrip coupled lines of (a) even mode (b) odd mode excitation.

Conventionally, any voltage or current excitation on the lines may be dissolved into even and odd components. In the even mode, signal coupling incurs through the magnetic field and in the odd mode this appears via the electric field. Even though both types of field contribute towards coupling, they may merge in either a constructive or destructive mood depending on lines excitation [4]. Hence, the coupling strength noticed is due to an interaction of these two effects. In microstrip coupled lines, the even and odd mode propagate at marginally different phase velocities due to the different field distributions.

An equivalent lumped element model of a pair of coupled transmission lines is presented in Fig. 2-6, where  $L_1$ ,  $C_1$ ,  $L_2$  and  $C_2$  are the self inductance and shunt capacitance per unit length of line 1 and line 2 respectively and  $L_m$  and  $C_m$  are the mutual inductance and capacitance per unit length between the two lines. The terminal voltages and currents in general are described by the differential equations (2.26)-(2.29).

$$\frac{dV_1}{dz} = L_1 \frac{dI_1}{dt} + L_m \frac{dI_2}{dt} \quad (2.26)$$

$$\frac{dV_2}{dz} = L_m \frac{dI_1}{dt} + L_2 \frac{dI_2}{dt} \quad (2.27)$$

$$\frac{dI_1}{dz} = C_{1g} \frac{dV_1}{dt} + C_m \frac{d(V_1 - V_2)}{dt} \quad (2.28)$$

$$\frac{dI_2}{dz} = C_m \frac{d(V_2 - V_1)}{dt} + C_{2g} \frac{dV_2}{dt} \quad (2.29)$$

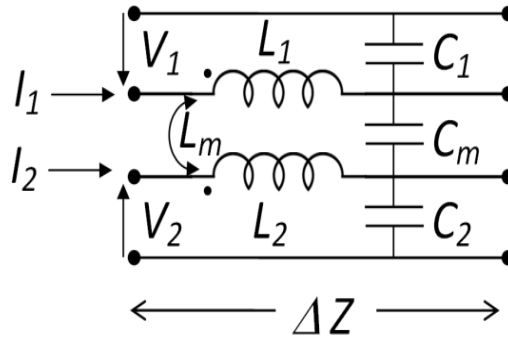


Fig. 2-6: Lumped element circuit model of coupled transmission lines

For an even mode excitation, the terminal voltages  $V_1 = V_2 = V$  and currents  $I_1 = I_2 = I$  are assumed. By applying these conditions to the above equations give (2.30)-(2.35), where  $C_1 = C_{1g} + C_m$  and  $C_2 = C_{2g} + C_m$  are the self capacitances per unit length of the lines 1 and 2 respectively.

$$\frac{dV}{dz} = L_1 \frac{dI}{dt} + L_m \frac{dI}{dt} = (L_1 + L_m) \frac{dI}{dt} \quad (2.30)$$

$$\frac{dV}{dz} = L_m \frac{dI}{dt} + L_2 \frac{dI}{dt} = (L_2 + L_m) \frac{dI}{dt} \quad (2.31)$$

$$\frac{dI}{dz} = C_{1g} \frac{dV}{dt} = (C_1 - C_m) \frac{dV}{dt} \quad (2.32)$$

$$\frac{dI}{dz} = C_{2g} \frac{dV}{dt} = (C_2 - C_m) \frac{dV}{dt} \quad (2.33)$$

The equations in the following state that the even mode equivalent inductance is  $L_1 + L_m$  and  $L_2 + L_m$  while the related capacitance is  $C_1 - C_m$  and  $C_2 - C_m$  for line 1 and 2 respectively.

Hence, the even mode characteristic impedance of line 1 may be defined by (2.34) and the corresponding impedance of line 2 can be derived by using similar approach.

$$Z_{even} = \sqrt{\frac{L_1 + L_m}{C_1 - C_m}} \quad (2.34)$$

In a similar argument for the odd mode where the applied conditions are  $V_1 = -V_2$  and currents  $I_1 = -I_2$  yields the odd mode equivalent inductance as  $L_1 - L_m$  and  $L_2 - L_m$  and corresponding capacitance as  $C_1 + C_m$  and  $C_2 + C_m$  for line 1 and 2 respectively. Therefore, the odd mode characteristic impedance of line 1 may be defined by (2.35) and the corresponding impedance of line 2 may be defined likewise.

$$Z_{odd} = \sqrt{\frac{L_1 - L_m}{C_1 + C_m}} \quad (2.35)$$

Another important factor particularly for filter design is the coupling coefficient as it characterises interaction of two resonators and offers a fairly accurate value for a direct synthesis of narrow-band filters and provide initial estimate structure parameters for optimisation synthesis of wideband filters. the coupling coefficient can be defined by the ratio of the coupled energy to the stored energy. The normalized electric and magnetic coupling coefficients  $K_E$  and  $K_M$  are given by (2.36) and (2.37) respectively.

$$K_E = \frac{C_m}{\sqrt{C_1 C_2}} \quad (2.36)$$

$$K_M = \frac{L_m}{\sqrt{L_1 L_2}} \quad (2.37)$$

## 2.4 Filter Design Theories

Filter design is generally begin with the lowpass prototype filter, which later can be transformed into any other form of filters, namely bandpass, highpass, and bandstop filters as in Fig. 2-7. The lowpass prototype may have various form of representation, depending on filter topology and characteristics as shown in Fig. 2-8. This section covers only lowpass to bandpass transformation theories, which are pertinent to the key objective of this research.

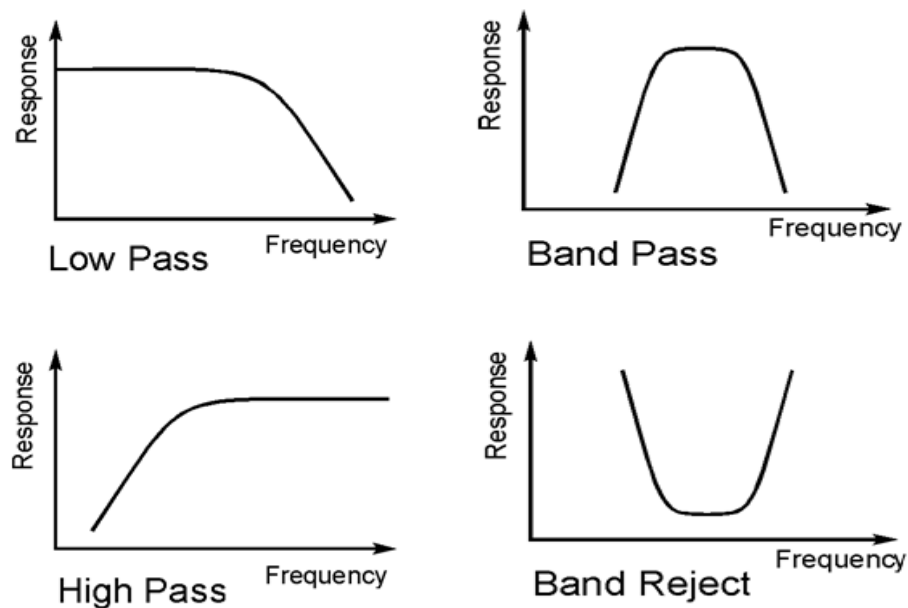


Fig. 2-7 Frequency behaviour of four basic types of filter

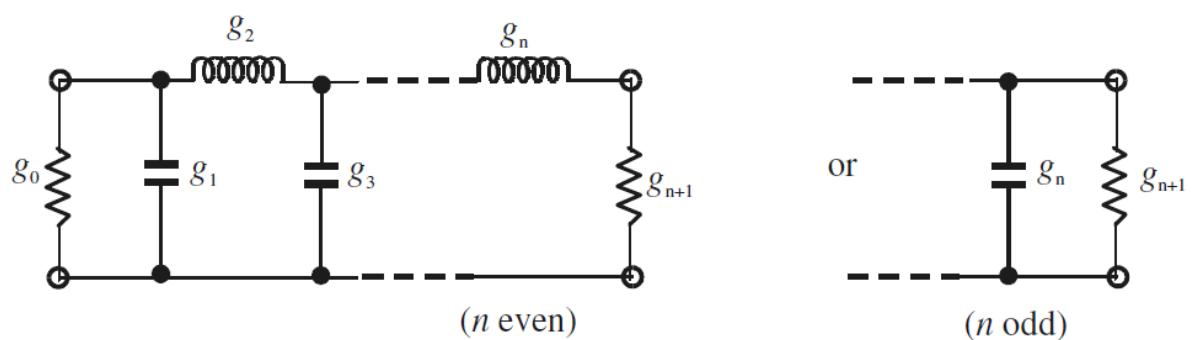


Fig. 2-8 Lowpass filter with degree of  $n$

To obtain the prototype element values in Fig. 2-8 and transform to a lowpass to a bandpass state, an convenient synthesis formulas are derived in the following:

The design procedure for a filter with given specifications, such as cutoff frequency, passband return loss or passband ripple factor in few cases, stopband attenuation at frequency  $f_s$ ,

1) The passband ripple level should be found from the expression for minimum passband return loss:  $L_R = 10\log_{10}\left(1 + \frac{1}{\varepsilon^2}\right)$  then  $\varepsilon^2 = \left(10^{L_R/10} - 1\right)^{-1}$  (2.38)

or the expression for passband ripple factor can be used to find the passband ripple level:

$$L_r = 10\log_{10}(1 + \varepsilon^2) \text{ Then passband ripple level } \varepsilon^2 = 10^{L_r/10} - 1 \quad (2.39)$$

2) The number of the element should be found at designated stopband frequency  $f_s$  from the expression for insertion loss:  $L_I = 10\log[1 + \varepsilon^2 T_n^2(\omega')]$  (2.40)

In this expression the  $T_n(\omega')$  is the  $n^{\text{th}}$  degree Chebyshev polynomial of the first kind which is defined by the expression:

$$\begin{aligned} T_n(\omega') &= \text{Cosh}[n \text{ArCosh}(\omega')] \text{ for } |\omega'| \geq 1 \\ T_n(\omega') &= \text{Cos}[n \text{ArCosh}(\omega')] \text{ for } 0 < |\omega'| < 1 \end{aligned} \quad (2.41)$$

where the normalised cutoff frequency can be found from the expression:

$$\omega' = \frac{\omega_s}{\omega_c} = \frac{2\pi f_s}{2\pi f_c} = \frac{f_s}{f_c} \quad (2.42)$$

3) The prototype element values should be defined form the provided table or using expressions:

$$g_0 = 1; g_1 = \frac{2\text{Sin}\left(\frac{\pi}{2n}\right)}{\text{Sin}\left(\frac{1}{n}\text{Sinh}^{-1}\frac{1}{\varepsilon}\right)}; g_i g_{i+1} = \frac{4\text{Sin}\left(\frac{2i-1}{2n}\pi\right)\text{Sin}\left(\frac{2i+1}{2n}\pi\right)}{\text{Sinh}^2\left(\frac{1}{n}\text{Sinh}^{-1}\frac{1}{\varepsilon}\right) + \text{Sin}^2\left(\frac{i\pi}{n}\right)}; i=1,2,\dots,(n-1) \quad (2.43)$$

4) The lumped elements values should be determined using prototype element values from equation:

The inductance for series inductors:

$$L_i = g_i \left( \frac{Z_0}{\omega_c} \right) = g_i \left( \frac{Z_0}{2\pi f_c} \right) \quad (2.44)$$

The capacitance for shunt capacitors:

$$C_i = g_i \left( \frac{1}{Z_0 \omega_c} \right) = g_i \left( \frac{1}{Z_0 2\pi f_c} \right) \quad (2.45)$$

Where the prototype element value  $g_i$  can be defined by using (2.43) and  $Z_0$  is arbitrary characteristic impedance.

5) Frequency transformation are needed to map the response in the lowpass filter prototype frequency domain,  $\Omega$ , to that in the frequency domain,  $\omega$ . By which a practical filter response such as bandpass, bandstop, and highpass characteristics can be obtained. The frequency transformation may have an effect on the reactive elements but no effect on the resistive elements. The required frequency transformation with having a passband  $\omega_2 - \omega_1$ , where  $\omega_1$  and  $\omega_2$  indicate the passband-edge angular frequency can be derived by following expression

$$\Omega = \frac{\Omega_c}{FBW} \left( \frac{\omega}{\omega_0} - \frac{\omega_0}{\omega} \right) \quad (2.46)$$

with

$$FBW = \frac{\omega_2 - \omega_1}{\omega_0} \quad \text{and} \quad \omega_0 = \sqrt{\omega_1 \omega_2}$$

The above frequency transformation may be applied to the reactive element of the lowpass prototype by using below derivation

$$j\Omega g = j\omega \frac{\Omega_c g}{FBW \omega_0} + \frac{1}{j\omega} \frac{\Omega_c \omega_0 g}{FBW} \quad (2.47)$$

The above expression (2.47) implies that an inductive/capacitive element  $g$  in the lowpass prototype in Fig. 2-8 is transformed to a series/parallel LC resonant circuit in the bandpass filter as shown in Fig. 2-9.

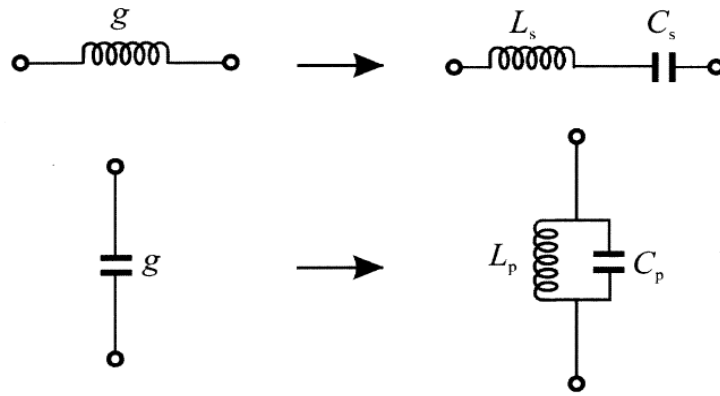


Fig. 2-9 Lowpass to Bandpass element transformation

The elements for the series  $LC$  resonator in the bandpass filter can be defined by

$$L_s = \left( \frac{\Omega_c}{FBW \omega_0} \right) \gamma_0 g$$

$$C_s = \left( \frac{FBW}{\omega_0 \Omega_c} \right) \frac{1}{\gamma_0 g} \quad (2.48)$$

where  $g$  representing prototype element value and  $\gamma_0$  is impedance scaling factor.

and the elements for the parallel  $LC$  resonator in the bandpass filter are expressed as follows

$$C_p = \left( \frac{\Omega_c}{FBW \omega_0} \right) \frac{g}{\gamma_0}$$

$$L_p = \left( \frac{FBW}{\omega_0 \Omega_c} \right) \frac{\gamma_0}{g} \quad (2.49)$$

6) The lengths of microstrip line ( $l_L$ ) to replace inductors should be determined using expression:

$$l_L = l_L = \frac{\lambda_{gL}}{2\pi} \text{Sin}^{-1} \left( \frac{2\pi f_c L}{Z_{0L}} \right), \text{ where the guide wavelength is } \lambda_g = \frac{\lambda_0}{\sqrt{\epsilon_{eff}}} = \frac{c}{f_c \sqrt{\epsilon_{eff}}} \quad (2.50)$$

The lengths of microstrip line ( $l_C$ ) to replace capacitors should be determined using expression:

$$l_L = \frac{\lambda_{gC}}{2\pi} \text{Sin}^{-1} (2\pi f_c C Z_{0C}) \quad (2.51)$$

7) The width ( $w$ ) of microstrip line for chosen characteristic impedance  $Z_{0L}$  for inductive transmission line and  $Z_{0C}$  for capacitive transmission line. By using the expressions (2.6) and (2.8), the effective dielectric constant and a width of narrow and wide microstrip line for inductor and capacitor can be derived.

## 2.5 References

[2-1] D. M. Pozar, Microwave engineering, 3<sup>rd</sup> edition, New York: John Wiley & Sons, 2004.

[2-2] T.C. Edward, M.B. Steer, "Foundation of interconnect and microstrip design 3<sup>rd</sup> edition", New York: Wiley, 2000.

[2-3] Kai Chang, Inder Bahl and Vijay Nair, "RF and Microwave Circuit and Component Design for Wireless Systems", Wiley and Sons, 2002.

[2-4] J.-S Hong and M. J. Lancaster, Microstrip filters for RF/microwave applications, New York: John Wiley & Sons, 2001.

[2-5] S. B. Cohn, "Dissipation Loss in Multiple-Coupled-Resonator Filters", Proceedings of the IRE, vol. 47, no. 8, pp. 1342 - 1348, Aug. 1959.

---

## 3.0 COMPACT RECONFIGURABLE UWB BANDPASS FILTERS

---

Ultra wideband (UWB) filters have seen a sharp rise in demand recently due to the commercialisation of the 3.1 GHz – 10.6 GHz band. However, this band is divided into a lower and upper band of 3.1 GHz - 5 GHz and 6.2 GHz – 10.6 GHz respectively to avoid the 5.0 GHz – 6.0 GHz band used by IEEE 802.11a. UWB filters is one of the essential components in different kinds of communication applications, for instance, indoor and handheld systems such as wireless peripheral interfaces, position tracking, radar, sensors etc. Currently extensive research and development efforts have been put into utilizing ultra-wideband (UWB) technology and linear broader bandwidth reconfigurable filters are in increasing demand for developing modern microwave communication systems. For filter realisation, planar circuits such as microstrip filter structures have become popular due to ease in integration and manufacture. Bandpass filters comprised of quarter wavelength ( $\lambda_g/4$ ) or half wavelength ( $\lambda_g/2$ ) stubs are quite alluring owing to the advantages of obtaining relatively wide bandwidth and less insertion loss around passband. For instance, quarter wavelength ( $\lambda_g/4$ ) resonators have been adopted to implement the interdigital and combine filters [1]-[4].

Recently reconfigurable UWB filter based on stub-types resonators has been proposed in [5] where four PIN diodes have been incorporated in order to switch between a bandpass and bandstop response. However, the filter experiences comparatively high loss and signal distortion due to nonlinear characteristics of the diode. Another quarter wavelength ( $\lambda_g/4$ ) open-circuited stub approach is employed in [6], where reconfigurability has been achieved by using a switchable notch in the passband. However, the filter circuit consumes a large space and the notch provides relatively narrowband in nature so that it is not possible to completely block the entire passband.

Various techniques are used recently for tuning include varactor diodes, RF MEMs, ferroelectrics, liquid crystals and optical switches. The use of varactor diodes has many disadvantages including high insertion loss and unacceptable distortion. RF MEMs offer low loss, high Q and good linearity but have very poor switching speeds. Ferroelectric materials also introduce high dielectric losses although they are readily tuned. Liquid crystals have high linearity, require low tuning voltages but very have slow switching times [7]. In contrast, the PIN diode provides lower losses and limits the degradation in the passband width and filter operation [8]. In addition, a PIN diode offers high power handling capability, quick switching speed as well as providing  $Q > 50$  below 10 GHz with reduced cost, easier packaging and a lower bias voltage. On the other hand, optically controlled silicon switches offer high power handling capability, immunity to electromagnetic interference, excellent isolation between the microwave and switch control circuits and very low distortion. Optically controlled resonators [9], couplers [10] and antennas [11] have already been demonstrated.

Although there is extensive literature on reconfigurable filters for wireless applications, the following important issues need to be addressed:

- ❖ Explore in depth to arrive at an equivalent circuit model, which is used as the basis for filter design.
- ❖ Small and low profile structures to suite modern communication systems.
- ❖ Independent control of switching frequency states within the same spectrum without affecting the filter characteristics.
- ❖ Filters performance in its operating environment by altering switches.

This chapter addresses the above issues with some novel concepts.

The aim of the section 3.1 is to introduce the filter topologies used in this research along with respective design equations and theories. This derivation can be used for acquiring the physical parameters of the resonator from the prototype networks values.

Then, in section 3.1.1, a novel reconfigurable filter is proposed, which can be switched from a bandpass to a bandstop state using PIN diode and Optical switch. The feasibility of the switches have been explored and the linearity of the filters using switches are evaluated.

Finally, in section 3.2, a filter based on similar transmission line prototype is coupled with T-shape resonator implemented in order to eliminate the unwanted interferences within the specified band limit (e.g. W-LAN, Bluetooth, UMTS for UWB). The proposed notch structure is analysed to conceive the resonator behaviour and realise the switches best locations. In this case, a significant size reduction and notched band operation has been achieved with small T-shaped structure.

The independent control concept that was discussed as above is achieved in all filters presented in this chapter and hence the filters response can be controlled over a wide frequency range. This feature provides an additional level of freedom for the filter designer to design the filters to any other band of interests.

### 3.1 Analysis and Equivalent Circuit

The topology described in Fig. 3-1 is heavily used in current and later chapters; therefore this section describes the structure in great detail with all theory, design equations and circuits clearly illustrated. The proposed filter is a third-order bandpass filter composed of a single half wavelength ( $\lambda_g/2$ ) resonator, which is placed between a pair of quarter wavelength ( $\lambda_g/4$ ) short circuited resonators shown in Fig. 3-1. The electrical length of the  $\lambda_g/4$  length and the  $\lambda_g/2$  resonators have been calculated at a centre frequency of the filter. For a given filter degree, the stub bandpass filter characteristics will then depends on the characteristic admittances of the stub lines denoted and the characteristic impedance of the connecting line. Since quarter wavelength ( $\lambda_g/4$ ) short circuited stubs look like parallel resonant circuit [12], they can be used as the shunt parallel LC resonators for bandpass filters. In contrast, the half wavelength ( $\lambda_g/2$ ) transmission line behaves as series resonant circuit, consists of series LC components.

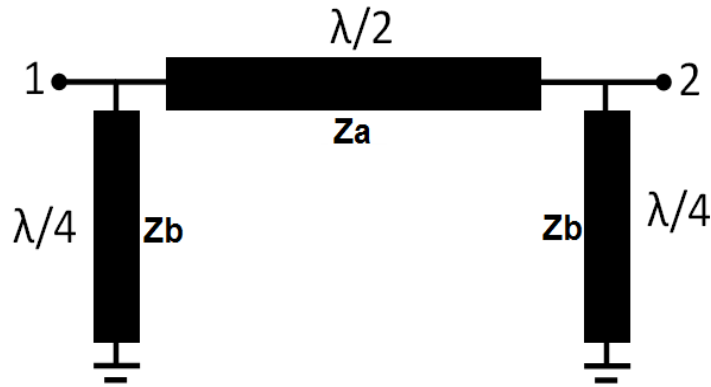


Fig. 3-1 Equivalent transmission line model of the proposed filter

As shown in Fig. 3-1, the equivalent circuit of the proposed filter where a series LC resonator is used to realise the connecting transmission line ( $\lambda_g/2$ ) between two shunt stubs, the shunt LC resonators connect in parallel are used to realise quarter wavelength short circuited ( $\lambda_g/4$ ) stubs. The design equations are derived for the connecting transmission line and stubs characteristic impedances, in terms of the element values of a low-pass prototype having the desired response. This can be accomplished by using equivalent circuits for the resonant stubs and connecting line, and equating the response to that of a lumped element bandpass filter.

The characteristic impedance of the connecting transmission line and admittance of the two shunt short-circuited stubs can be defined by using the following equations (3.1)-(3.6),

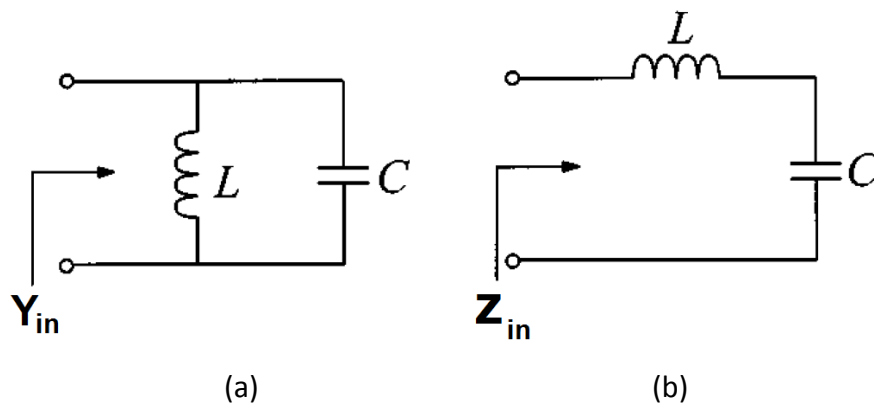


Fig. 3-2 Equivalent circuits of (a) Quarter wavelength ( $\lambda_g/4$ ) and Half wavelength ( $\lambda_g/2$ ) transmission line.

If  $X_{in}$  and  $X_a$  are the input reactance of the transmission line and the series LC resonator, respectively, then,

$$X_{in}(\omega) = Z_a \tan \beta l = Z_a \frac{\sin\left(\frac{2\Pi}{\lambda}\right)}{\cos\left(\frac{2\Pi}{\lambda}\right)} l \quad (3.1)$$

and the impedance near resonance of the series LC network can be approximated as

$$X_a(\omega) = \omega L - \frac{1}{\omega C} \quad (3.2)$$

Let the reactance slope parameter of  $X_{in}$  and  $X_a$  equals to each other at  $\omega_0 = \sqrt{1/LC}$ , we get,

$$Z_a = \frac{2\omega_0 L}{\pi} \quad \text{when} \quad \theta = \frac{\lambda_g}{2} \quad (3.3)$$

On the other hand, If  $B_{in}$  and  $B_a$  are the input susceptance of the transmission line and the shunt LC resonator, respectively, then,

$$B_{in}(\omega) = -Y_b \cot \beta l = Y_b \frac{\cos\left(\frac{2\Pi}{\lambda}\right)}{\sin\left(\frac{2\Pi}{\lambda}\right)} l \quad (3.4)$$

and the admittance near resonance of the shunt LC network can be approximated as

$$B_a(\omega) = \omega C - \frac{1}{\omega L} \quad (3.5)$$

Let the susceptance slope parameter of  $B_{in}$  and  $B_a$  equals to each other at  $\omega_0$ , we get,

$$Y_b = \frac{1}{Z_b} = \frac{4\omega_0 C}{\pi} \quad \text{when} \quad \theta = \frac{\lambda_g}{4} \quad (3.6)$$

The lumped elements values in Fig. 3-2 should be determined using prototype element values from equation (3.7):

For series tuned series elements:

$$L_i = g_i \frac{Z_0}{2\pi\Delta\omega}; \quad C_i = \frac{2\pi\Delta\omega}{g_i Z_0 \omega_0^2}$$

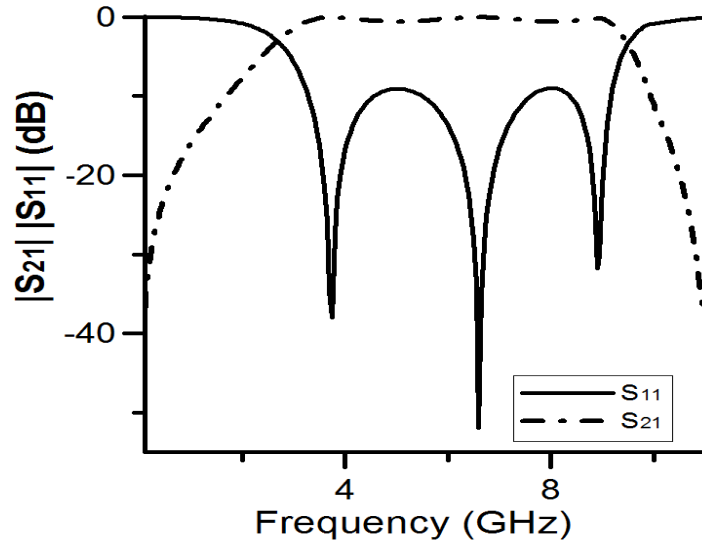


Fig. 3-3 Calculated filter frequency response.

For shunt tuned shunt elements:

$$L_i = \frac{2\pi Z_0 \Delta\omega}{g_i \omega_0^2}; \quad C_i = \frac{g_i}{2\pi Z_0 \Delta\omega} \quad (3.7)$$

where  $g_i$  is the prototype element values and  $Z_0$  is arbitrary characteristic impedance.

The frequency response as in Fig. 3-3 of the stubs filter circuit can be calculated using the equivalent circuit in Fig. 3-1. The ABCD matrix of the filter circuit is

$$\begin{aligned} \begin{bmatrix} A & B \\ C & D \end{bmatrix} &= \begin{bmatrix} 1 & 0 \\ Y_b & 1 \end{bmatrix} \begin{bmatrix} \cos \theta_0 & jZ_a \sin \theta_0 \\ j \frac{\sin \theta_0}{Z_a} & \cos \theta_0 \end{bmatrix} \begin{bmatrix} 1 & 0 \\ Y_b & 1 \end{bmatrix} \\ &= \begin{bmatrix} \cos \theta_0 + jZ_a Y_b \sin \theta_0 & jZ_a \sin \theta_0 \\ Y_b \cos \theta_0 + j \frac{\sin \theta_0}{Z_a} + Y_b (Y_b jZ_a \sin \theta_0 + \cos \theta_0) & Y_b jZ_a \sin \theta_0 + \cos \theta_0 \end{bmatrix} \quad (3.8) \end{aligned}$$

Finally, the scattering matrix can be derived by,

$$S_{11} = \frac{A_0 + B_0 + C_0 Z_0 - D_0}{A_0 + B_0 / Z_0 + C_0 Z_0 + D_0}$$

$$S_{21} = \frac{2}{A_0 + B_0 / Z_0 + C_0 Z_0 + D_0} \quad (3.9)$$

where

$$A_0 = D_0 = \cos \theta_0 + jZ_a Y_b \sin \theta_0$$

$$B_0 = jZ_a \sin \theta_0$$

$$C_0 = Y_b \cos \theta_0 + j \frac{\sin \theta_0}{Z_a} + Y_b (Y_b jZ_a \sin \theta_0 + \cos \theta_0)$$

In Fig. 3-3 shows that in terms of the return loss  $|S_{11}|$  dB, three reflection zeros appear at  $f_0$ ,  $f_1$  and  $f_2$ , where  $f_0$  is the filter resonator centre frequency and  $f_1$  and  $f_2$  can be derived from (3.10) and (3.11) with  $Z_a / Z_0$  and  $Z_b / Z_0$ , as  $Z_0$  is the system impedance,

$$f_1 = \frac{1}{\pi} \tan^{-1} \sqrt{\frac{(1+k)k}{(1+k) - Z_a^2}} \quad (3.10)$$

$$f_2 = \frac{1}{\pi} \left[ \pi - \tan^{-1} \sqrt{\frac{(1+k)k}{(1+k) - Z_a^2}} \right] \quad (3.11)$$

where  $Z_a, Z_b$  is the line impedance of  $\lambda_g/2, \lambda_g/4$  and  $k = Z_a/Z_b$ .

In contrast, wireless applications require bandstop filters (BSFs) to block unwanted signals while allowing desired signals to pass through. Over the recent years, several techniques have been proposed to generate a bandstop operation such as

- ❖ Combine a quarter wavelength line with a coupled line section [12]
- ❖ Connect two quarter wavelength coupled line sections where one short-circuited and the other open-circuited [13]
- ❖ Signal Interference technique using two signal paths [14]

A typical bandstop arrangement is shown below in Fig. 3-4, which is a cascade of  $90^\circ$  open circuit stub connecting with  $90^\circ$  transmission line [15]:

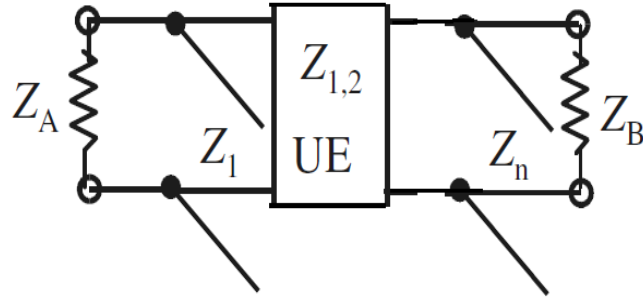


Fig. 3-4 Transmission line network of the bandstop filter

In order to design such a filter, the section is synthesized using the following transfer function:

$$|S_{21}(f)|^2 = \frac{1}{1 + \varepsilon^2 F_N^2(f)} \quad (3.12)$$

where  $\varepsilon$  is the passband ripple constant and  $F_N(f)$  is the filtering function given by,

$$F_N(f) = T_n\left(\frac{t}{t_c}\right) T_{n-1}\left(\frac{t\sqrt{1-t_c^2}}{t_c\sqrt{1-t^2}}\right) - U_n\left(\frac{t}{t_c}\right) U_{n-1}\left(\frac{t\sqrt{1-t_c^2}}{t_c\sqrt{1-t^2}}\right) \quad (3.13)$$

in which  $t$  is the Richard's transform variable

$$t = j \tan\left(\frac{\pi}{2} \frac{f}{f_0}\right) \quad (3.14)$$

$$t_c = j \tan\left(\frac{\pi}{4} (2 - FBW)\right)$$

Finally, for a given reference  $Z_0$  the line impedances are determined by,

$$Z_i = \frac{Z_0}{g_i} \text{ and } Z_{i,i+1} = \frac{Z_0}{J_{i,i+1}} \quad (3.15)$$

### 3.1.1 Reconfigurable UWB Filter (Bandpass to Bandstop)

Based on the discussion in section 3.0, this section tackles the following points:

- ❖ Reduce the size of the filter.
- ❖ Independent control of the frequency bands (Bandpass to Bandstop) with less complexity.
- ❖ Studying the effect of the altering switches (PIN diode and Optical Switch) in the filter response.
- ❖ Reduce the number of switches to improve the filter linearity.

Hence, the filter proposed in this section is focused on using stub-based ring shape to introduce reconfigurable frequency states and to minimise the size of the filter. The proposed design was optimised to operate at single band for use in lower UWB (3.1-5.2 GHz) applications. Alternative frequency can be attained by changing key dimensions of the filter.

This section presents a simple third order UWB reconfigurable filter. First, start with a third pole ( $n=3$ ) Chebyshev lowpass prototype with a 0.1 dB passband ripple. The prototype parameter are  $g_0 = g_4 = 1$ ,  $g_1 = 1.1468$ ,  $g_2 = 1.3712$ ,  $g_3 = 1.9750$ . By following the design equations, the lumped element values in Fig. 3-2 are determined by using equations from (3.7) and the corresponding element values are  $L_{\text{series}} = 5.6$  nH,  $L_{\text{parallel}} = 0.403$  nH, and  $C_{\text{series}} = 0.322$  pF,  $C_{\text{parallel}} = C_3 = 4.5$  pF. The presented design equations are extremely useful in filter design as it allows prototype parameters to be estimated relatively accurately from the given filter specifications.

Due to the wideband passband response and its simple design structure, the stub-type ring shape topology is chosen. As depicted in Fig. 3-1, the electrical length of the two  $\lambda_g/4$  lengths and the  $\lambda_g/2$  resonators have been calculated at a centre frequency of 4.15 GHz (lower band of UWB) using the microstrip design equations described in chapter 2 and the line impedance was found 58.8  $\Omega$ , which corresponded to lines of width 1.2 mm.

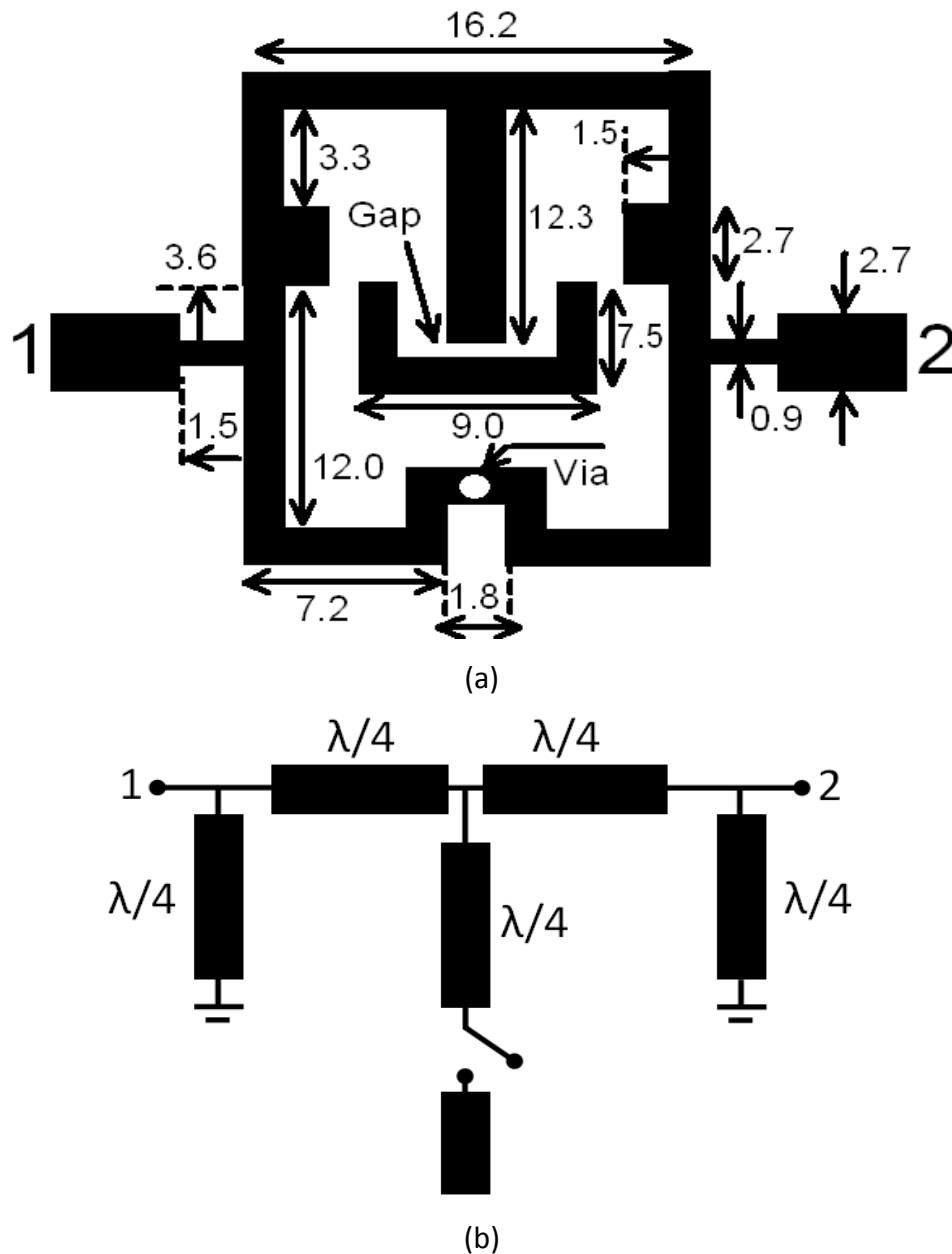
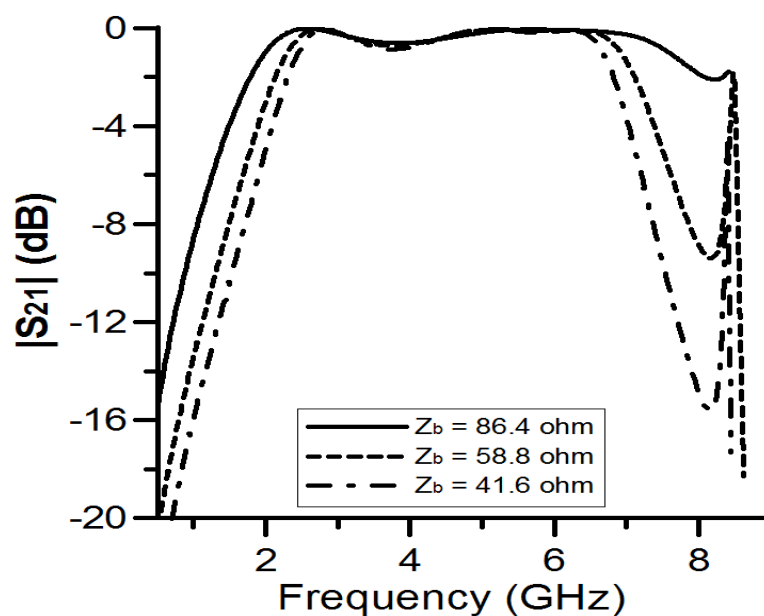


Fig. 3-5 (a) Layout of the proposed UWB filter (dimensions in millimetres), (b) Equivalent transmission line model.

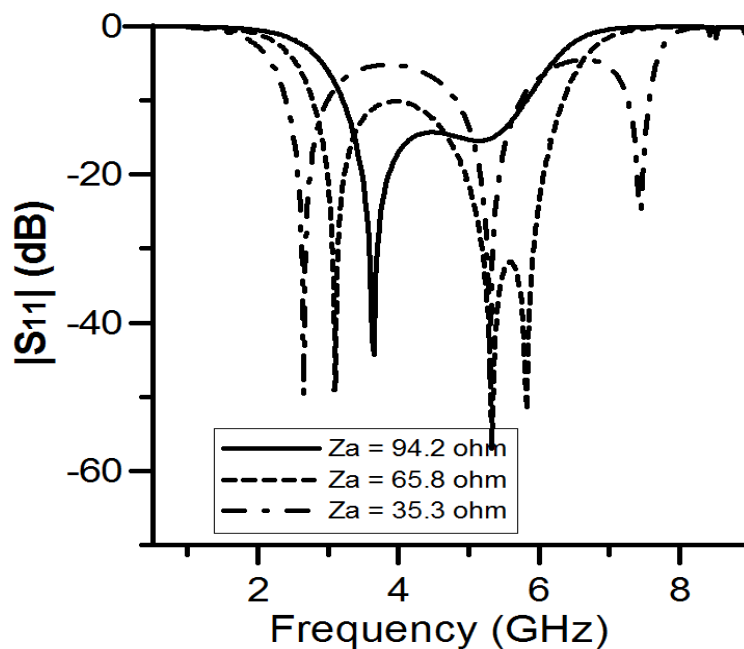
A sample filter is designed with an specifications of 3-dB passband from 3.1–5.2 GHz with a mid-band frequency of 4.15 GHz and 50  $\Omega$  terminal impedance. In one setting, the filter behaves as a bandpass filter with a passband between 3.1 GHz to 5.2 GHz while in the other mode, it behaves as a bandstop filter in the same band. The layout of the proposed filter and the corresponding transmission line model is illustrated in Fig. 3-5 where the filter is inductively coupled to the source and load as illustrated. Folding both short circuited resonators inwards allowed the use of a common ground via to be utilised, which makes the structure compact in size. In addition, slow wave technique which can be obtained by

retarding the phase velocity on a transmission line either increasing the series  $L$  or the shunt  $C$ , is utilised to shrink the resonator wavelength further down.

For the bandpass case, the response is developed by constructing filter structure with a single  $\lambda_g/2$  resonator, which is placed between a pair of  $\lambda_g/4$  short circuited resonators in Fig. 3-5(b). As discussed in the previous section, the stub bandpass filter characteristics will depend on the characteristics admittance of the stub lines and the characteristics impedance of the connecting line. Hence, with properly selected transmission line impedances, wideband bandpass response can be achieved. In Fig. 3-6(a) indicates that with increasing the impedance of the the  $Z_b$ , while keeping the  $Z_a$  is  $50 \Omega$ , the broader the bandwidth and higher the attenuation level can be achieved. In contrast, in Fig. 3-6(b) shows by changing the  $Z_a$  to the higher impedance with constant  $Z_b = 50 \Omega$ , the narrower the bandwidth can be obtained.



(a)



(b)

Fig. 3-6 Bandwidth of the proposed filter is influenced by (a) changing impedance of  $Z_b$ ,  
changing impedance of  $Z_a$

On the other hand, as in Fig. 3-5(b) depicts a transmission line network of a bandstop filter with open-circuited stub, where the shunt quarter wavelength ( $\lambda_g/4$ ) open-circuited stub is separated by connecting lines that are quarter wavelength ( $\lambda_g/4$ ) at the mid band frequency. This section is synthesized using equations (3.12)-(3.15) and extract the impedance value of the open-circuited stub is  $36.8 \Omega$  at a centre frequency 4.15 GHz, which is leading to 2.4 mm wide. The open-circuited stub is placed in the symmetry plane of the filter in order to reconfigure the frequency response. With the switch in the OFF state, the open-circuited stub presents a short circuit at the main transmission line and generates a transmission zero when its electrical length is about  $90^\circ$  at the filter mid-band frequency and the filter operates as a bandstop filter. In the ON state, the length of the stub is increased and the transmission zero is shifted to 2.2 GHz. The transmission zero and its first harmonic at  $3f_0$  improve the attenuation and selectivity of the bandpass filter in the lower and upper stopbands.

### 3.1.2 Switching Elements

Microwave switches consists of Pin and Varactor diodes, MEMS switches and optically controlled photoconductive switches are widely being researched to reconfigure wireless communication systems. Optical switches are seen as an attractive option as there is a high isolation between the controlling optical beam and the RF input signal. In the application of reconfigurable filters this may allow improved insertion loss pattern by eliminating interference from metallic biasing lines used to control circuit. In addition, due to the absence of a junction in a photoconductive silicon die switch, the voltage at which the switch experiences breakdown is considerably higher, and hence there is potential for greater power handling capability.

The optical switch consists of a 1 x 3 mm n-type doped silicon wafer whose conductivity may be altered with illumination. It may be modelled with an equivalent circuit as shown Fig. 3-7 (a) and the response is in the 'ON' state given in Fig. 3-7(b). Experimental data suggests that  $R_G$  and  $R_S$  decrease when the optical switch is ON while  $C_G$  and  $C_S$  increase [11]. In [10], the performance of a single optical switch was evaluated and was found to have an overall insertion-loss of around 0.68 dB in the ON state (under 200 mW of optical power). In the OFF state, the total series resistance increased significantly while  $C_G$  and  $C_S$  decreased. The EM simulations however were conducted with an open gap to model the switch in the OFF state and a bridged gap to model the switch in the ON state.

In contrast, pin diodes are popular switching elements, especially in MIC designs, where in addition to high switching speed, they offer ruggedness. Equivalent circuits of the pin diode in the ON and OFF states are given in Fig. 3-8(a) and the response is in the 'ON' state given in Fig. 3-8(b). In the ON state, the pin diode is essentially a current controlled resistor, whose resistance may be described by (3.16),

$$R_S = \frac{k}{\tau I_F} \quad (3.16)$$

where  $k$  is a device constant,  $I_F$  is the forward bias current and  $\tau$  is the minority carrier lifetime. In the OFF state, there is a large series resistance in parallel with a capacitance  $C_p$ , which degrades the high frequency isolation of the device.

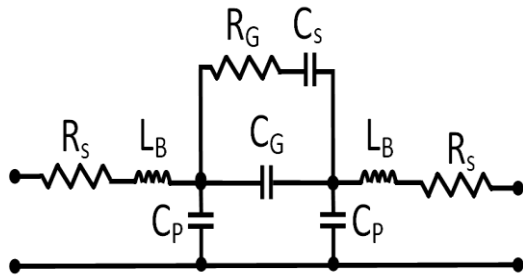
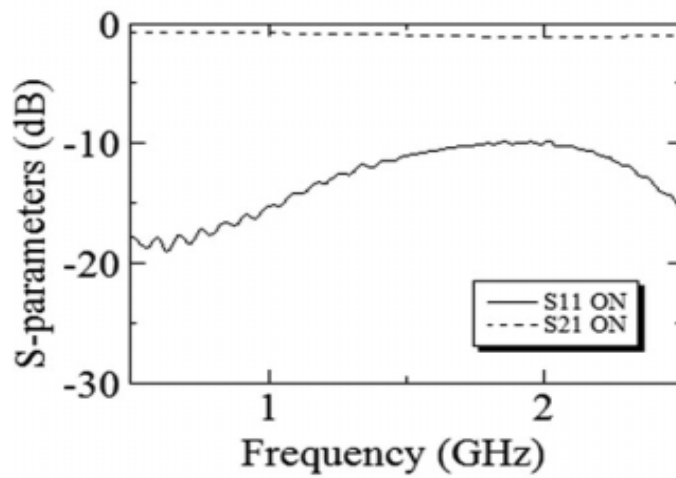


Table I R, L, C values as a function of laser power (Optical Switch)		
ON (200 mW)	$L_B = 41 \text{ nH}$ $R_S = 50 \Omega$ $C_p = 23 \text{ pF}$	$C_G = 23 \text{ pF}$ $R_G = 50 \Omega$ $C_S = 23 \text{ pF}$
OFF (0 mW)	$L_B = 1 \text{ nH}$ $R_S = 800 \Omega$ $C_p = 1 \text{ pF}$	$C_G = 1 \text{ pF}$ $R_G = 800 \Omega$ $C_S = 1 \text{ pF}$

(a)

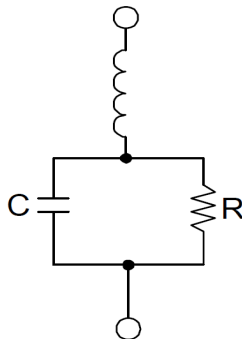


(b)

Figure 3-7 (a) Equivalent circuit of optical switch, and (b) corresponding response in the 'ON' state using 50 Ω transmission line.



(a)



(b)

Table II (Pin switch)	
ON	OFF
$R_s = 0.9 \Omega$ $L = 0.6 \text{ nH}$	$C_p = 0.8 \text{ pF}$ $R_p = 10 \text{ K}\Omega$ $L = 0.9 \text{ nH}$

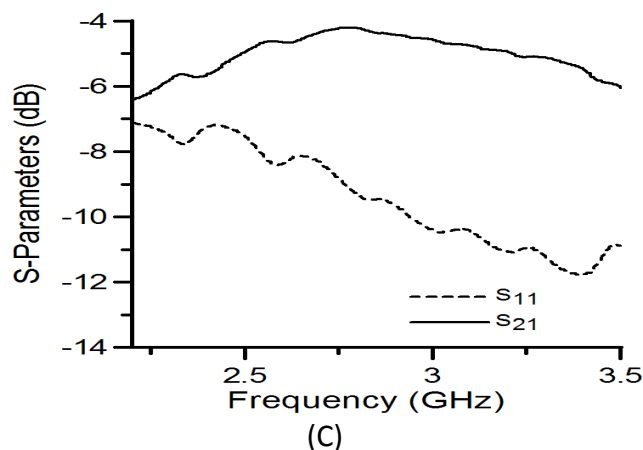


Figure 3-8 Equivalent circuit of PIN diode, (a) in Forward bias or 'ON', (b) in Reverse bias or 'OFF', and (C) corresponding response in 'ON' state using 50  $\Omega$  transmission line.

### 3.1.3 Simulated and Experimental Results

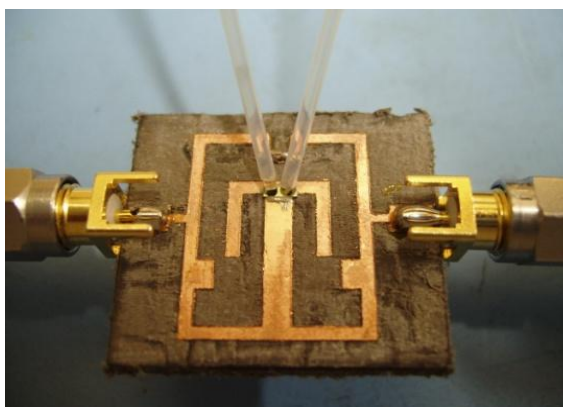
In order to validate the argument, the filter was fabricated on RT Duroid 5880 substrate with  $\epsilon_r = 2.2$  and  $h = 1.575$  mm. The overall filter size was 20.4 mm x 16.2 mm. In order to realise the switching performance in simulation, the S-parameters of the Optical switch and the PIN diode are measured first in a 50 $\Omega$  line at 4.15 GHz and the lumped element values are then created to match the S-parameters. The 0.3 mm gap labelled in Fig. 3-5(a) is overlaid with Optical and PIN diode switch (BAP65-02).

#### 3.1.3.1 Using Optical Switch

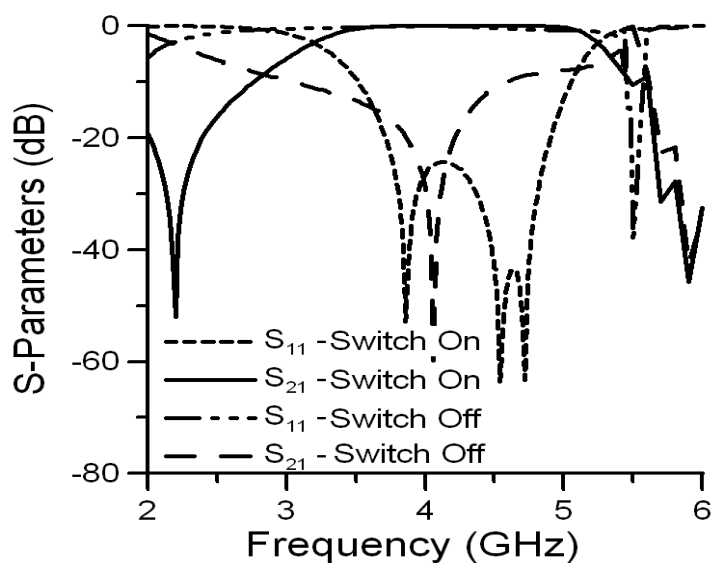
A 1 mm x 3 mm Silicon switch was fixed in place using a conducting silver epoxy. Two 1mm diameter glass fibre optic cables were positioned over the silicon wafer as shown in Fig. 3-9 (a). The simulated results for the filter in both ON and OFF states are depicted in Fig. 3-9(b). In measurement, under the ON state each cable delivered 200mW of optical power in the 980 nm near infra-red range. If a smaller switch was used, activation could be performed with just one fibre optic cable. The S-parameters of the filter with the optical switch in ON and OFF states were measured with an Anritsu Lightning 37397D Vector Network Analyzer and are shown in Fig. 3-9(c). The group delay of the filter in the ON state is given in Fig. 3-9(d), where the filter performs a flat group delay within the passband of about 0.45-0.65 ns

between 3-4.8 GHz but a sharp peak has been noticed at around 5 GHz due to poor conductivity of the optical switch.

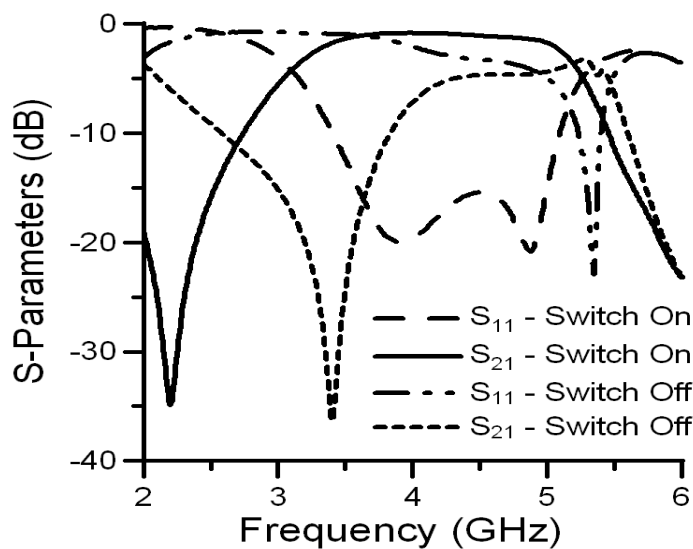
With the switch in the ON state, the measurements show the notch at a slightly lower frequency (3.4 GHz) than expected. Even in the OFF state, the silicon wafer acts as a dielectric causing  $C_G$  to be larger. As a result, the length of the stub is effectively elongated slightly and therefore, the transmission zero is not quite at the desired frequency. This can be corrected by increasing the width of the gap to compensate for the increase in capacitance. Measurements show that a rejection of better than 30 dB can be obtained at the centre frequency and a minimum of 10 dB rejection can be achieved across the desired band, which is an improvement to [5], where the minimum rejection was around 5 dB. The measured passband insertion-loss of the bandpass filter was 0.84 dB with fractional bandwidth 48.2% and minimum passband return loss of 15 dB is observed.



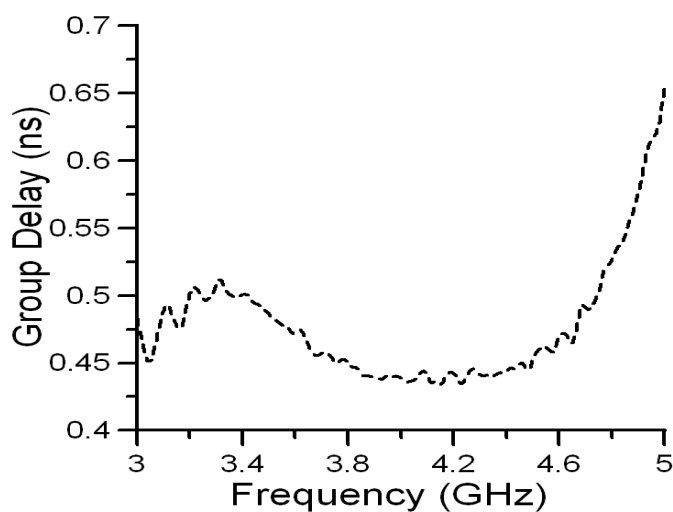
(a)



(b)



(c)



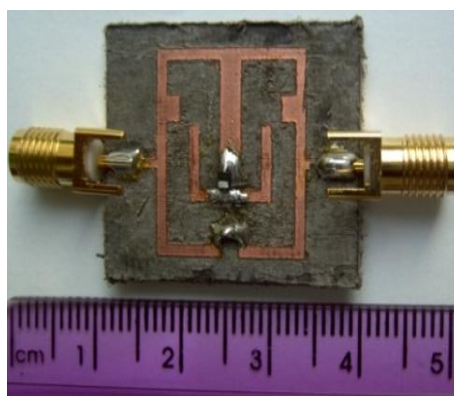
(d)

Fig. 3-9 (a) Photograph of fabricated filter with optical switch, (b) Simulated response of filter with the gap in the ON and OFF states, (c) Measured response of the fabricated filter with the optical switch in the ON and OFF states, and (d) Measured group delay of bandpass filter in the ON state.

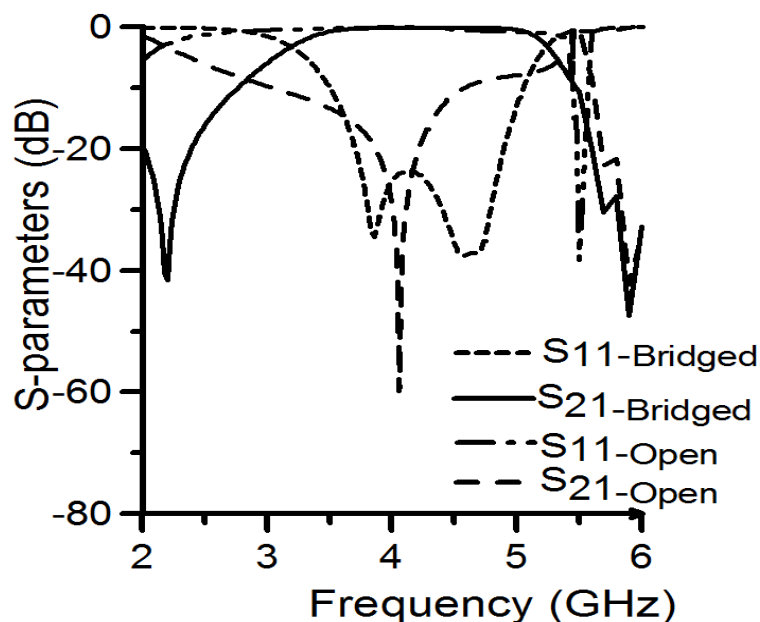
### 3.1.3.2 Using PIN Diode

In this experiment, the PIN diode NXP BAP65-02 SOD523 is chosen in order to match with the switching circuit parameters which has typical value of  $0.9 \Omega$  resistance,  $0.6 \text{ nH}$  inductance and  $0.8 \text{ pF}$  of capacitance [16]. To turn on the diodes, the external dc voltage is  $3\text{V}$ , and the current is  $1\text{mA}$ . The dc blocking capacitance is  $33 \text{ pF}$  and the resistor  $1\text{k}\Omega$  is used

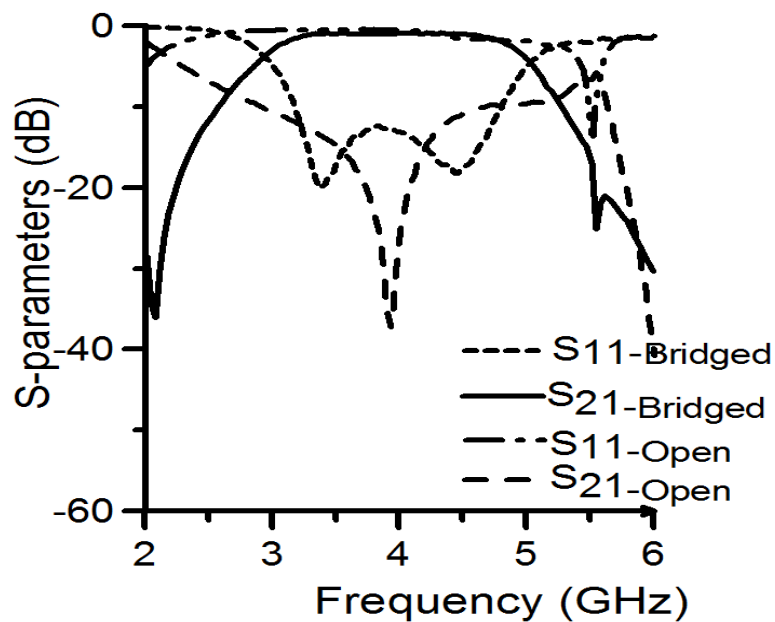
for biasing. A photograph of the fabricated filter is shown in Fig. 3-10(a). The S-parameters of filter with the PIN diode (BAP65-02) in ON and OFF position were measured with a vector network analyzer and are shown in Fig. 3-10 (b)-(c). When the PIN diode is ON, results from both circuits are in agreement. The measured passband insertion-loss of the bandpass filter was 0.15 dB and a minimum return loss of 20 dB is observed. A slight deviation from specifications and less return loss are observed between the simulated and measured results and this may be attributed to the various fabrication errors involved such as finite inductances of via hole, parasitic capacitances in PIN diode. The group delay of the filter in the ON state is given in Fig. 3-10(d) in which the filter experiences fluctuated group delay of about 0.55-0.75 ns between 3-5 GHz because of inherent non linearity of the PIN diode.



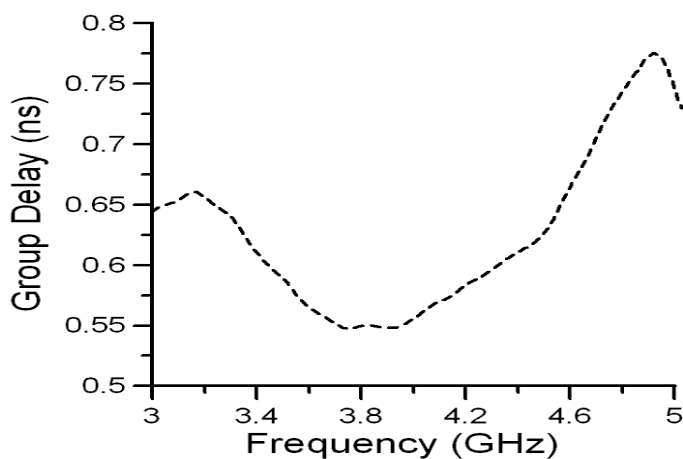
(a)



(b)



(c)



(d)

Fig. 3-10 (a) Photograph of fabricated filter with PIN diode, (b) Simulated response of filter with the gap in the bridged and open states, (c) Measured response of the fabricated filter with the PIN diode in the ON and OFF states, and (d) Measured group delay of bandpass filter in ON state.

### 3.1.3.3 Linearity

A key performance indicator of the filter was its linearity. The use of the filter lies in applications where presence of nonlinear elements can distort the output spectrum considerably due to other interfering unwanted signals. For linearity validation purposes, the linearity characteristics of the optical switch are assessed using Quadrature Phase Shift

Keying (QPSK) modulation schemes as input signals. Input power ( $P_{in}$ ) ranging from -10 dBm to 10 dBm produced excellent linearity performance for the signal at 4.1 GHz, as shown in Fig. 3-11. The distortion levels are only measured for the filter with optical switch in the ON state and this measurements were taken with the switch under illumination of 200 mW. An experimental setup was created using a signal generator for QPSK signal with the filter under discussion as Device Under Test (DUT). As expected the distortions measured at higher power levels are more in comparison to lower values of input power and in this case the proposed filter using optical switch was achieved a good linearity with IIP3 of 63 dBm at 4.1 GHz.

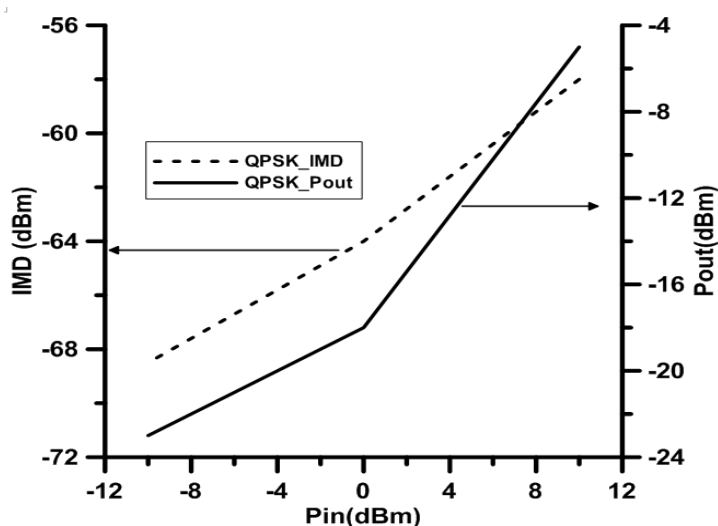
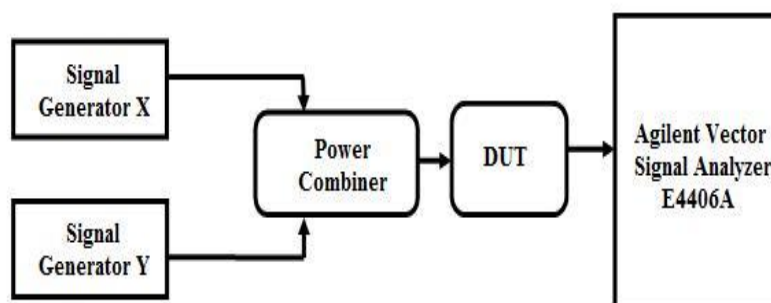


Fig. 3-11 Pout vs Pin and IMD vs Pin for QPSK digitally modulated Signal for 4.1 GHz Frequency in the ON state.



(a)

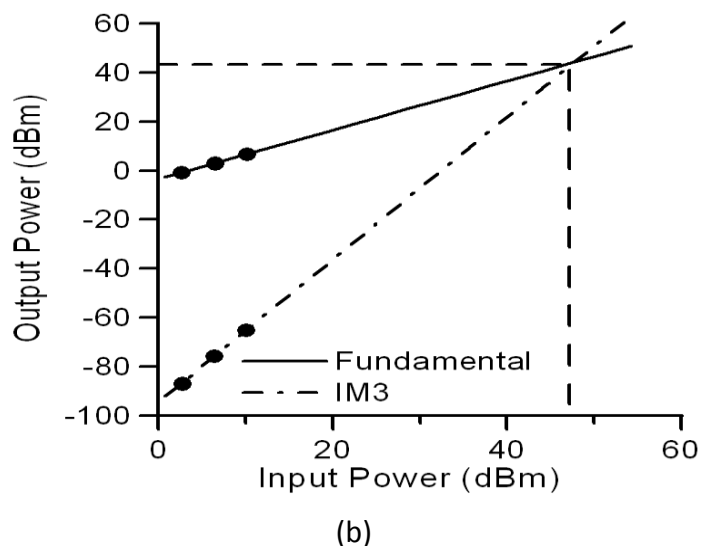


Figure 3-12 (a) Two-tone test setup, (b) Measured power of fundamental tones and third-order intermodulation product (IM3) plotted against input power for pin switch.

In contrast, for the pin switch, the third order intermodulation performance was assessed by the two-tone test setup illustrated above in Fig. 3-12(a). The test was conducted with the two tones at 3.99 GHz and 4.01 GHz, with a forward bias voltage of 30V with a DC isolation resistance of 1 k $\Omega$  to prevent RF leakage into the DC supply. The input and output referred third-order intercept points were measured at 47 dBm and 42 dBm, respectively, as shown in Fig. 3-12(b).

### 3.1.4 Summary

A linear reconfigurable microstrip UWB filter is demonstrated. The outlined filter design procedure allows bandpass filters to be realized from lowpass prototype networks. Given the lowpass prototype element values, the equations presented allow the physical parameters of the resonators to be attained quickly, with accuracy especially for wideband filter designs. The proposed filter achieves over 50% size reduction relative to the filters in [5] and higher stopband attenuation level.

A single PIN diode (BAP65-02) and an optical switch is shown to reconfigure the structure as either a bandpass or a bandstop filter. In this experiment, the overall simulation results are in good agreement to the measurements for both the optical and pin reconfigurable

filters. The linearity of the optical switch and the PIN based filters are evaluated experimentally at various passband frequencies and excellent linearity performances have been observed e.g. 63 dBm for an Optical switch and 47 dBm for PIN diode. From this investigation, it has been observed that an Optical switch could be a better alternative of a PIN diode due to having additional feature such as they do not require bias circuit, easier fabrication, good linearity and group delay characteristics. Moreover, this highly linear reconfigurable filter has great potential in UWB based applications in terms of cost saving and easier fabrication.

## 3.2 UWB Bandpass Filters with Reconfigurable Notched Band

UWB band (3.1 GHz - 10.6 GHz) covers a very wide frequency and is overlapped with range of other wireless services (e.g. WLAN band). These services potentially interfere with UWB signals and therefore causing signal distortion as well as loss of sensitivity. In order to best use that frequency band, filtering is essential. One of the possible and effective solutions for this problem is to realize narrow rejection bands (notches) within the passband of a UWB bandpass filters. Many efforts have been carried out to produce a UWB bandpass filters with notch and some of these techniques are as follows:

- ❖ Using defected ground structure (DGS) [17]
- ❖ An embedded open-circuited stub [18]
- ❖ Asymmetric parallel coupled line [19]

In [17], compact defected ground structures are used to create the notch. A third-order suspended strip line (SSL) filter was added to achieve the band rejection. Unfortunately, this configuration consumes a large size. UWB filter which consists of five short-circuit stubs along with embedded open-circuit stubs in the first and the last connecting lines is presented to reject the undesired signal [18]. However, the lower band (3.1-5 GHz) and the upper band (6-10.6 GHz) cannot be suppressed satisfactory. In contrast, notch



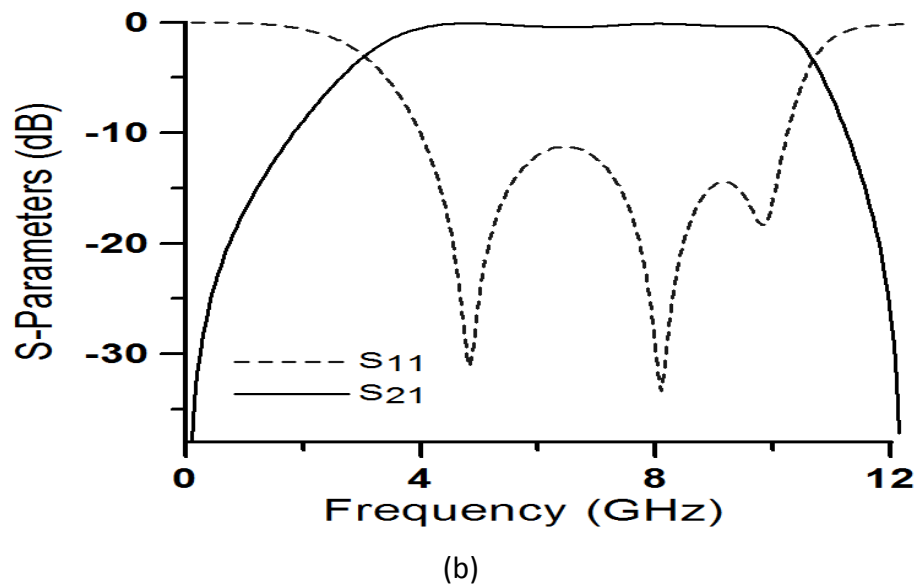


Fig. 3-11 (a) Layout of the proposed UWB filter with reconfigurable notch structure, (b) EM simulated response of the proposed UWB filter without reconfigurable notch structure.

### 3.2.1 Design of External Notch Structure

The proposed notch band can be achieved by simply combining the T-shaped resonator and the design scheme of T-shaped resonator will be discussed step by step. The proposed notch structure is designed with basic structure T-shape stepped impedance resonator as illustrated in Fig 3-12. The structure is comprised of four segments where  $Z_A$ ,  $Z_B$  and  $Z_C$  are the impedances and  $\theta_A$ ,  $\theta_B$  and  $\theta_C$  are corresponding to their electrical lengths, respectively.

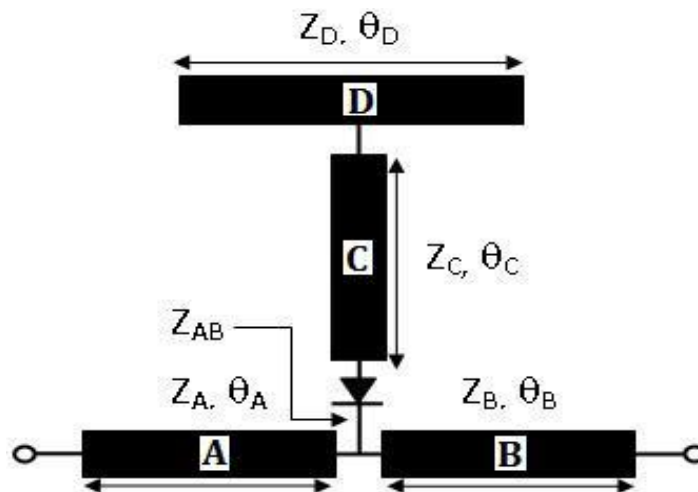


Fig. 3-12 Layout of the switchable notch structure

The input impedance of each transmission line can be analysed by the basic transmission line equation,

$$\frac{Z_{in}}{Z_0} = \frac{Z_L + jZ_0 \tan \beta l}{Z_0 + jZ_L \tan \beta l} \quad (3.17)$$

where  $\beta l = \theta$  and  $Z_{in}$ ,  $Z_L$ ,  $Z_0$  are the input impedance, load impedance and characteristic impedance.

As sections A and B are terminated by open circuit,  $Z_L = \infty$ , this leads to,

$$Z_A = -jZ_A \cot \theta_A \quad (3.18)$$

$$Z_B = -jZ_B \cot \theta_B$$

$Z_{AB}$  is a combination of two sections  $Z_A$  and  $Z_B$ , hence

$$Z_{AB} = -j \frac{Z_A Z_B \cot \theta_A \cot \theta_B}{Z_A \cot \theta_A + Z_B \cot \theta_B} \quad (3.19)$$

From the equation (3.18) and (3.19), it can be found that the effect of transmission line A and B are capacitive. The impedance looking into transmission line section C is given by,

$$\frac{Z_C}{Z_{0c}} = \frac{Z_{AB} Z_{0c} (1 + \tan^2 \theta_C)}{Z_{0c}^2 + Z_{AB}^2 \tan^2 \theta_C} + \frac{j(Z_{0c}^2 - Z_{AB}^2) \tan \theta_C}{Z_{0c}^2 + Z_{AB}^2 \tan^2 \theta_C} \quad (3.20)$$

where  $Z_{0c}$  is the line impedance of section C. In the final part, section D consists of a coupled line and can be modeled like [17] as a capacitive  $\pi$ -network which couples via the gap between the transmission line and the resonant elements:

$$Z_D = \frac{1/Z_C + j\omega(C_{11} + C_{12})}{j\omega C_{12}(1/Z_C + j\omega C_{22}) + j\omega C_{11}[1/Z_C + j\omega(C_{11} + C_{12})]} \quad (3.21)$$

where  $C_{11}$ ,  $C_{22}$  represent the capacitor to ground and  $C_{12}$  is the capacitance between the two lines without any ground plane.

In the expression for calculating S-parameters from ABCD matrix all line impedances are normalised by characteristic impedance of the network  $Z_0$ .

The ABCD matrix for T-network which consists of section A, B and C is equals:

$$\begin{bmatrix} A_1 & B_1 \\ C_1 & D_1 \end{bmatrix} = \begin{bmatrix} 1 + \frac{Z_A}{Z_B} & Z_A + Z_B \frac{Z_A Z_B}{Z_C} \\ \frac{1}{Z_C} & 1 + \frac{Z_B}{Z_C} \end{bmatrix} \quad (3.22)$$

where  $Z_A$ ,  $Z_B$ , and  $Z_C$  are impedances as it is shown in the Figure 3-14.

For transmission line of section D's ABCD matrix is equal:

$$\begin{bmatrix} A_2 & B_2 \\ C_2 & D_2 \end{bmatrix} = \begin{bmatrix} \cos \theta_D & jZ_0 \sin \theta_D \\ j \frac{\sin \theta_D}{Z_D} & \cos \theta_D \end{bmatrix} \quad (3.23)$$

The overall ABCD matrix of two networks is equal:

$$\begin{bmatrix} A & B \\ C & D \end{bmatrix} = \begin{bmatrix} A_1 & B_1 \\ C_1 & D_1 \end{bmatrix} \cdot \begin{bmatrix} A_2 & B_2 \\ C_2 & D_2 \end{bmatrix} = \begin{bmatrix} A_1 A_2 + B_1 C_2 & A_1 B_2 + B_1 D_2 \\ C_1 A_2 + D_1 C_2 & C_1 B_2 + D_1 D_2 \end{bmatrix} \quad (3.24)$$

Finally, the scattering matrix  $S_{11}$  and  $S_{21}$  can be derived as equation (3.8). The intended notch frequency or transmission zero occurs when  $S_{21} = 0$ .

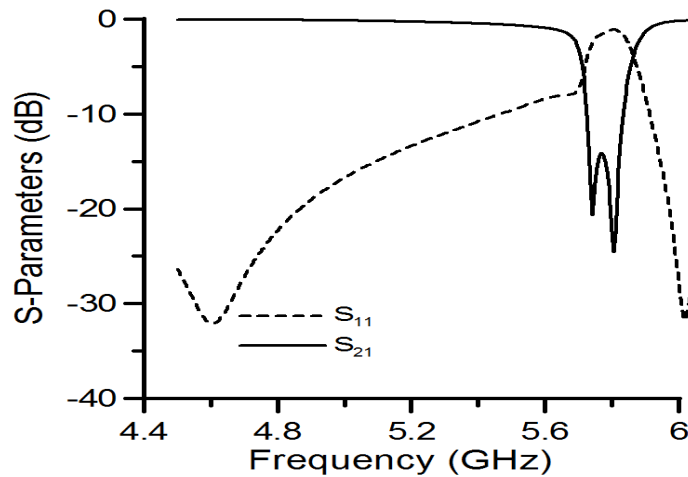


Fig. 3-13 Transmission response of the reconfigurable notch structure.

The PIN diode is placed as shown in Fig 3-12. When the PIN diode is in the forward bias or ON state, the sections A and B generate capacitive effect from equations (3.19) and the proposed section is formed a series LC resonator, which presents a short circuit at the main transmission line and creates a transmission zero at 5.8 GHz within the UWB passband as shown in Fig 3-14(a). On the other hand, in reverse bias or OFF state, there is no connection between sections A,B and section C, which turns the section C ineffective by cutting the length less than  $\lambda_g/4$ , provides an all pass response as shown in Fig 3-14(c).

To validate the circuit concept, the filter is designed and fabricated on Taconic RF-35 substrate with  $\epsilon_r = 3.5$  and  $h = 0.76$  mm and tested with a single PIN diode (BAP65-02) for switching the notch in the passband. In our experiment, The PIN diode was modelled by using a capacitor of value 0.8 pF in the OFF state and a resistor value of 0.9  $\Omega$  in the ON state. The full wave simulated S-parameters of the filter in ON/OFF states together with the corresponding measurements, taken with Agilent vector network analyzer E38361A, are shown in as shown in Fig 3-14(b).

The measured passband insertion-loss of the bandpass filter is < 1.3 dB. The notch rejection at 5.8 GHz in the ON state was observed at approximately 15 dB with fractional bandwidth 5.3%. The small discrepancies between the simulated and measured responses may be attributed to the various fabrication errors involved.

In addition, the existence of sections A and B induce further tuning features by varying the length of both sections A and B the notched band can be easily set at the desired frequency. Also, notched band bandwidth can be varied (over 26%) with the change of section C width. This feature provides extra degree of freedom in the design as shown in Fig. 3-15. Also, the filter group delay is presented in Fig. 3-16.

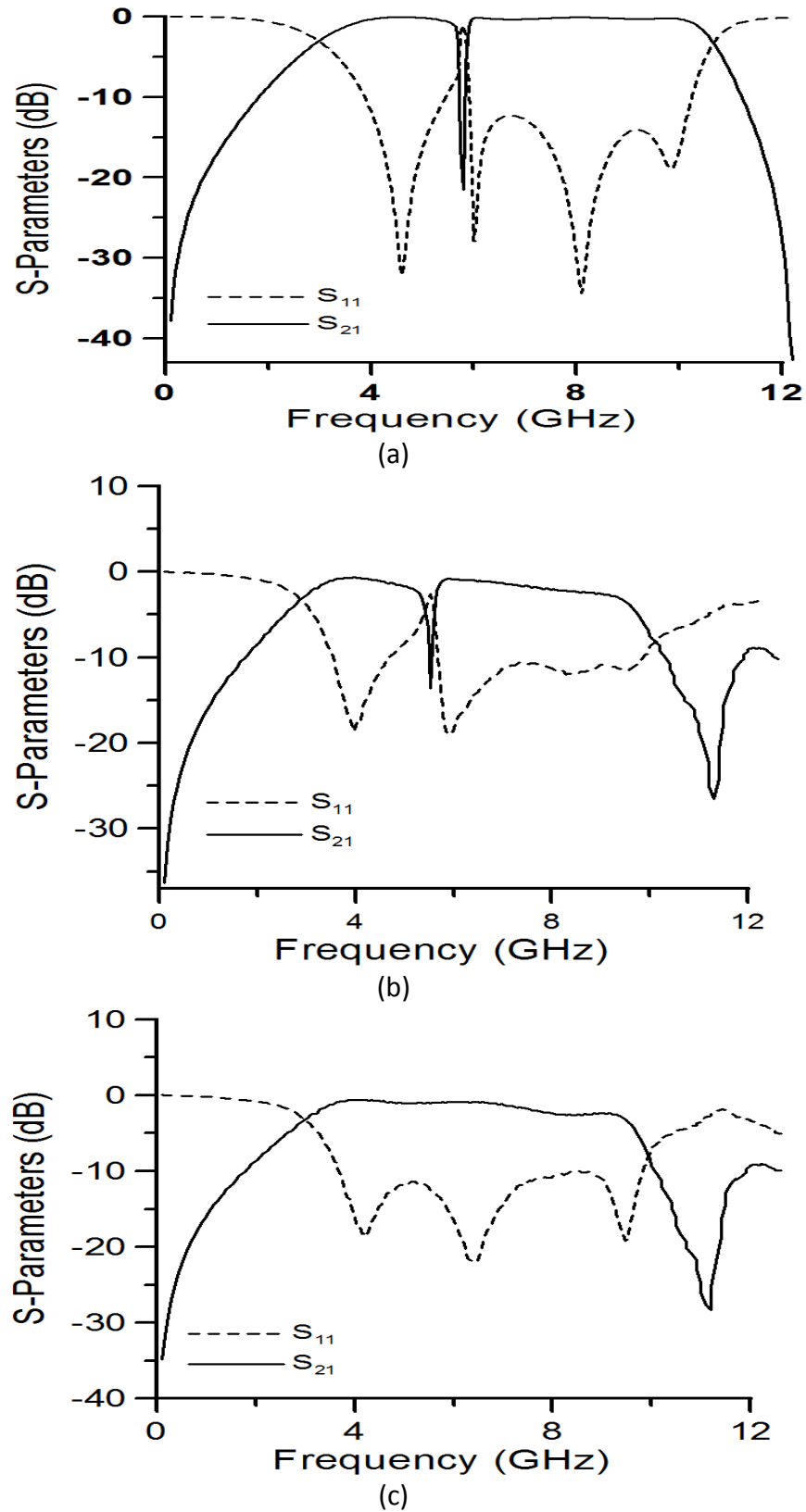
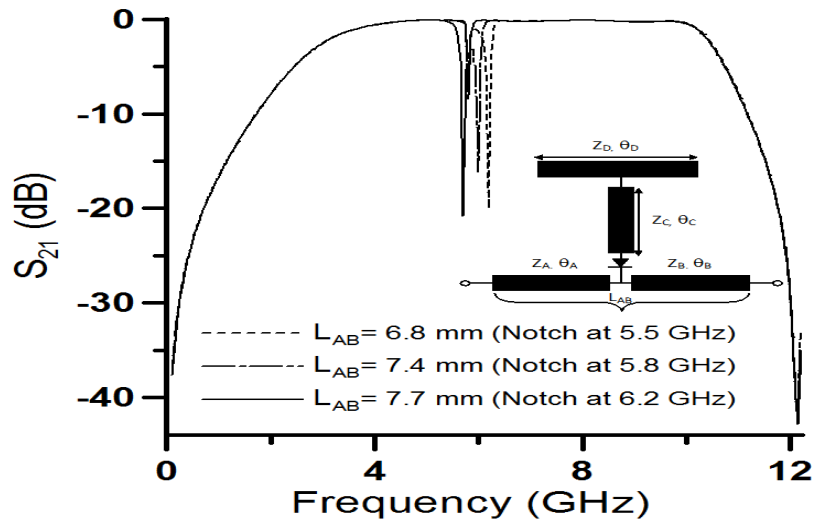
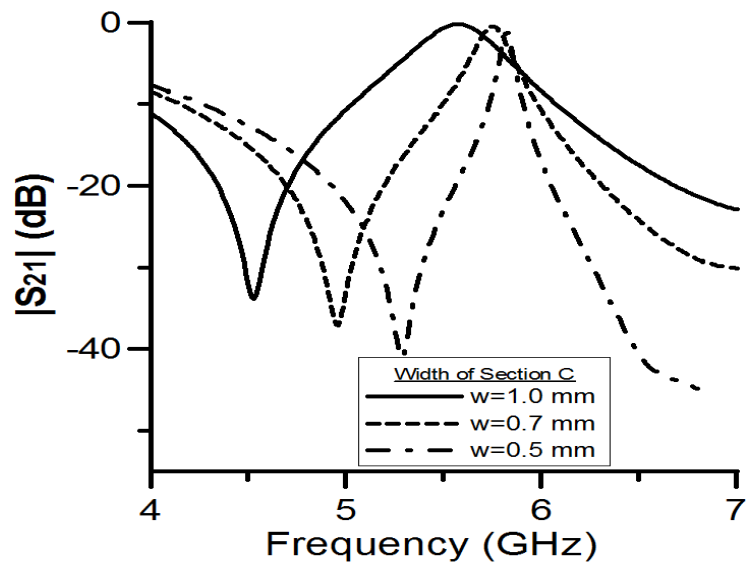


Fig. 3-14 (a) Simulated  $s$ -parameter response of filter in the ON states (b) Measured  $s$ -parameter response of the fabricated filter in the ON states, (c) Measured  $s$ -parameter response of the fabricated filter in the OFF states.



(a)



(b)

Fig 3-15 Simulated S-parameter responses [insertion loss ( $S_{21}$ )] of the proposed notch frequency with varying (a) length ( $L_{AB}$ ) of section A, B and (b) width of section C.

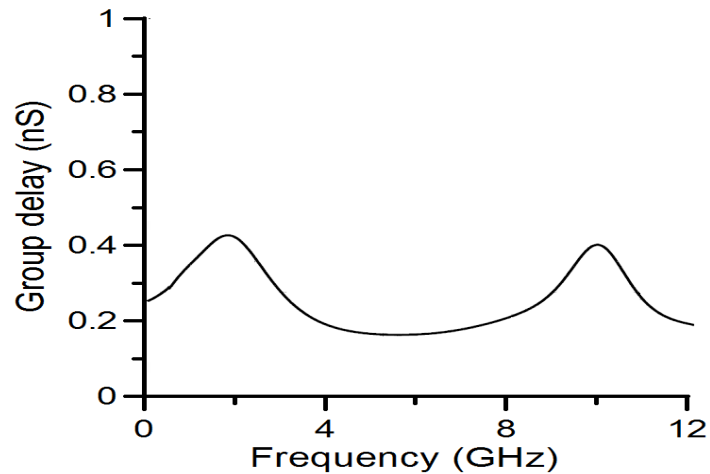


Fig 3-16 Measured Group delay response using PIN diode OFF

### 3.2.2 Summary

A compact reconfigurable UWB bandpass filter with external coupled T-shaped resonator has been presented. The desired notched band is introduced by a predesigned external coupled structure, which produces sharp rejection at the desired band. Also, the notch frequency can be controlled by the proper selection of the parameters of T-shape structure. Furthermore, it was shown that a switching element may be inserted within the notch structure in order to allow the notch band to be made reconfigurable. Design procedure is supplemented with simulated and experimental results to show the performance and highlight the compactness achieved with these configurations especially in comparison to other research work.

In this experiment, the proposed reconfigurable filter using a PIN diode has shown good agreement with simulations. A PIN diode is used instead of other switching elements to achieve compactness, high switching speed and easier fabrication. The obtained results indicate that the proposed reconfigurable filter is suitable to be applied in the modern UWB systems.

## **3.3 References**

[3-1] G. L. Matthaei, "Interdigital bandpass filters," IEEE Transactions on Microwave Theory and Techniques, vol. MTT-10, no. 7, pp. 479–491, Jul. 1962.

[3-2] J. S.Wong, "Microstrip tapped-line filter design," IEEE Transactions on Microwave Theory and Techniques, vol. MTT-27, no. 1, pp. 44–50, Jan. 1979.

[3-3] D. G. Swanson, "Narrow-band microwave filter design," IEEE Microwave Magazine, pp. 107–114, Oct. 2007.

- [3-4] E. G. Cristal, "Tapped-line coupled transmission lines with application to interdigital and combline filters," *IEEE Transactions on Microwave Theory and Techniques*, vol. 23, no. 12, pp. 1007–1012, Dec. 1975.
- [3-5] M.F. Karim, Y.X. Guo, Z.N. Chan and L.C. Ong, "Miniaturized reconfigurable and switchable filter from UWB to 2.4 GHz WLAN using PIN diodes", *IEEE MTT-S*, pp. 509-512, Jun. 2009.
- [3-6] Y.H. Chun, H. Shamman, J.S. Hong, "Switchable embedded notch structure for UWB bandpass filter", *IEEE Microwave and Wireless Component Letters*, vol. 18, no. 9, pp. 590 – 592, Sep. 2008.
- [3-7] D. Draskovic and D. Budimir, "Optically controlled negative refractive index transmission lines", *European Conference on Antennas and Propagation*, pp. 1672-1674, Mar. 2009.
- [3-8] Alexander Miller, J.S. Hong, "Wideband Bandpass Filter With Reconfigurable Bandwidth", *IEEE Microwave and Wireless Component Letters*, Vol. 20, No. 1, pp. 28-30, Jan. 2010.
- [3-9] G. Zouganelis and D. Budimir, "Silicon gap-loaded microstrip slit-tetragonal resonator under IR-radiation", *Microwave and Optical Technology Letters*, vol. 49, pp. 699-702, Mar. 2007
- [3-10] D. Draskovic and D. Budimir, "Optically reconfigurable dual-band compact branch-line couplers", *European Conference on Antennas and Propagation*, pp. 1-3, Nov. 2007.
- [3-11] C.J. Panagamuwa, A. Chauraya and J.Y.C Vardaxoglu, "Frequency and beam reconfigurable antenna using photoconducting switches", *IEEE Transactions of Antennas and Propagation*, vol. 54, No. 2, pp. 449 -454, Feb. 2006.

- [3-12] M.-Y. Hsieh and S.-M. Wang, "Compact and wideband microstrip bandstop filter," *IEEE Microw. Wireless Compon. Lett.*, vol. 15, no. 7, pp. 472–474, Jul. 2005.
- [3-13] M. K. Mandal, K. Divyabramham, and S. Sanyal, "Compact, wideband bandstop filters with sharp rejection characteristic," *IEEE Microw. Wireless Compon. Lett.*, vol. 18, no. 10, pp. 665–667, Oct. 2008.
- [3-14] M. K. Mandal and P. Mondal, "Design of sharp-rejection, compact, wideband bandstop filter," *IET Microw. Antenna. Propag.*, vol. 2, no.4, pp. 389–393, Apr. 2008.
- [3-15] J.-S. Hong and M. J. Lancaster, *Microstrip filters for RF/microwave applications*, New York: John Wiley & Sons, 2001.
- [3-16] [http://www.nxp.com/documents/data\\_sheet/BAP65-02.pdf](http://www.nxp.com/documents/data_sheet/BAP65-02.pdf) (2013)
- [3-17] W. Menzel and P. Feil, "Ultra-wideband (UWB) filter with WLAN notch", *European Conference on Antennas and Propagation*, Munich, Germany, pp.595–598, Sep. 2006.
- [3-18] H. Shaman and J.S. Hong, "Ultra-wideband (UWB) bandpass filter with embedded band notch structures", *IEEE Microwave Wireless Components Letters*, Vol. 17, 193–195, Mar. 2007.
- [3-19] Yang, G.-M., R. Jin, C. Vittoria, V. G. Harris, and N. X. Sun, "Small ultra-wideband (UWB) bandpass filter with notched band," *IEEE Microwave Wireless Components. Letters*, Vol. 18, 176–178, Mar. 2008.
- [3-20] R. Ludwig and P. Bretchko, "RF Circuit design. Theory and application", Prentice Hall, Upper Saddle River, NJ, 2000.

---

## 4.0 HIGHLY SELECTIVE RECONFIGURABLE UWB FILTERS

---

In recent years, there are increasing demands for broader bandwidth, research on UWB devices has greatly accelerated but characterisation, design, and fabrication of UWB filter have been a challenging task compared to narrow-band filters such as high selectivity and low insertion loss over the frequency range is important to minimise distortions of the signal. To achieve better selectivity, much effort has been made by generating transmission zeros, for example, in [1] reported five short-circuited stub for the developments of UWB filter with pairs of transmission zeros but the filter suffered poor out-of-band performance as well as large size. In [2] reported the quintuple-mode UWB bandpass filter with sharp roll-off and super-wide upper stopband. Although the aperture-backed structure can raise the coupling degree of the I/O lines, the fabrication procedure would become complexity. On inspection, it is clear that designing miniaturized high selectivity UWB bandpass filters with attenuation at lower and upper is found a great hurdle to filter designer and most of the UWB bandpass filter designs basically cover the entire passband range but very few address the techniques to mitigate interference with other wireless systems.

Moreover, bandpass filters utilising distributed elements suffer from spurious passbands due to the periodicity of the distributed elements. Because of having the presence of spurious bands, such bandpass filters fail to enclose the entire signal within the assigned spectrum and therefore they are not appropriate for certain applications. Hence, Several techniques have been proposed to restrict spurious passband. For example, step-impedance resonators are used to shift the second harmonic passband to higher frequency [3] and changes of the input and output tapping could have extra transmission zeros in the stopband [4]. Furthermore, the EBG/DGS-based filter structure has over 20 dB restriction at the second harmonic [5]-[6]. The shunt quarter wavelength stubs were introduced to produce

transmission zeros at the stopband [7]. Another method to restrict harmonics is to using asymmetric parallel-coupled units [8]. However, these methods are still accompanied by complicated design or process limitation. Additionally, some of them would also affect the insertion loss in the passband and increase the overall circuit size. Also, in modern wireless communication systems, a single filter cannot executes the requisites for all operating bands and use of multiple filters consume a large space as well as incur extra cost. Hence, reconfigurable and switchable filter constitute a lucrative solution to resolve this problem. Recent research into UWB BPFs with notched band and Bandpass to Bandstop state have been quoted in [3]-[5]. But to date, filter with compact in size, highly selective, reconfigurable feature associates with a switchable notched band option at the same time have not been reported.

To base on the aforementioned studies in the previous and current section, the issues can be summarised as:

- ❖ Proposed filters experience low selectivity and poor out of band rejection level; In addition, most designs are based on complex geometry, causes difficulties in fabrication and circuit board mounting.
- ❖ Mostly provide single function whereas multiple functions are demanding in the future wireless systems. Also, the filter can offer additional features when using more than one switch. However, the switches will add complexity to the systems as the biasing will be more complicated. Hence, reconfigurable filters with less switches is desirable.
- ❖ The number of services increases with the increase in size. The challenges is not only to reduce the circuit size but also to make the filter capable of operating in various wireless applications.

To address all these drawbacks, in section 4.1 discusses the design theories of the proposed filter structure with wide out of band suppression technique. The equivalent circuit model parameters can be obtained by using the derived equations.

Then, in section 4.2 reveals a novel miniaturized, highly selective stub resonator based UWB bandpass filter with dual functional capabilities such as at one setting the filter performs

reconfigurable feature from a bandpass to a bandstop state within the same spectrum and at the another setting it behaves bandpass filter with a switchable notched band for UWB applications.

Later, a new L-shape notched structure is proposed, which can be reconfigured using PIN diode and Optical switch. The suggested notch topology is achieved significant size reduction (25%) and required a lesser switching conductivity in compare with T-shape structure in section 3.2, which is compatible with Optical switch. Finally, the proposed L-shape structure is extended further in section 4.3 and it has been shown that this resonator can be used for obtaining multi-notched characteristics without enlarging circuit size, which is suitable for UWB applications because of having other multiple wireless services (e.g. WLAN, WiMAX, WiFi) within the specified bandwidth.

## 4.1 Analysis of the Proposed Filter Resonator

The proposed stub based resonator in its most simple form, consists of a single  $\lambda_g/2$  resonator, which is placed initially between a pair of  $\lambda_g/4$  short circuited resonators. To sharpen the out-of-band rejection skirt, the shunt short-circuited stubs are stretched by two times, i.e., from  $\lambda_g/4$  to  $2\lambda_g/4$  which turns the section from short to open-circuited stub and as shown in Fig. 4-1, which contributes two attenuation poles on each side of the passband. To verify the origination of transmission zeros, three states are selected and simulated results are presented in Fig. 4-2. Also, corresponding transmission line model is shown in Fig. 4-3.

For a given filter degree  $n$ , the stub bandpass filter characteristics will then depends on the characteristic admittances of the stub lines denoted by  $Y_{ia}$ ,  $Y_{ib}$  and the characteristic impedance of the connecting line between two shunt stubs.

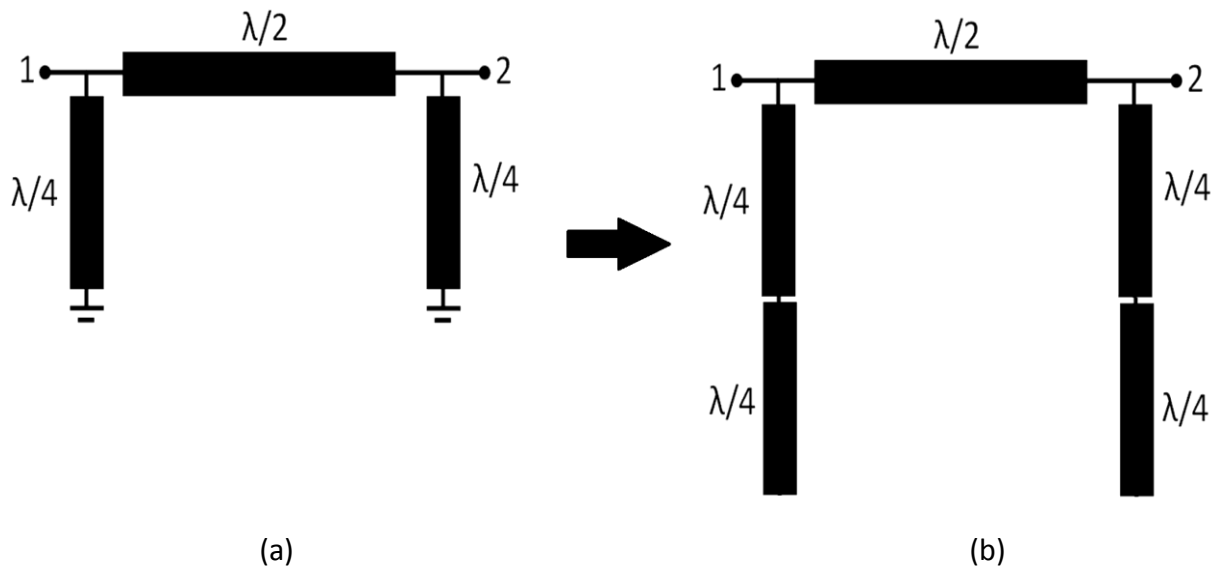
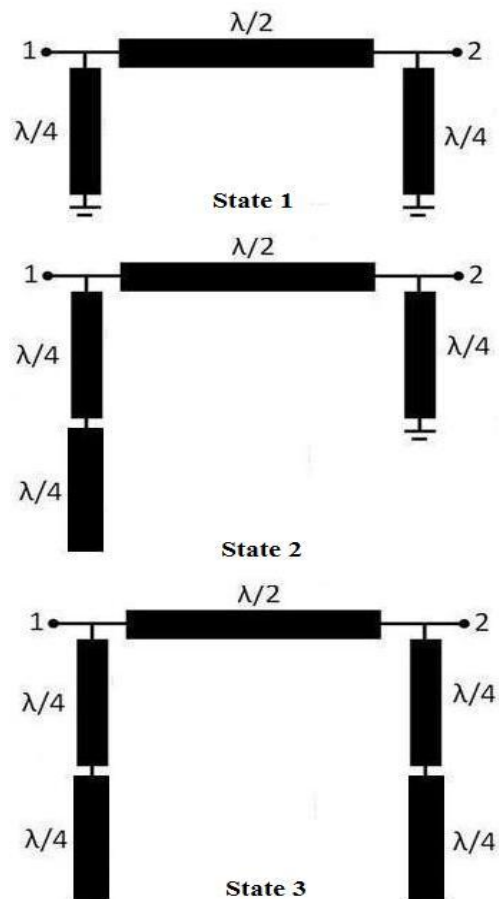


Fig. 4-1 (a) Initial configuration of the UWB bandpass filter with shunt short-circuited stubs, (b) Replacing short-circuited stubs with two sections of open-circuited stubs for generating transmission zeros.



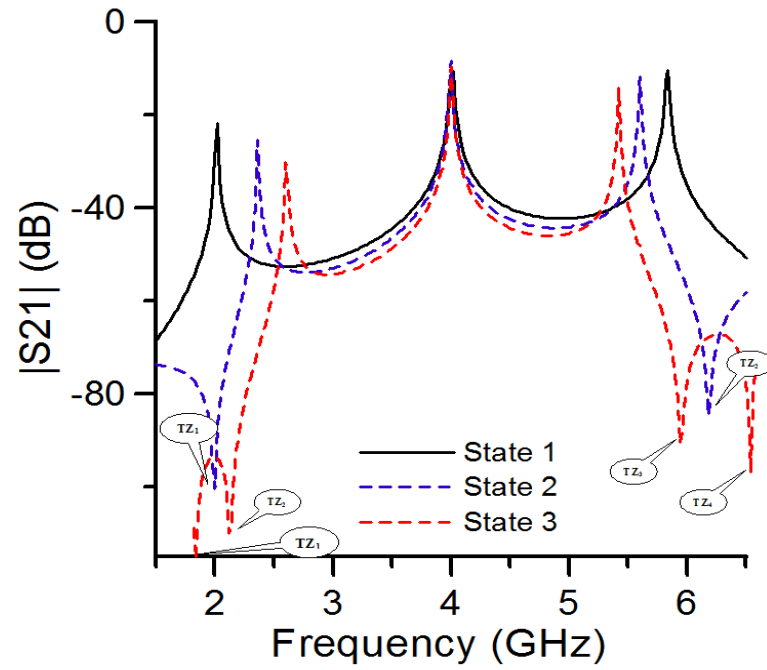


Fig. 4-2 Comparison between conventional and modified BPF.

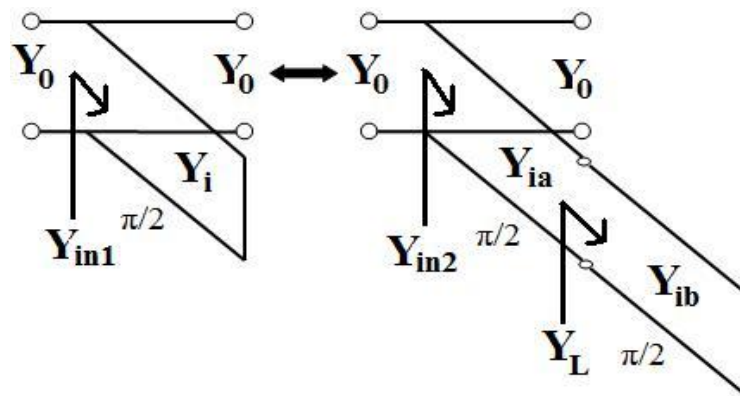


Fig. 4-3 Transmission line model of short to open-circuited stub configuration

$$Y_{in1} = \frac{Y_i}{j \tan \theta} \quad (4.1)$$

$$Y_{in2} = Y_{ia} \frac{Y_L + jY_a \tan \theta}{Y_{ia} + jY_L \tan \theta}$$

where  $Y_L = jY_{ib} \tan \theta$

$$Y_{in2} = Y_{ia} \frac{jY_{ib} \tan \theta + jY_{ia} \tan \theta}{Y_{ia} - Y_{ib} \tan^2 \theta} \quad (4.2)$$

Equivalence of the two input admittance  $Y_{in1}$  and  $Y_{in2}$  in Fig. 4-3 can be expressed by the below equation with an assumption  $Y_{ia} = \alpha_i Y_{ib}$ ,

$$Y_{in1} = Y_{in2} = \frac{Y_i}{j \tan \theta} = Y_{ia} \frac{jY_{ib} \tan \theta + jY_{ia} \tan \theta}{Y_{ia} - Y_{ib} \tan^2 \theta}$$

$$\frac{Y_i}{j \tan \theta} = Y_{ia} \frac{j\alpha_i Y_{ia} \tan \theta + jY_{ia} \tan \theta}{Y_{ia} - \alpha_i Y_{ia} \tan^2 \theta}$$

$$\frac{Y_i}{j \tan \theta} = Y_{ia} \frac{j(\alpha_i + 1) jY_{ia} \tan \theta}{1 - \alpha_i \tan^2 \theta}$$

$$Y_{ia} = \frac{Y_i(\alpha_i \tan^2 \theta - 1)}{1 - \alpha_i \tan^2 \theta} \quad (4.3)$$

where the parameter  $\alpha_i$  is given by,

$$\alpha_i = \cot^2 \left( \frac{\pi f_{zi}}{2 f_0} \right) \quad \text{for } f_{zi} < f_1 \quad (4.4)$$

where  $f_1$  is the low band-edge frequency of the passband,  $f_0$  is the centre frequency and  $f_{zi}$  is a frequency at which the shunt open-circuited stub presents a short circuit to the main transmission line and causes a transmission zero.

In order to verify the design equation, a sample filter can be designed with the given design equations. Using the equations (4.1)-(4.3) yields the characteristics admittance and length of

the open-circuited stubs and (4.5) yields the characteristics impedance and length of the connecting line.

$$Z_{in} = \frac{2\omega_0 L}{\pi} \quad \text{when} \quad \theta = \frac{\lambda_g}{2} \quad (4.5)$$

Furthermore, the proposed filter schematic and the equivalent circuit is presented in Fig. 4-4 and the corresponding circuit model response is shown in Fig. 4-5. The lumped element values in Fig. 4-4(b) are determined by using equations from (3.7);

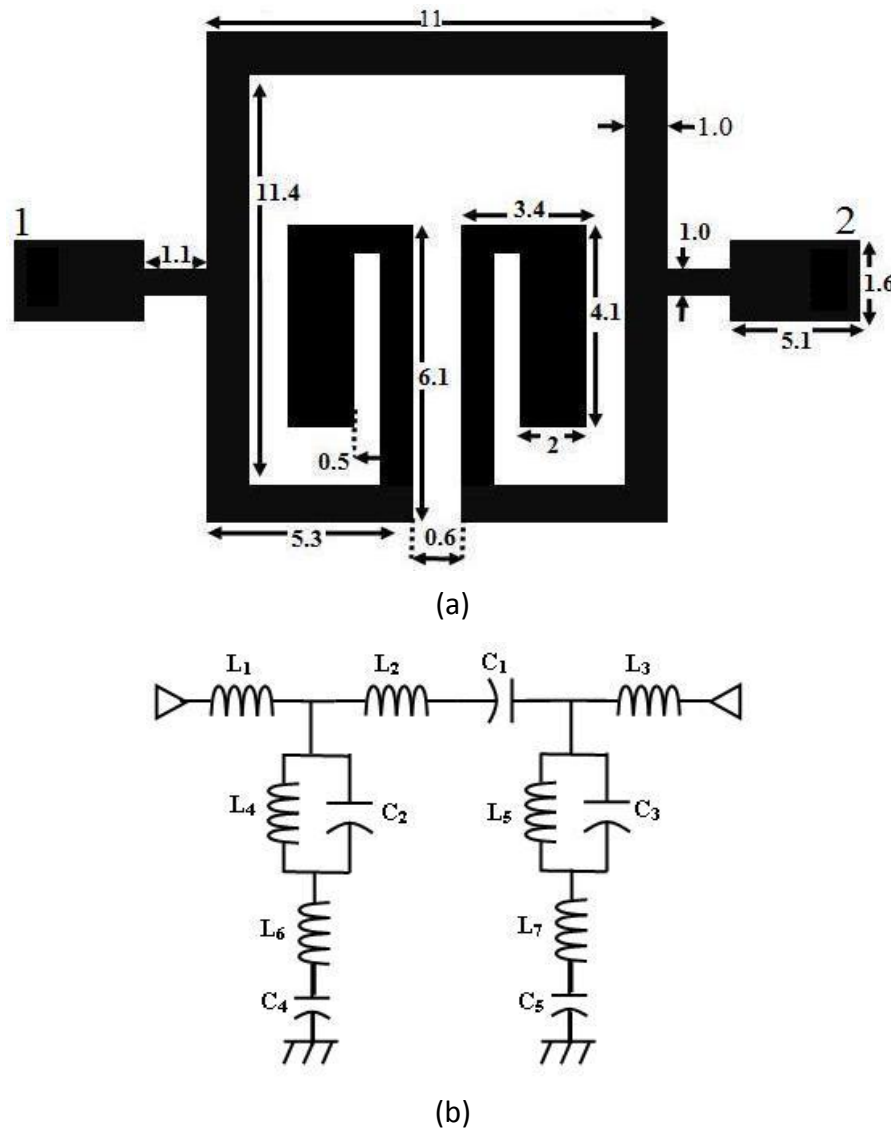


Fig. 4-4 (a) Schematic layout (dimensions in mm) and (b) Equivalent circuit ( $L_1= L_3=0.2$  nH,  $L_2=5.6$  nH,  $L_4= L_5=0.403$  nH,  $L_6=0.524$  nH,  $L_7=0.202$  nH,  $C_1=0.322$  pF,  $C_2= C_3=4.5$  pF,  $C_4=8.4$  pF,  $C_5=6.0$  pF) of the proposed UWB bandpass filter.

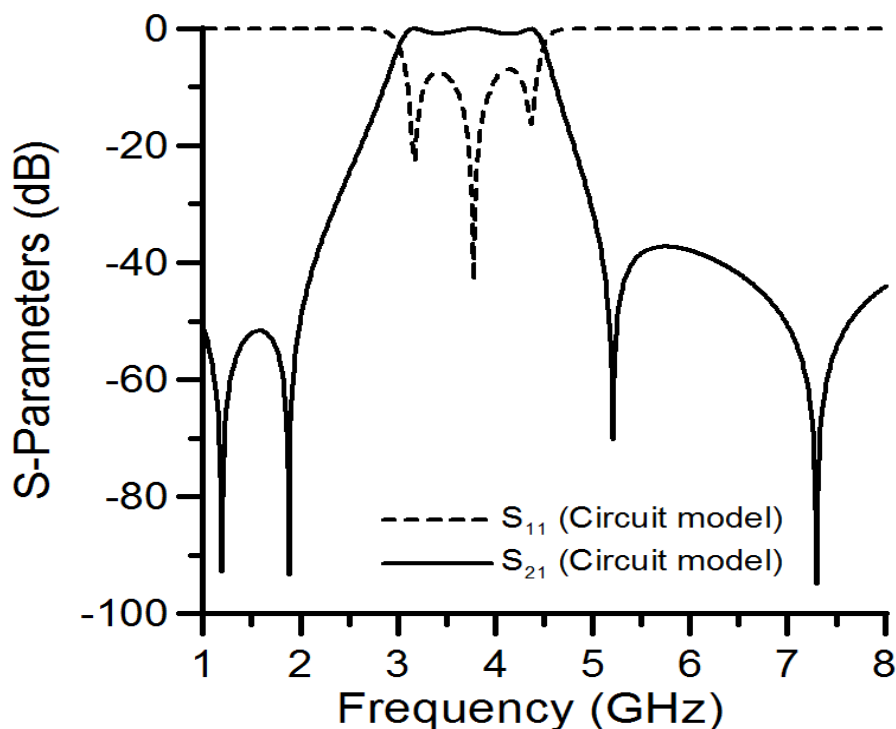


Fig. 4-5 Equivalent circuit model response of the proposed filter.

#### 4.1.1 Filter with Improved Stopband

In this section, a convenient method for wide out of band suppression is proposed without effecting the filter response. A drawback of this type of filter structure will have an additional passband in the vicinity of  $2f_0$ . To restrict the spurious band in the stopband without increase the overall size, this section proposes a shunt open-circuited stubs as shown in Fig. 4-6(a) which are placed in between the outer  $\lambda_g/4$  stubs and the lengths are assigned to be  $45^\circ$  at the fundamental frequency. Therefore, at the second harmonic, the electrical length of the shunt stubs would be  $90^\circ$ , and the stubs behave like a bandstop filter to suppress the second harmonics. The open stub lines has great attenuation in its resonant frequency but has small insertion loss ( $<0.3$  dB) within other frequency band as in Fig. 4-6(b). From the figure it is observed that the characteristic of passband is almost not affected by the substitution while the stopband is greatly optimised.

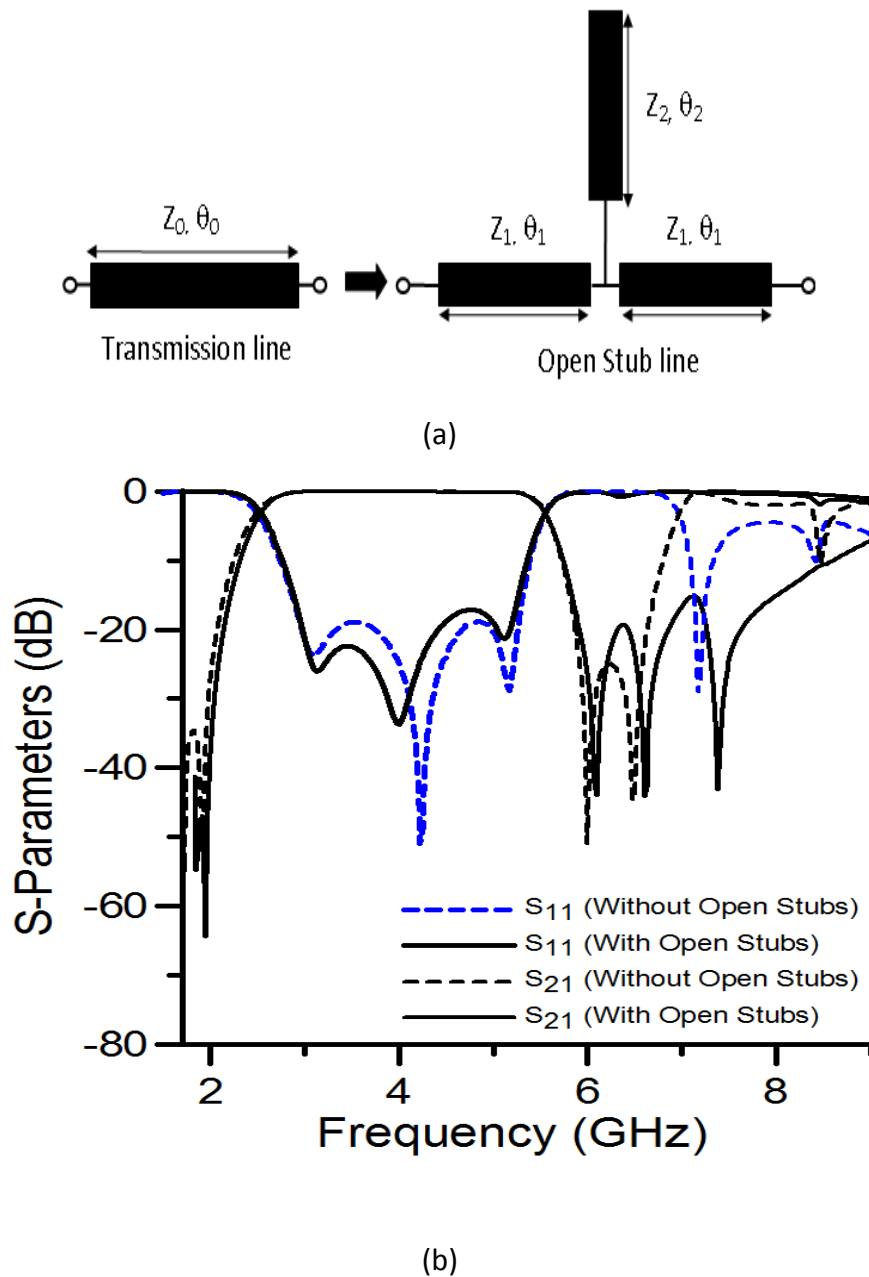


Fig. 4-6 (a) Series transmission line is replaced by open stub T-shaped and (b) Transmission response of conventional and modified filter with T-shaped structure

An equivalent transmission line model for the proposed structure as in Fig. 4-6(a) is analysed to find its design parameter:

Suppose the characteristic impedance of transmission line is  $Z_0$  and its electrical length is  $\theta_0$ . The characteristic impedance of the connected line and the open stub line are respectively  $Z_1$  and  $Z_2$  and their electrical lengths are  $\theta_1$  and  $\theta_2$ .

The ABCD matrix of the normal transmission line is

$$M_0 = \begin{bmatrix} \cos \theta_0 & jZ_0 \sin \theta_0 \\ j \frac{\sin \theta_0}{Z_0} & \cos \theta_0 \end{bmatrix} \quad (4.6)$$

The proposed structure consists of two side connected line and one open stub and their ABCD matrix respectively,

$$M_1 = \begin{bmatrix} \cos \theta_1 & jZ_1 \sin \theta_1 \\ j \frac{\sin \theta_1}{Z_1} & \cos \theta_1 \end{bmatrix} \quad M_2 = \begin{bmatrix} 1 & 0 \\ \frac{j \tan \theta_2}{Z_2} & 1 \end{bmatrix} \quad (4.7)$$

Considering the cascading of these two networks with respect to ignore discontinuity and open end effect, the equivalent ABCD matrix of the proposed structure,

$$M_T = M_1 M_2 M_1 \quad (4.8)$$

If we substitute the open stub line for the series transmission line, the following equation must hold true,

$$M_T = M_0 \quad (4.9)$$

With (4.6)-(4.9),

$$\begin{aligned} Z_1 &= Z_0 \cot \theta_1 \\ Z_2 &= Z_0 \frac{\cos^2 \theta_1}{1 - 2 \sin^2 \theta_1} \end{aligned} \quad (4.10)$$

Equation (4.10) is the design relation between the normal transmission line and the open stub line, when  $\theta_1 = \pi/4$ ,  $Z_1 = Z_0$  and  $Z_2 \rightarrow \infty$ , which is equivalent to open circuit.

## 4.2 Reconfigurable and Switchable Notched Band UWB Filter

This section discusses the following points:

- ❖ Derives an accurate lumped element and the corresponding transmission line model to facilitate the filter design with the proposed stub resonator. The model can be used to accelerate the conversion of a lumped network to a distributed filter.
- ❖ The multiplicity of services generated from one filter so that the filter can serve more than one application. A novel switchable notched band technique through mismatching coupled lines, followed by a reconfigurable frequency states (bandpass to bandstop) without compromising filter performances is introduced.
- ❖ The simplicity of the resonator to reduce the size and fabrication cost.

The proposed filter is a third-order bandpass filter composed of a single  $\lambda_g/2$  resonator ( $\theta_1$ ) shown in Fig 4-7 and a pair of  $\lambda_g/4$  short circuited resonators ( $\theta_2$  and  $\theta_3$ ). The electrical length of the  $\lambda_g/4$  length and the  $\lambda_g/2$  resonators have been calculated at a centre frequency of 4.15 GHz and the corresponding line impedance for both lengths is 68.4  $\Omega$ . The proposed filter layout integrate with notched band and harmonic suppression structure and the equivalent lumped elements model is shown in Fig. 4-8. To sharpen the out-of-band rejection skirt, the shunt short-circuited stubs ( $\theta_2, \theta_3$ ) are stretched by two times, i.e., from  $\lambda_g/4$  to  $2\lambda_g/4$  which turns the section from short to open- circuited stub ( $\theta_2+\theta_4$ ) and ( $\theta_3+\theta_5$ ) which contributes two attenuation poles on each side of the passband as shown in Fig. 4-9. Additionally, two shunt open-circuited stubs ( $\theta_6, \theta_7$ ) are designed to have rejection at the second harmonic of the filter as both lengths ( $\theta_6, \theta_7$ ) are assigned to be  $45^\circ$  at the fundamental frequency and the relevant transmission line response with modified structure is presented in Fig. 4-6(b).

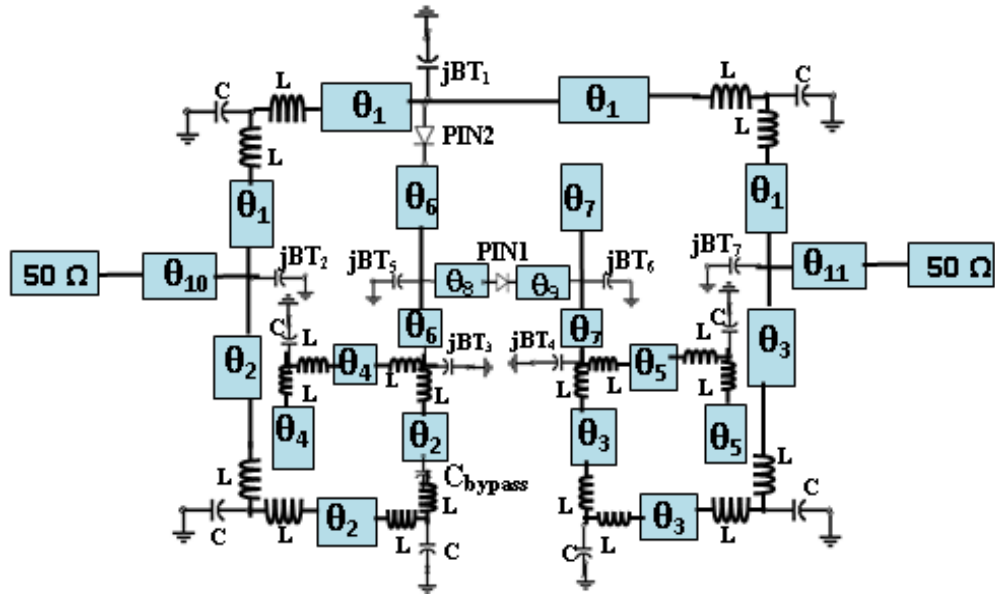
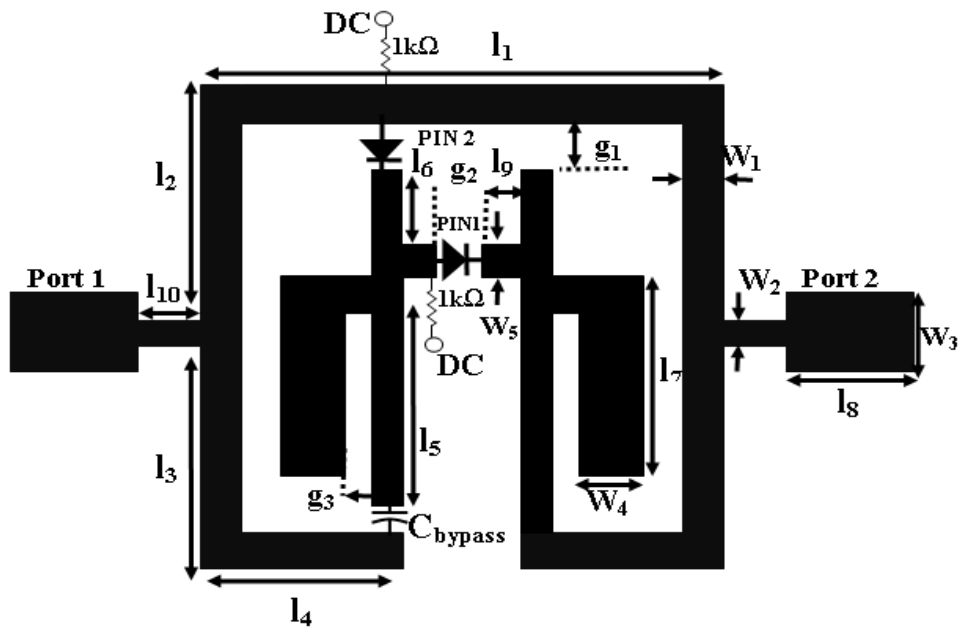
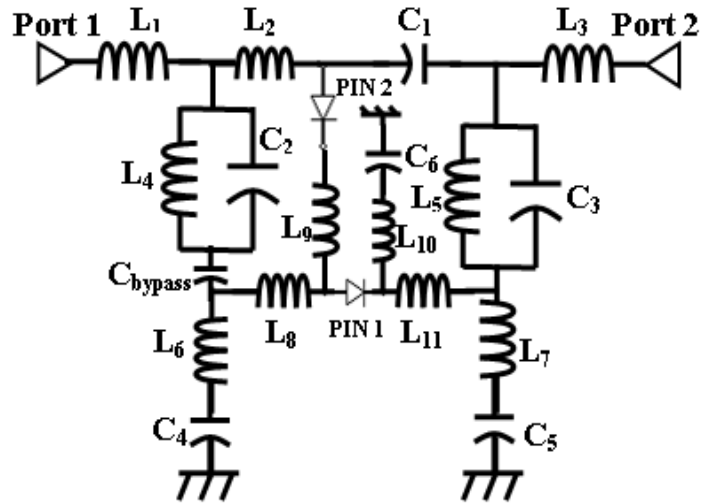


Fig. 4-7 Equivalent transmission line model of the proposed filter where  $\theta_{1-n}$  are the electrical lengths of transmission lines, inductance (L) and capacitance (C) are the parasitic elements (bending circuit), and capacitance  $jBT_{1-n}$  are the T-junction parasitic elements between connecting transmission lines.

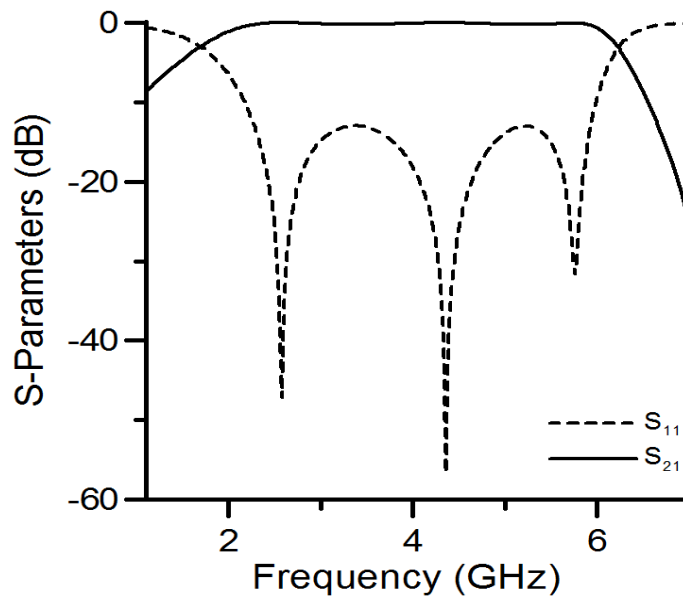


(a)



(b)

Fig. 4-8 Schematic of the proposed reconfigurable UWB bandpass filter ( $l_1=11$ ,  $l_2=4.5$ ,  $l_3=4.5$ ,  $l_4=4.1$ ,  $l_5=6.5$ ,  $l_6=1.5$ ,  $l_7=5.2$ ,  $l_8=5.1$ ,  $l_9=0.9$ ,  $l_{10}=0.9$ ,  $W_1=0.9$ ,  $W_2=1.0$ ,  $W_3=1.6$ ,  $W_4=2.0$ ,  $W_5=1.0$ ,  $g_1=0.5$ ,  $g_2=0.5$ ,  $g_3=0.6$  (dimensions in mm)), (b) Circuit schematic for the filter prototype ( $L_1=L_3=0.2$  nH,  $L_2=5.6$  nH,  $L_4=L_5=0.403$  nH,  $L_6=0.524$  nH,  $L_7=0.202$  nH,  $L_8=0.508$  nH,  $L_9=0.404$  nH,  $L_{10}=0.303$  nH,  $L_{10}=0.508$  nH,  $C_1=0.322$  pF,  $C_2=C_3=4.5$  pF,  $C_4=2.4$  pF,  $C_5=2.0$  pF,  $C_6=2.7$  pF,  $C_{\text{bypass}}=33$  pF).



(a)

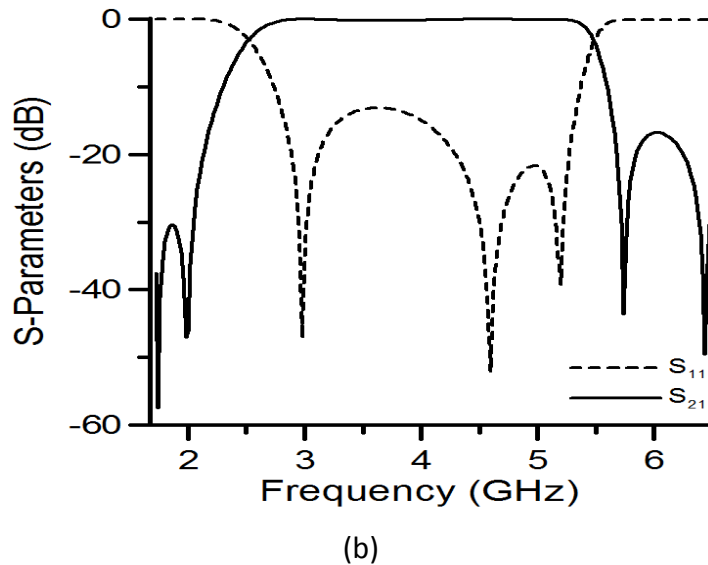


Fig. 4-9 (a) Conventional and (b) Modified Bandpass transmission response.

#### 4.2.1 UWB Filter with a Switchable Notched Band

In this section, a novel switchable notched band technique is introduced, which bypassed the signal traffic without affecting the original BPF characteristics and creates a phase mismatch between two couple lines, therefore, a narrow notch is generated. An analysis of the structure is illustrated to describe comprehensively the operation of the unit. To reject the undesired WiMAX signal (3.4-3.6 GHz, 5.71% FBW) at 3.5 GHz, a section of diode loaded (PIN1) transmission line ( $\theta_8 + \theta_9$ ) is placed between a pair of shunt open-circuited stub ( $\theta_6, \theta_7$ ) as shown in Fig. 4-7. A bypass capacitor  $C_{\text{bypass}}$  in Fig. 4-8 is used to avoid a short circuit for the dc bias applied to the PIN diode. The equivalent circuit of the notch structure is presented in Fig. 4-10.

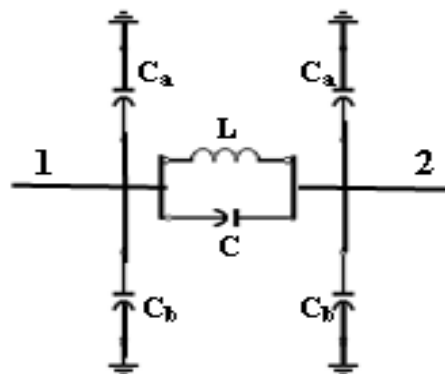


Fig. 4-10 Equivalent circuit of the notch structure

The equivalent element values can be derived from [9],

$$j\omega_0 L = jZ_0 \sin \beta \quad (4.11)$$

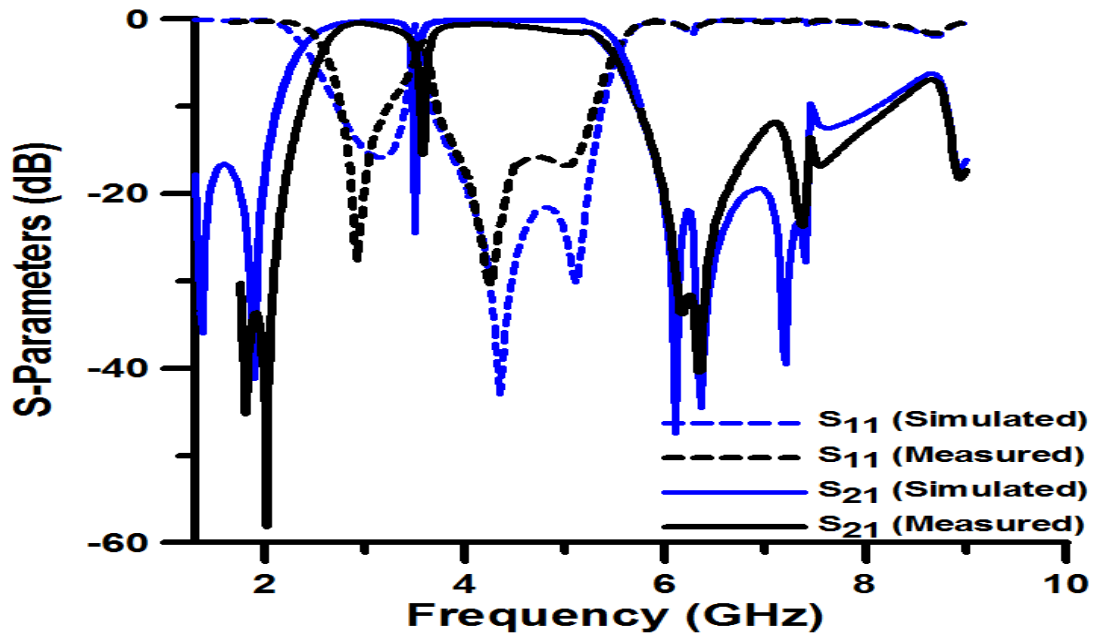
$$j\omega_0 C = j \frac{Y_{0o} - Y_{0e}}{2} \tan \phi \quad (4.12)$$

$$j\omega_0 C_a = jY_0 \tan \frac{\beta}{2} \quad (4.13)$$

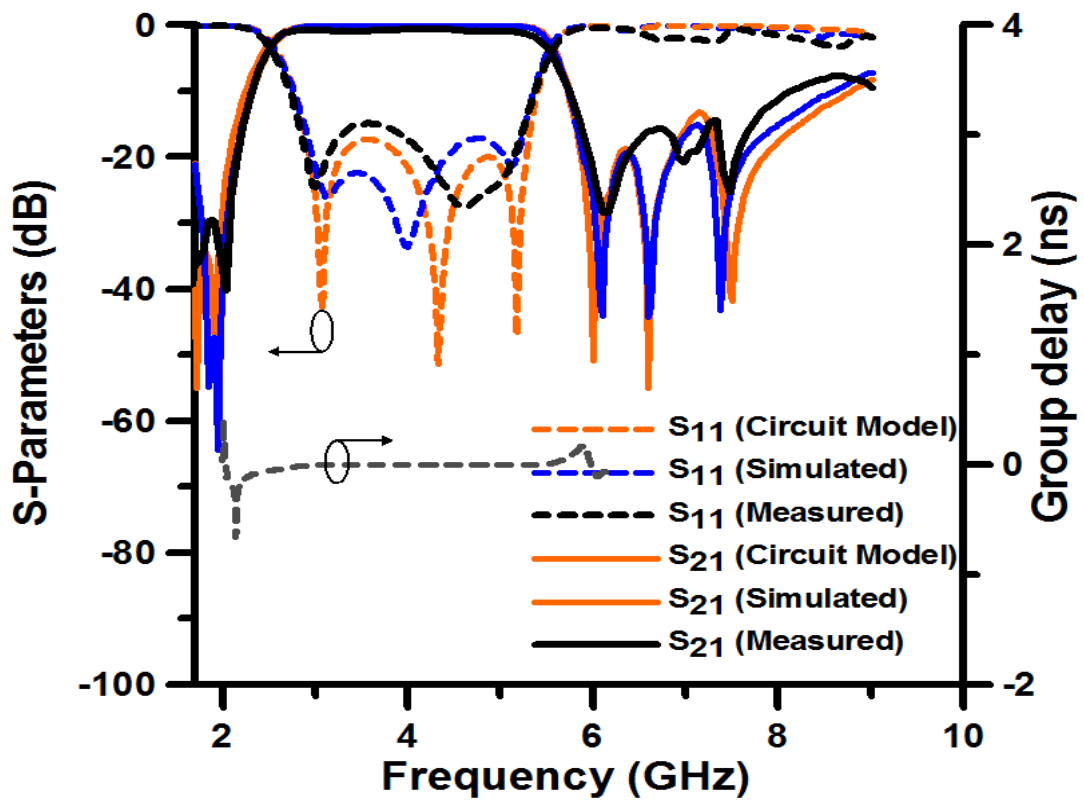
$$j\omega_0 C_b = jY_{0e} \tan \phi \quad (4.14)$$

where  $Z_0$  characteristic impedance of the transmission line,  $Z_{0o}$  &  $Z_{0e}$  even and odd mode impedance of coupled line,  $\beta$  is the propagation constant, and  $\phi$  is electrical length of coupled line.

In the forward bias or on state, the PIN diode behaves like a small resistance so that this section ( $\theta_8 + \theta_9$ ) creates an alternate path ( $\theta_1 + \theta_2 + \theta_3 + \theta_8 + \theta_9$ ) to propagate the main signal. Hence the signal paths along the two coupling lines ( $\theta_2, \theta_4$ ) become out-of-phase and equal magnitude in which transmission signal is cancelled, thus generating a notch band at 3.5 GHz without affecting the original BPF characteristics as illustrated in Fig 4-11(a). Conversely, in the zero bias or off state, the alternate pathway is broken and the filter structure reinstates to its position, provides full passband response as shown in Fig 4-11(b); Also the corresponding coupling coefficient with respect to vary the section ( $\theta_8 + \theta_9$ ) position is demonstrated in Fig. 4-12.



(a)



(b)

Fig. 4-11 Simulated and measured response of the fabricated filter with the pin switch (a) Bandpass filter with a notched band at 3.5 GHz in the PIN1 ON state and PIN2 OFF state, (b) Bandpass filter with full passband in the PIN1 OFF state and PIN2 OFF state.

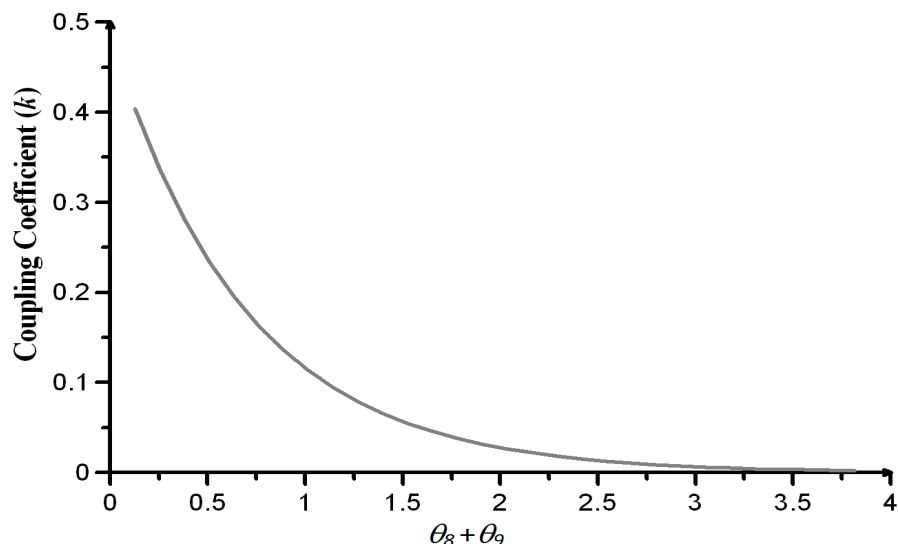


Fig. 4-12 Coupling coefficient ( $k$ ) with respect to vary the section ( $\theta_8 + \theta_9$ ) position

#### 4.2.2 UWB Filter with Reconfigurable Frequency States

To achieve reconfigurability, a single PIN diode (PIN2) is inserted at one end of the first shunt open-circuited stub ( $\theta_6$ ) as shown in Fig. 4-7. With the PIN diode in the forward bias or on state, the open stub joined to the main transmission line. In this case, the lines ( $\theta_1, \theta_2, \theta_6$ ) are connected at their two ends. When a signal is applied at one end of the structure, it is divided into two components. After propagating through these lines, the signals interfere at the other end with different phases and magnitudes due to the lengths and characteristic impedances of the lines. In this state, the structure operates as a bandstop filter as shown in Fig. 4-13 and transmission zero is created because of destructive interference of the signals propagating through the two paths. In contrast, in zero bias or off state, there is no connection between the open stub and the main transmission line so that the section gives a bandpass response as shown in Fig 4-11(b).

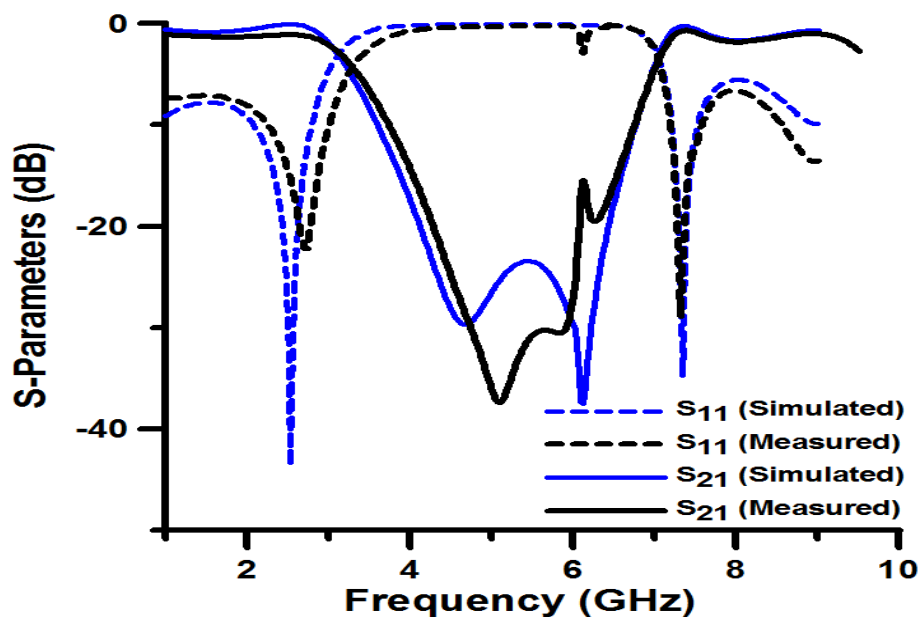


Fig. 4-13 Bandstop filter in the PIN1 OFF state and PIN2 ON state

To validate the circuit concept, the filter is designed and fabricated on Taconic RF35 substrate with  $\epsilon_r = 3.5$  and  $h = 0.76$  mm. The overall filter dimension is approximately  $0.15\lambda_g \times 0.13\lambda_g$  (excluding feed lines), where  $\lambda_g$  is the microstrip guided wavelength on the substrate at centre frequency. The filter is optimised by EM Sonnet software as the EM Sonnet use method of moments (MoM) numerical computational method to solve electromagnetic problem, which is based on reducing the operator equations to a system of linear equation that is written in matrix form. The corresponding measurements are taken with Agilent vector network analyzer E38361A. In order to realise the electronic switching, the S-parameters of the PIN diode are measured first in a  $50\Omega$  line at 3.5 GHz and the lumped element values are then created to match the S-parameters, which is equivalent to  $0.9\Omega$  forward resistance,  $0.6$  nH parasitic inductance in the forward bias case; In contrast, the reverse bias circuit is equivalent to  $0.9$  nH parasitic inductance,  $0.8$  pF capacitance with  $10$  k $\Omega$  parallel resistance. In this experiment, the PIN diode NXP BAP65-02 SOD523 is chosen in order to match with the switching circuit parameters which has typical value of  $0.9\Omega$  resistance,  $0.6$  nH inductance and  $0.8$  pF of capacitance [10]. To turn on the diodes, the external dc voltage is 3V, and the current is 1mA. The dc blocking capacitance is 33 pF and the resistor 1k $\Omega$  is used for biasing. A photograph of the fabricated filter is shown in Fig. 4-14.

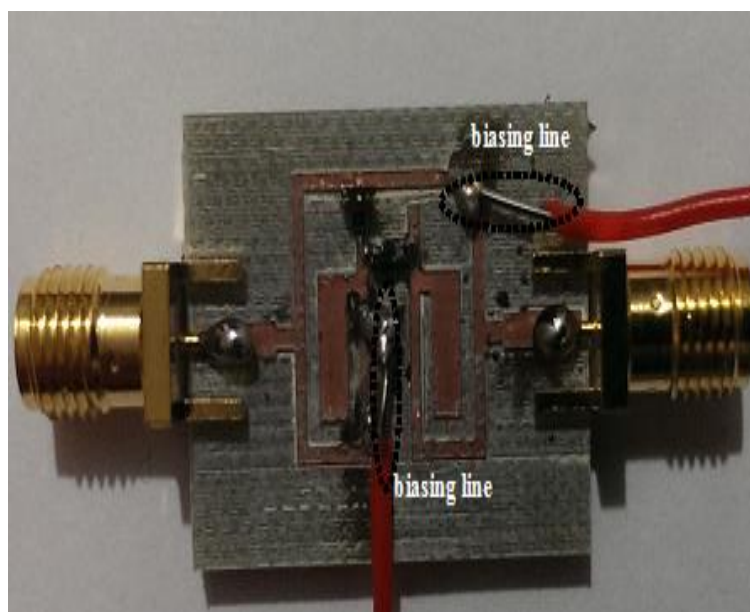


Fig. 4-14 Photograph of the fabricated filter

**Table 1** Comparison of various Reconfigurable BPFs

Ref.	No. of Zeros	Upper passband	Category & Switch	Size reduction
[1]	None	$<2f_0$	Dual-functional & 04	40%
[2]	Two	$<3.5f_0$	Single- functional & 01	15.7%
[3]	One	$>1.6f_0$	Single- functional & 02	57%
[4]	Two	$>2.5f_0$	Single- functional	85%
[5]	One	$<1.7f_0$	Single- functional & 01	89%
This work	Five	$\approx 2f_0$	Dual- functional & 02	

In the switchable notched band case shown in Fig. 4-11(a), the notched band centred at 3.56 GHz has 5-dB rejection fractional bandwidth of about 5.2% and the attenuation at the centre of the notched band is around 16 dB. In contrast, the case for reconfigurable filter, the attenuation in most of the passband has been observed approximately 35 dB in the bandstop state. Also, in Fig. 4-13, the measured passband of the bandpass state centred at 4.15 GHz has 3-dB fractional bandwidth of 2.6 GHz (2.8-5.4 GHz) and measured minimum insertion and return loss of 0.9 & 17 dB. Moreover, the filter performs a flat group delay within the passband of about 0.27-0.38 ns in both cases. The small discrepancies between

the simulated and measured responses may be attributed to the various fabrication tolerances, parasitic of pin diode, and capacitor.

### 4.2.3 Summary

A reconfigurable microstrip filter associates with a novel switchable notched band technique has been presented for the lower UWB band (3.1-5.2 GHz) application. A comprehensive analysis of the proposed filter resonator and the relevant circuit model is shown to verify the calculations. An approach is displayed by which harmonic can be suppressed without effecting filter response and enlarging circuit diameter. Considering the inaccuracies involved in practical realization of the proposed pin based UWB filter, the agreement between simulation and measurement is very good. In addition, this filter has achieved significant size reduction via folding both open-circuited resonators inward avoids enlarging the size problem of the filter structure and also eliminates the need for ground connection with the circuit. The obtained results indicate that the proposed reconfigurable filter is promising for modern UWB systems as well as solving the problem of WiMAX interferences allocated in the UWB spectrum.

### 4.3 Single and Multi-Notched Band Technique

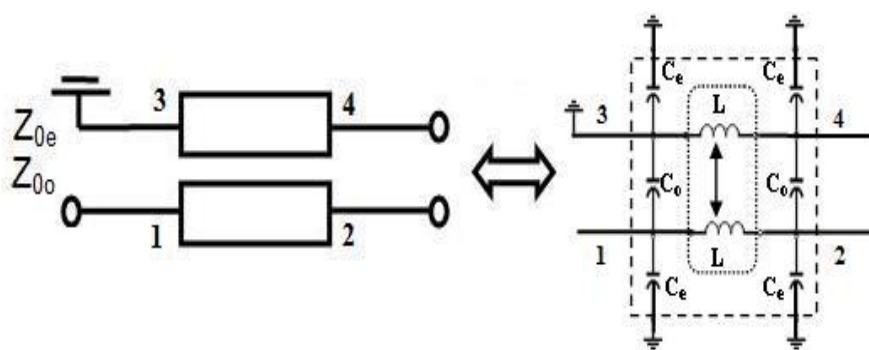
UWB communication spectrum covers a very wide frequency band and is overlapped with WiMAX (3.5 GHz) in the lower band and with WLAN (5.8 GHz) in the upper band. These services potentially interfere with UWB signals and therefore may cause signal distortion. One of the possible and effective solutions for this problem is to realize narrow rejection bands within the passband of a UWB bandpass filter. The reason tends to focus on reconfigurable notch features in order to avoid possibility of interferences on the increasingly crowded spectrum and achieve multi-functionality using a single filter.

To overcome these interferences, this section explores the following features:

- ❖ A rejection band technique utilising capacitively coupled short-circuited L-shape stub to the main filter structure.
- ❖ Independent control of the notched band structure with different switching elements (Optical switch and PIN diode).
- ❖ Multi-notched bands characteristic using L-shape topology without occupying additional circuit space.

#### 4.3.1 Single Switchable Notched Band for UWB Filter

The design of rejection filters in this work is based on the configuration of coupled transmission line bandstop filter. As illustrated in Fig. 4-15, the first order notch filter is attained by loading a pair of coupled transmission lines with a gap in between for switch insertion.



(a)

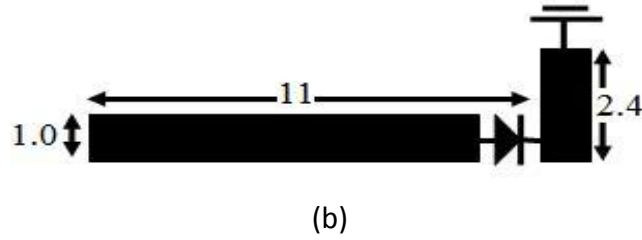


Fig. 4- 15 Notch structure (a) Notch equivalent circuit, (b) Notch layout

If the impedances of coupled line such as the even-mode and odd-mode ( $Z_{0o}$ ,  $Z_{0e}$ ) are matched with port impedance  $Z_0 = 50 \Omega$ , then

$$Z_0 = \sqrt{Z_{0o} Z_{0e}} \quad (4.15)$$

In Fig. 4-15, port 3 is grounded and port 4 is terminated by load  $Z_L$ . With these terminations on ports 3 and 4, the coupled line become a two-port with S-parameters

$$S_{11} = -\frac{\beta^2}{1 + \alpha^2 \Gamma_{L4}} \quad (4.16)$$

$$S_{21} = \alpha \left( 1 - \frac{\beta^2 \Gamma_{L4}}{1 + \alpha^2 \Gamma_{L4}} \right) \quad (4.17)$$

where  $\alpha = \sqrt{1 - C^2} / \sqrt{1 - C^2} \cos \theta + j \sin \theta$

$$\beta = jC \tan \theta / \sqrt{1 - C^2} + j \tan \theta \quad (4.18)$$

$$\Gamma_{L4} = \frac{Z_L - Z_0}{Z_L + Z_0}$$

Coupling coefficient C in is defined as,

$$C = (Z_{0e} - Z_{0o}) / (Z_{0e} + Z_{0o}) \quad (4.19)$$

The resonant frequency is given by,

$$f_r = \frac{1}{2\pi\sqrt{L(C_e + C_o)}} \quad (4.20)$$

To reject the undesired WiMAX signal at 3.5 GHz, a section of L-shaped parallel coupled transmission line with a grounded end is added as illustrated in Fig 4-15 (b). The electrical length of the stub is chosen  $90^\circ$  at 3.5 GHz in order to create a transmission zero at this frequency as coupled lines coupling maximize at  $\beta l = \lambda_g/4$ . The switch is placed as shown in Fig 4-15 (b). When the switch (either pin diode or optical switch) is in the on state, the joined section length is equivalent to  $\lambda_g/4$  and it reaches at maximum coupling stage which contributes a narrow reject band within the filter passband at 3.5 GHz as in Fig. 4-16(a). Conversely, in the off state presents in Fig. 4-16(b), there is no connection between the open-stub and the L-shaped section provides full passband response due to low coupling between two coupled lines.

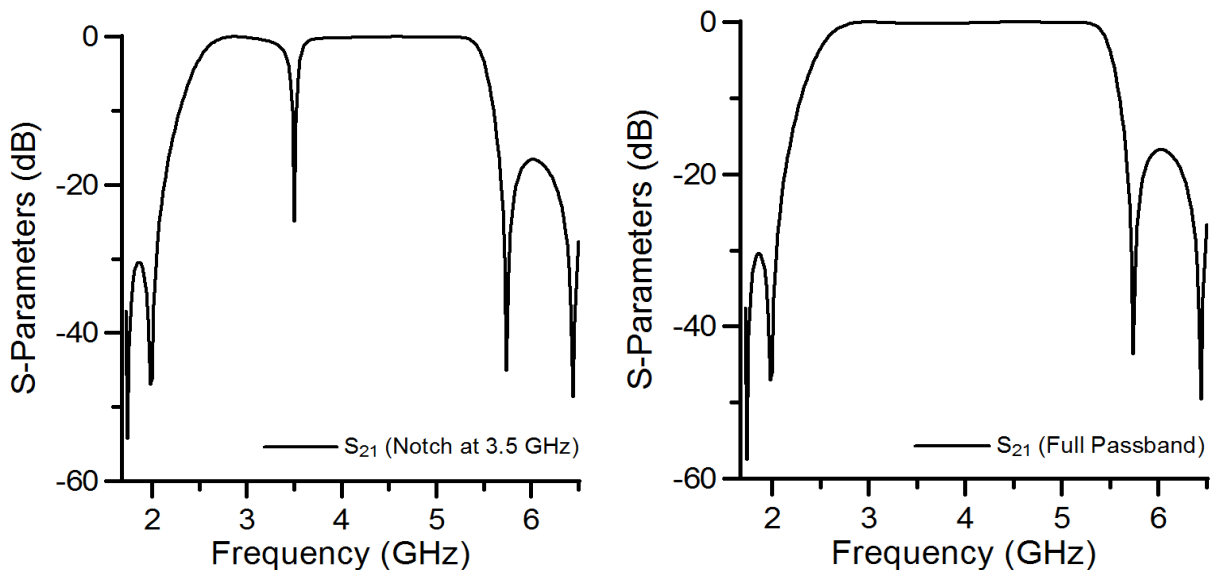


Fig. 4-16 Simulated response of the reconfigurable notch structure (a) With switch ON (b) With switch OFF.

The 0.3 mm gap is overlaid with a PIN diode switch (BAP65-02) as shown above in Fig. 4-15 (b) in one filter circuit and the other is overlaid with a 1 x 3 mm silicon dice. The PIN diode was modelled by using a capacitor of value 0.8 pF in the OFF state and a resistor value of 0.9  $\Omega$  in the ON state. The silicon wafer has a conductivity of 16.7 mS/m in the dark which increases to 150 S/m when illuminated by 200mW of 980 nm wavelength laser light.

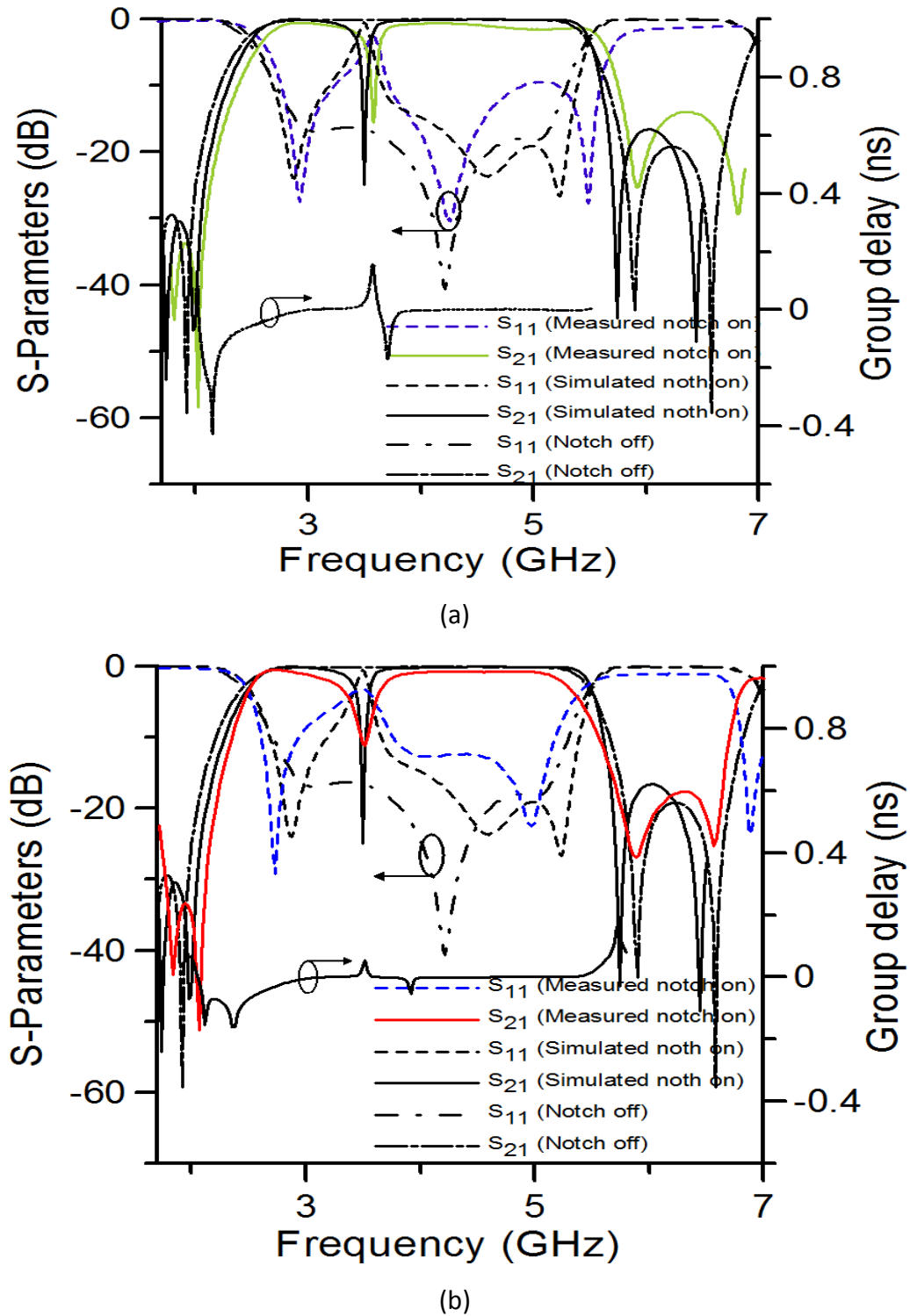
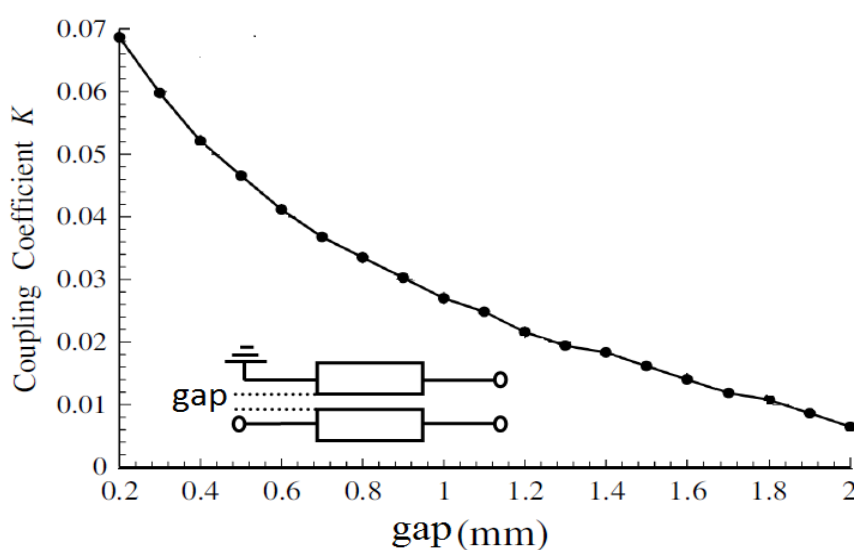


Fig. 4-17 Simulated and measured results (a) with pin diode and (b) with optical switch

To validate the circuit concept, the filter is designed and fabricated on Taconic RF35 substrate with  $\epsilon_r = 3.5$  and  $h = 0.76$  mm and tested with a pin/optical switch. The overall filter dimension is approximately  $0.25\lambda_g \times 0.23\lambda_g$ , where  $\lambda_g$  is the microstrip guided

wavelength on the substrate at centre frequency. The full wave simulated S-parameters of the filter with pin diode in ON & OFF states with the corresponding measurements, are taken with Agilent vector network analyzer E38361A and presented in Fig. 4-17(a) while filter with the optical switch are measured using an Anritsu Lightning 37397D Vector Network Analyzer and demonstrated in Fig. 4-17(b).

In the switchable notched band case with pin diode, the notched band centered at 3.52 GHz has 5-dB rejection fractional bandwidth of about 3.2% and the attenuation at the centre of the notched band is around 16 dB, also measured minimum insertion loss of 0.7 dB as shown in Fig. 4-17(a). In contrast, using optical switch, the notch rejections were observed at 3.54 GHz at approximately 12 dB and passband insertion-loss of the bandpass filter was 1.0 dB as illustrated in Fig. 4-17(b). The proposed L-shape notch structure shows significance improvement filter performances such as less insertion loss ( $<0.6$  dB) in compare with T-shape topology that was discussed in chapter 3 and requires less switching conductivity ( $\sigma < 500$  s/m) than the aforementioned shape, which is suitable for optical switch. A photograph of the fabricated filter is shown in Fig. 4-18. Moreover, the filter performs a flat group delay within the passband of about 0.2-0.35 ns in both cases. The small discrepancies between the simulated and measured responses may be attributed to the various fabrication errors involved and poor conductivity of switches especially for optical switch.



(a)

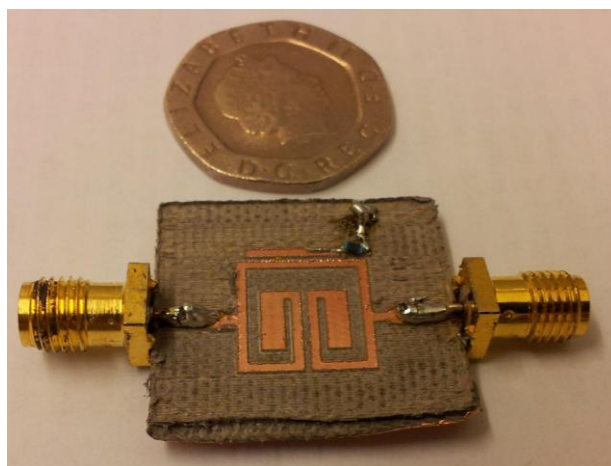


Fig. 4-18 (a) Coupling co-efficient ( $k$ ) between coupled transmission lines vs gap, and (b) A photograph of the fabricated filter

#### 4.3.2 Multi-Notched Band for UWB Filter

The technique presented in section 4.2.1 can be generalised in order to create multi-rejection bands in the band of a UWB filter. In this section, a similar third order filter employing the stub based square ring-shape structure is constructed with a desirable multi-notched bands. In Fig. 4-19 represents the proposed bandpass filter integrates with multi-notched structure. The concept of composite right/left handed as in Fig. 4-19(a) is used to develop the dual-notch structure and the third notch is created by following the similar procedure as explained in section 4.2.1, the notched band is generated employing quarter wavelength short-circuited resonator capacitively coupled to the main filter structure.



(a)

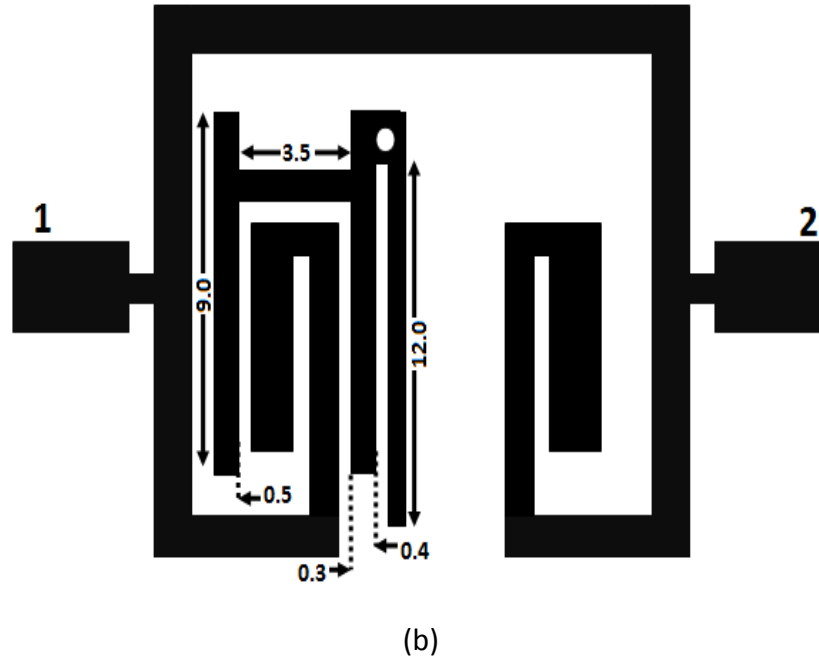


Fig. 4-19 (a) Geometry and equivalent circuit of the multi-notched structure and (b)UWB filter integrates with multi-notched structure

In accordance to [9], the composite right/left handed resonator posses inherent dual mode property and the two resonant frequencies are described by

$$\omega_1 = \frac{1}{\sqrt{L_B C}} \quad (4.21)$$

$$\omega_2 = \frac{\sqrt{1 + 4L_B / L_A}}{\sqrt{L_B C}} \quad (4.22)$$

where  $L_A$  is the series inductance realised by short-circuited high impedance line,  $L_B$  is the shunt inductance obtained by the grounded stub, and the capacitance  $C$  is added via open-end section. A simulated response using the composite right/left handed resonator is presented in Fig. 4-20 and in Fig. 4-21 shows the complete triple notch structure with corresponding measured results.

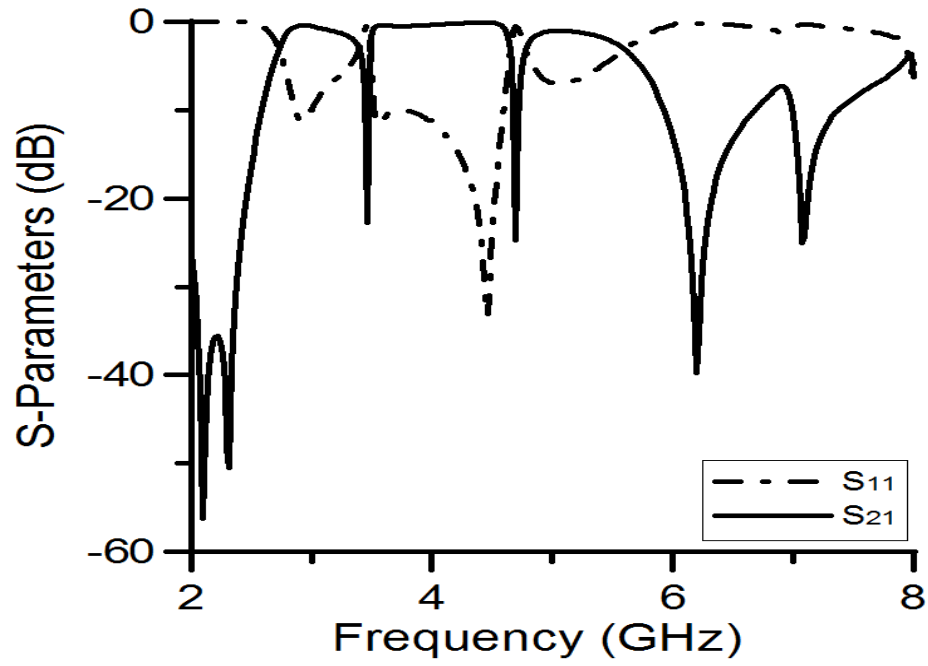
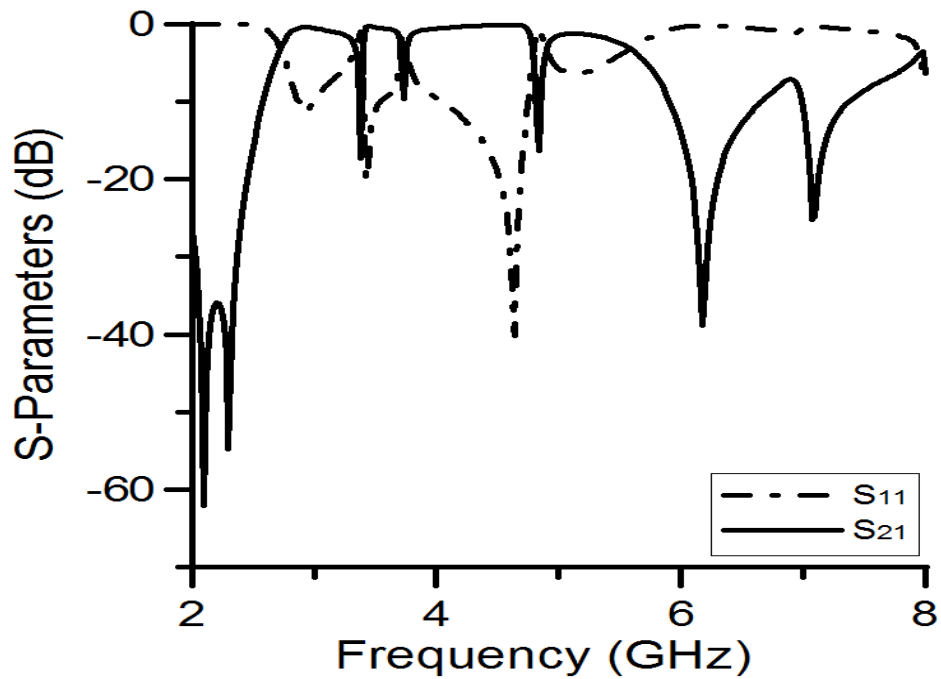


Fig. 4-20 UWB bandpass filter with dual notch using composite right/left handed resonator



(a)

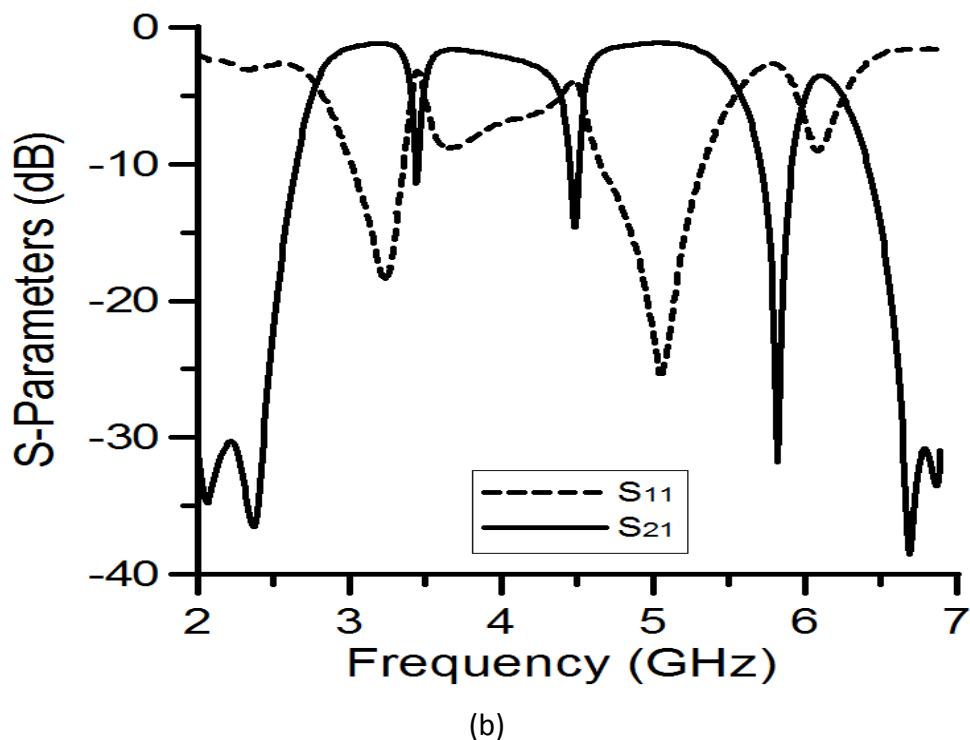


Fig. 4-21 UWB bandpass filter with triple notch using composite right/left handed resonator and a quarter wavelength short-circuited coupled resonator (a) Simulation, (b) Measured.

The filter is designed and fabricated on Taconic RF35 substrate with  $\epsilon_r = 3.5$  and  $h = 0.76$  mm. The overall filter dimension is approximately  $0.25\lambda_g \times 0.23\lambda_g$ . The filter is simulated by EM Sonnet software and the relevant measurements are taken with Agilent vector network analyzer E38361A. From the measured results in Fig. 3-21(b), the first notched band centred at 3.48 GHz has 5-dB rejection fractional bandwidth (FBW) of about 3.4% and the attenuation at 4.58 GHz with around 15 dB and 3.8% fractional bandwidth, and the third or final notched band centred at 5.82 GHz with around 33 dB rejection. The FBW of the proposed notched bands can be controlled by varying the coupling coefficients as in Fig. 4-18(a) between resonators as well the width of the structures. The measured minimum insertion loss is  $<1.2$  dB but it can be improved by selecting proper line impedances as shown in chapter 3.

### 4.3.3 Summary

First, for the first time, a microstrip filter with a reconfigurable notched band has been presented. A single pin diode and an optical switch have been used to reconfigure the notch at 3.5 GHz within the passbands of the UWB filter. In this experiment, the proposed filter has shown good agreement with simulations. Also promising features of optical switch have been shown as an alternative of pin diode. In addition, this filter has the merit of compact size and easier fabrication. The obtained results indicate that the proposed reconfigurable filter is promising for modern UWB systems solving the problem of WiMAX interferences allocated in the UWB spectrum.

Next, a technique for generating rejection notches in the passband of UWB filter using stub based square ring-shape structure is presented. The technique is effective and can be conveniently integrated with the proposed filter resonator, the single notch frequency is achieved by using short-circuited quarter wavelength and multiple notches are attained by the composite right/left handed resonator. In all cases, the results from the simulation and measurement are in good agreement.

## 4.3 References

[4-1] H. Shaman and J. Hong, "A novel ultra-wideband (UWB) bandpass filter (BPF) with pairs of transmission zeroes," *IEEE Microwave Wireless Components Letters*, vol. 17, no. 2, pp. 121-132, Feb. 2007.

[4-2] X.H. Wu, Q.X. Chu, X.K. Tian, X. Quyang, "UWB Quintuple-mode, Bandpass filter with sharp roll-off and super-wide upper stopband", *IEEE Microwave Wireless Components Letters*, vol. 21, no. 12, pp. 661–663, Dec. 2011.

- [4-3] Hsieh, L. H. and K. Chang, "Compact, broad-stopband elliptic-function lowpass filters using microstrip stepped impedance hairpin resonators," IEEE MTT-S International Microwave Symposium, pp. 1775-1778, Philadelphia, USA, Jun. 2003.
- [4-4] Kuo, J. T. and E. Shih, "Microstrip stepped impedance resonator bandpass filter with an extended optimal rejection bandwidth," IEEE Transactions on Microwave Theory and Techniques, Vol. 51, No. 5, pp. 1554-1559, May 2003.
- [4-5] Kong, Y. W. and S. T. Chew, "EBG-based dual mode resonator filter," IEEE Microwave Wireless Components Letters, Vol. 14, No. 3, pp. 124-126, Mar. 2004.
- [4-6] Ahn, D., J. S. Park, C. S. Kim, Y. Qian, and T. Itoh, "A design of lowpass filter using the novel microstrip defected ground structure," IEEE Transactions on Microwave Theory and Techniques, Vol. 49, No. 1, pp. 86-93, Apr. 2001.
- [4-7] Zhu, L. and W. Menzel, "Compact microstrip bandpass filter with two transmission zeros using a stub-tapped half-wavelength line resonator," IEEE Microwave Wireless Components Letters, Vol. 13, No. 1, pp. 16-18, Jan. 2003.
- [4-8] Gao, J. and L. Zhu, "Investigation on asymmetric parallel-coupled CPW for  $\lambda/4$  bandpass filters with broad rejection band," IEICE Electro. Express, Vol. 1, No. 11, pp. 1-6, Mar. 2004.
- [4-9] George L. Matthaei, Leo Young, E. M. T. John "Microwave Filters, Impedance Matching Networks and Coupling Structures", Artech House pp. 217-228, 1980.
- [4-10] [http://www.nxp.com/documents/data\\_sheet/BAP65-02.pdf](http://www.nxp.com/documents/data_sheet/BAP65-02.pdf) (2013)

---

## 5.0 MINIATURISED UWB FILTERS WITH RECONFIGURABLE BANDWIDTH AND FREQUENCY

---

Recent advances in modern wireless communication applications demand high performance, reconfigurability, and compact RF subsystems. Reconfigurable Microwave filters are often used to obtain wide-band coverage with the advantage of minimizing overall hardware size. These kinds of filters would be directed at supporting multiple wireless functions using common hardware hence decreasing the overall system complexity. The filter demonstrated in [1] can produce broad and narrow bandwidths by modifying inter-resonator couplings. A dual mode resonator can be found in [2], the filter employs a triangular patch resonator to achieve a two state reconfigurable bandwidths. In [3], the filter uses an interdigital capacitor with an open end gap and a rectangular ground plane below the interdigital capacitor or etched slots to achieve bandwidth reconfigurability.

In addition, the filter of adjustable fractional bandwidth or a constant bandwidth with varied centre frequency have been reported [4]-[8]. For instance, the reconfigurable filters with fractional bandwidth control were presented [4]-[5]. Also, the reconfigurable filters for transmission zeros reconfiguration and asymmetric frequency response were demonstrated in [6]-[7]. The varactor loaded combline design for the BPF with a tunable bandwidth was reported in [8]. However, the reconfigurable/tunable filters suffer from high in-band insertion loss, which limits the frequency tuning range.

In addition, several UWB bandpass filter (BPF) design techniques have been proposed such as the multi-mode resonators (MMR) [9]-[10], multilayer aperture-coupled patches [11] to achieve compactness. Moreover, to realise better selectivity, much effort has been made by generating transmission zeros, for example, in [12] demonstrated five short-circuited stub for the developments of UWB filter with pairs of transmission zeros but the filter

experienced poor out-of-band performance and consumed large size. In [13] reported the quintuple-mode UWB bandpass filter with sharp roll-off and super-wide upper stopband. Although the aperture-backed structure can raise the coupling degree of the I/O lines, it increases the fabrication complexity.

On the other hand, currently Microstrip-to-CPW (coplanar waveguide) transition or interconnects without bonding wires have been arousing endless interest due to several exclusive features of microstrip and CPW lines such as it facilitates easy shunt or series surface mounting of active and passive devices, eliminates the need for via holes as well as reduces radiation loss [14]-[16]. DML (doubly metalized line) has demonstrated a good medium for CPW and microstrip filters as it offers a wide range of advantages such as allowing use of both sides of the substrate, able to achieve high coupling factors and also easily integrate with CPW and microstrip circuits [17]-[18]. Reconfigurable UWB (3.1-5.0 GHz) filter using EBG structure has been proposed in [19] to switch between a bandpass and band-stop response. Another planar approach is employed in [20] where four Pin diodes have been utilised to switch between a bandpass and bandstop response. Both filters however suffer from relatively high loss as well as signal distortion due to the non-linear characteristics of the diode.

On inspection of the literatures, the following points can be observed:

- ❖ Most of the reported methods of bandwidth and centre frequency tunability are for narrowband applications.
- ❖ Less effort has been made in reconfigurability of bandwidth due to the lack of methods to vary the inter-resonator couplings.
- ❖ To achieve wide range tunability, additional bias circuits are used and this increases circuit complexity and incurs high losses.
- ❖ Most of the circuits occupies large space because of having excitation feeding line on the same plan.

Therefore, to address these issues, in section 5.1 presents a novel design approach using dual-mode resonator, which shows very low passband insertion loss and a wider fractional bandwidth (FBW) tuning range with almost unchanged selectivity. The proposed design

utilises stepped impedance resonator (SIR) for realization of bandpass filter (BPF) and employs a single varactor diode (BB135-NXP) for the purpose of reconfiguring bandwidth. Additionally, to improve the selectivity between passband edges, a cross-coupling between I/O feed lines is introduced which generated pairs of attenuation poles at each side of the passband.

Later, in section 5.2, a new compact CPW-fed reconfigurable UWB bandpass filter using DML lines concept is proposed, which has high selectivity filtering characteristics and relatively small size. An optical switch model is used in order achieve reconfigurability. The proposed filters are able to achieve significant size reduction as compared to the conventional bandpass filters with reconfigurable bandwidth and frequency states.

## 5.1 Proposed Filter Structure

This section focuses the following topics:

- ❖ A technique to analyse the filter topology in order to obtain equivalent circuit parameters conveniently.
- ❖ A method to attain high selectivity between passband edges without compromising filter performances.
- ❖ Independent control of the filter bandwidth over a wide range.
- ❖ Investigate a miniaturisation approach using dual mode resonator.

The proposed filter is a third-order BPF which is inductively coupled to the source and load shown in Fig. 5-1 and is excited via ports 1 and 2, where  $Z_0=50 \Omega$ . The resonator consists of a single stepped impedance based ring resonator and a shorted stubs is loaded with at the symmetry plane as shown above to achieve dual-mode performance.

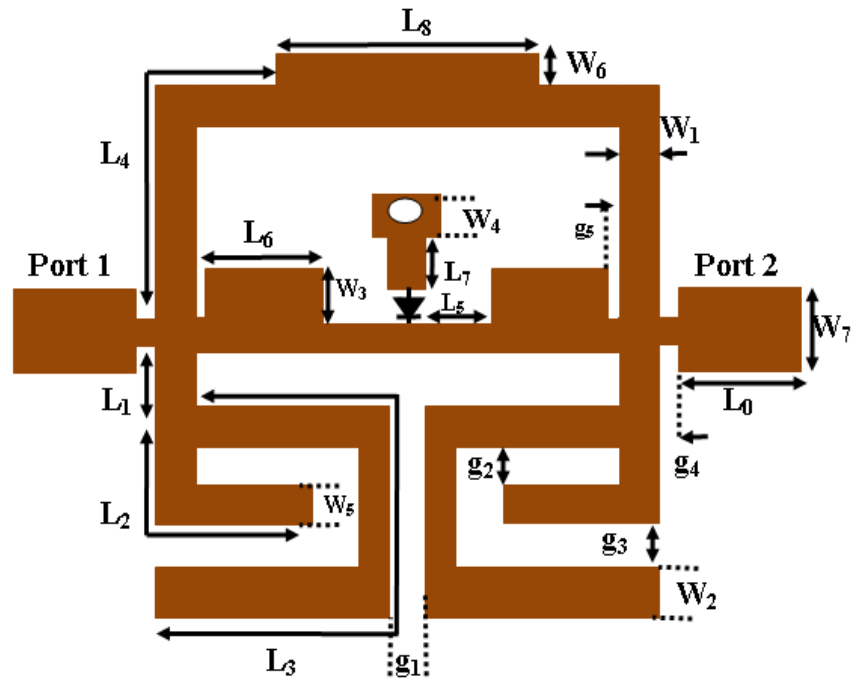


Fig. 5-1 Layout of the proposed bandpass filter with a reconfigurable notched band structure ( $L_0=5.1$ ,  $L_1=1.1$ ,  $L_2=2.4$ ,  $L_3=8.2$ ,  $L_4=4.7$ ,  $L_5=2.7$ ,  $L_6=1.7$ ,  $L_7=1.2$ ,  $L_8=4.8$ ,  $W_1=0.6$ ,  $W_2=0.9$ ,  $W_3=0.4$ ,  $W_4=1.1$ ,  $W_5=0.6$ ,  $W_6=0.6$ ,  $W_7=1.6$ ,  $g_1=0.4$ ,  $g_2=0.6$ ,  $g_3=0.5$ ,  $g_4=0.3$ ,  $g_5=0.3$ , and via diameter = 0.7 (Dimensions in mm))

### 5.1.1 Analysis of the Filter Unit

In order to gain a better insight into this resonator, excluding the bias circuitry, Fig. 5-2(a) shows the equivalent transmission line model for the proposed resonator BPF. Since the resonator is symmetrical, one can use even and odd-mode technique to analyse it. Odd and even-mode equivalents circuits are shown in Fig. 5-2(b).

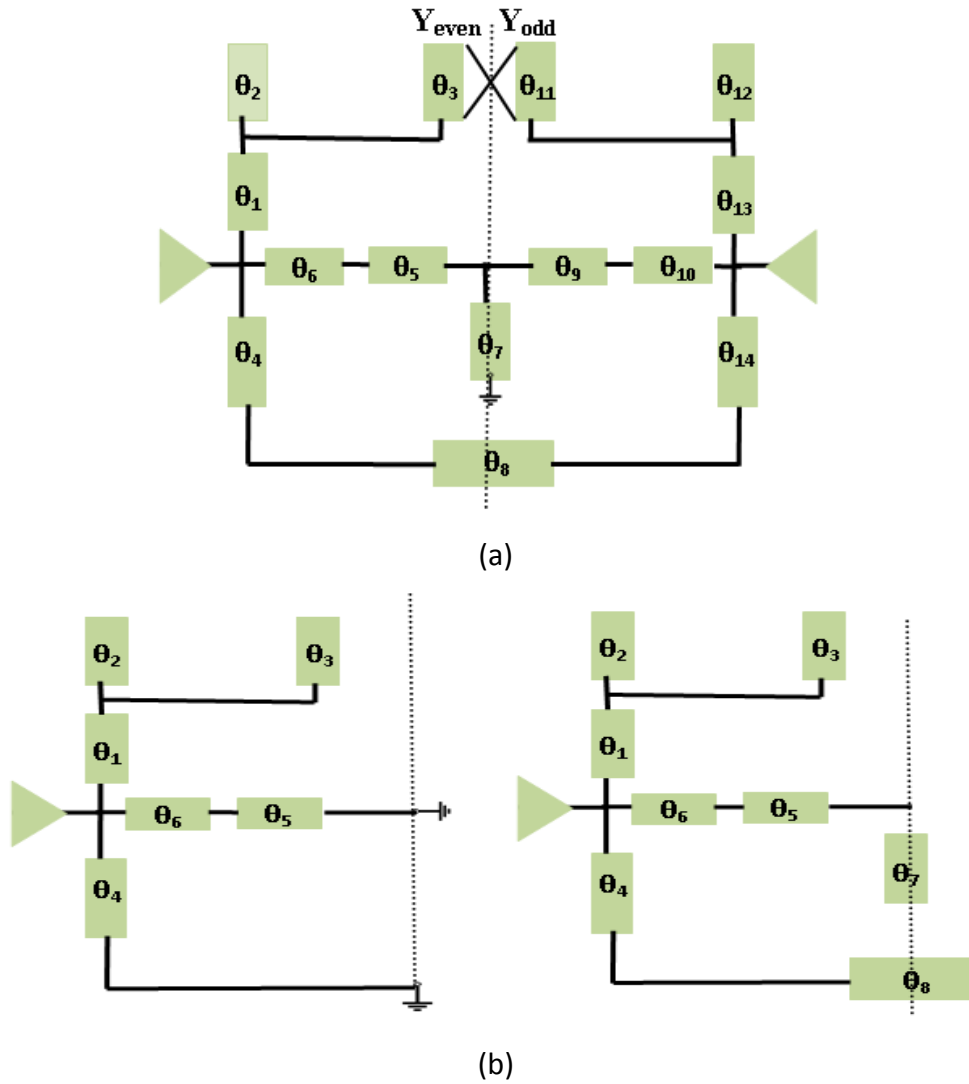


Fig. 5-2 (a) Equivalent filter transmission line model, (b) Equivalent odd-mode and even-mode circuit.

In the odd-mode excitation, the input admittance is,

$$\begin{aligned}
 Y_{in\,odd} = & Y_1 \frac{Y_{in23} + jY_1 \tan \theta_1}{Y_1 + jY_{in23} \tan \theta_1} + jY_4 \tan \theta_4 \\
 & + Y_6 \frac{j(Y_5 \tan \theta_5 + Y_6 \tan \theta_6)}{Y_6 + j(jY_5 \tan \theta_5)}
 \end{aligned} \tag{5.1}$$

with

$$Y_{in23} = \frac{Y_2 \tan \theta_2 + Y_3 \tan \theta_3}{jY_2 Y_3 \tan \theta_2 \theta_3}, \quad Y_1 = \frac{Y_2 Y_3 \tan \theta_2 \tan \theta_3}{Y_2 \tan \theta_2 + Y_3 \tan \theta_3}$$

$$Y_2 = j \tan \beta l_2, \quad Y_3 = j \tan \beta l_3$$

and  $\theta_1$  and  $\theta_2$  can be derived by using the following derivation,

$$\tan \theta_1 \cdot \tan \theta_2 = Z_1 / Z_2$$

$$L_n = \frac{\pi}{2} \left[ \theta_1 + \arctan \left( \frac{R_Z}{\tan \theta_1} \right) \right] \text{ where } R_Z = Z_2 / Z_1$$

when  $Y_{in\ odd} = 0$ , the odd-mode resonance as in Fig. 5-3 will occur and the conditions are,

$$Y_{in23} + jY_1 \tan \theta_1 = 0, \quad j(Y_5 \tan \theta_5 + Y_6 \tan \theta_6) = 0, \quad jY_4 \tan \theta_4 = 0 \quad (5.2)$$

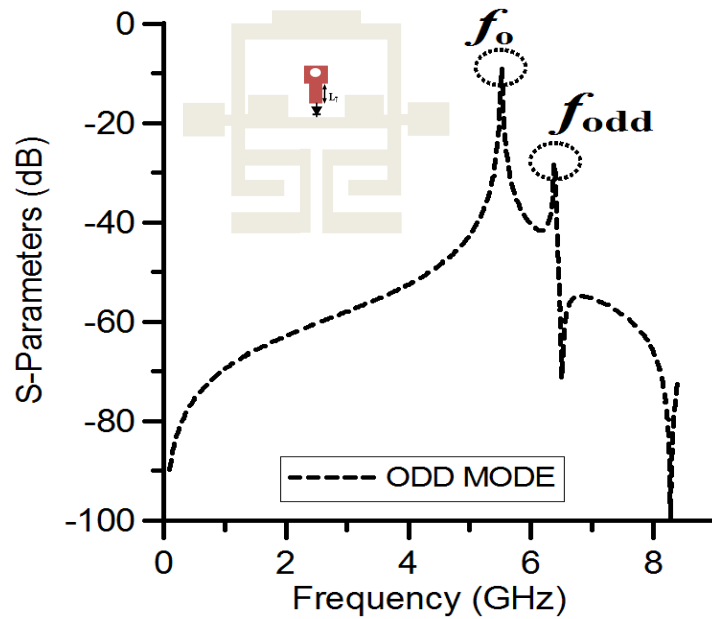


Fig. 5-3 Odd-mode resonance without the grounded  $L_7$  effect

Similarly, in the even-mode excitation, the input admittance is,

$$Y_{in\ even} = Y_1 \frac{Y_{in23} + jY_1 \tan \theta_1}{Y_1 + jY_{in23} \tan \theta_1} + Y_4 \frac{j(2Y_8 \tan \theta_8 + Y_4 \tan \theta_4)}{Y_4 + j(j2Y_8 \tan \theta_8)} + Y_6 \frac{Y_{in5} + jY_6 \tan \theta_6}{Y_6 + jY_{in5} \tan \theta_6} \quad (5.3)$$

and the even-mode resonance as shown in Fig. 5-4 occur at  $Y_{in\ even} = 0$  with the conditions are where the odd-mode resonance still exists by default due to sharing common structure,

$$Y_{in23} + jY_1 \tan \theta = 0, \quad j(2Y_8 \tan \theta_8 + Y_4 \tan \theta_4) = 0, \quad Y_{in5} + jY_6 \tan \theta_6 = 0 \quad (5.4)$$

The  $S_{21}$  parameters can be derived from (5.1) and (5.3),

$$S_{21} = \frac{Y_{in_{odd}} Y_0 - Y_{in_{even}} Y_0}{(Y_0 + Y_{in_{odd}})(Y_0 + Y_{in_{even}} Y_0)} = 0 \quad (5.5)$$

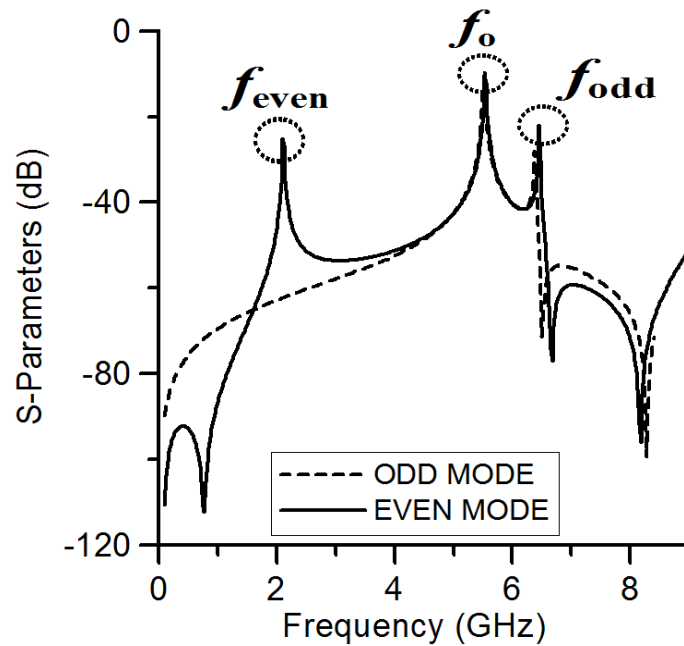


Fig. 5-4 Even-mode resonance with the grounded  $L_7$  effect

where  $\theta_i$  ( $i=1,2,3,\dots$ ,etc) are the electrical lengths of the transmission line sections and  $Y_i$  ( $i=1,2,3,\dots$ ,etc) are the characteristic admittance of the corresponding electrical length respectively.

The design steps are as following:

1. Choose centre frequency (4.9 GHz), fractional bandwidth (69%), and frequency response (Chebyshev with 0.1 dB ripple).
2. Calculate the frequencies of the three transmission poles in the passband [8]. Choose Table I parameters such that the pole frequencies are 3.25 GHz, 4.9 GHz, and 6.5GHz.
3. Using the formulation given above (5.1)-(5.5), the frequency response of this filter can be computed.
4. Final optimization in full-wave simulator such EM Sonnet (space mapping technique) in this case.

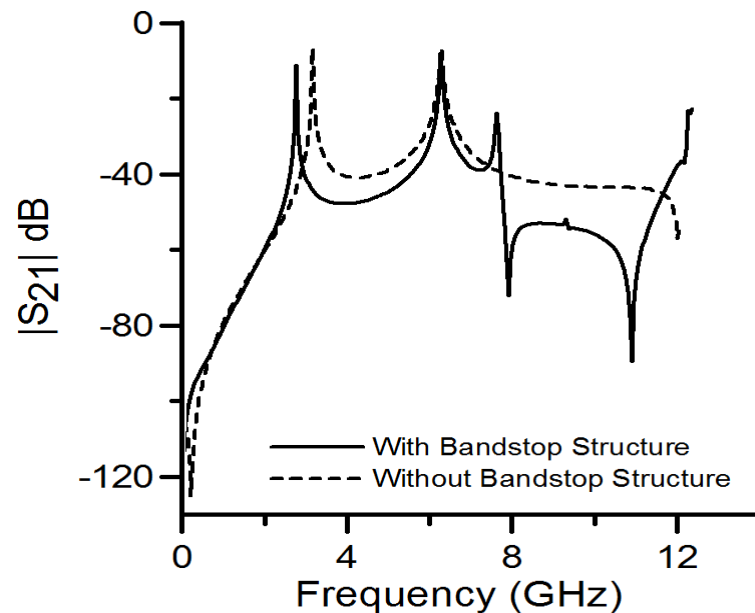
**Table I** Filter dimensions ( $f_0=4.9$  GHz)

Electrical length in	Transmission line
----------------------	-------------------

degree	impedance ( $\Omega$ )
$\theta_1=\theta_{13}= 25.9^\circ$	$Z_1=Z_{13}= 81.7 \Omega$
$\theta_2=\theta_{12}= 29.6^\circ$	$Z_2=Z_{12}= 81.7 \Omega$
$\theta_4=\theta_{14}= 28.7^\circ$	$Z_4=Z_{14}= 81.7 \Omega$
$\theta_5=\theta_9= 9.26^\circ$	$Z_5=Z_9= 81.7 \Omega$
$\theta_6=\theta_{10}= 26.6^\circ$	$Z_6=\theta_{10}= 47.0 \Omega$
$\theta_7 = 14.8^\circ$	$Z_7= 81.7 \Omega$
$\theta_8= 46.25^\circ$	$Z_8= 54.4 \Omega$
$\theta_3=\theta_{11}= 89.37^\circ$	$Z_3=Z_{11}= 81.7 \Omega$

### 5.1.2 Attainment of transmission zeros

In order to produce transmission zeros at desired frequencies to improve filter selectivity, two techniques have been adopted, firstly, a broadband bandstop section is developed by stretching two shunt stubs ( $\theta_1$  &  $\theta_{13}$ ) as shown in Fig. 5-2(a) to achieve one wavelength ( $\lambda_g$ ) electrical length ( $\theta_1+\theta_4$ ,  $\theta_{13}+\theta_{14}$  &  $\theta_8$ ) which parallels with a with a half-wavelength ( $\lambda_g/2$ ) transmission line ( $\theta_5+\theta_6$  &  $\theta_9+\theta_{10}$ ) for contributing transmission zeros as in Fig. 5-5 at the upper stopband.



(a)

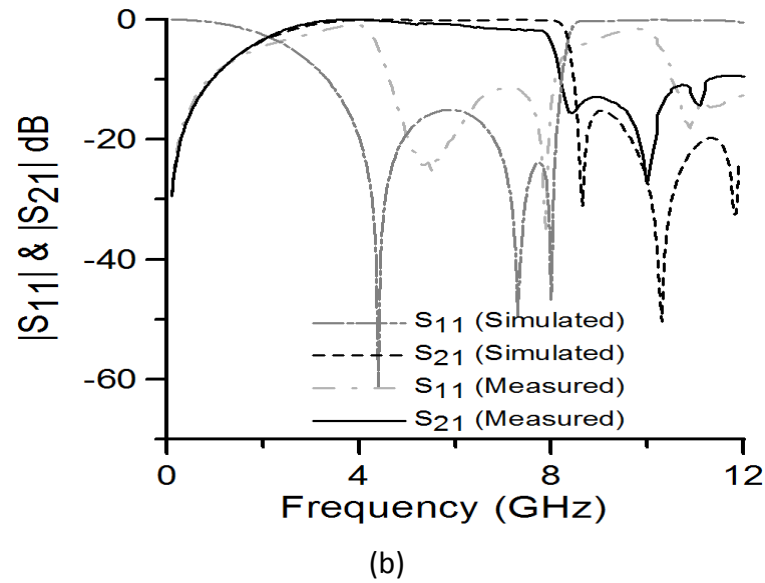


Fig. 5-5 Modified Dual-Mode Resonator with Improved Upper Stopband using bandstop structure (a) Pole response, (b) Transmission response

Later, two quarter-wavelength ( $\lambda_g/4$ ) open stubs ( $\theta_2$  &  $\theta_{12}$ ) are employed to increase the insertion loss of the bandstop filter. The electrical length of the  $\lambda_g$ ,  $\lambda_g/4$  length and the  $\lambda_g/2$  resonators have been calculated at a centre frequency of 7.8 GHz. Furthermore, secondly, a cross coupling between the I/O feedlines has been introduced by placing a section of U-shaped ( $L_2+L_5+L_9$ ) transmission line as shown in Fig. 5-1 on the two shunt open-circuited stub which generates pairs of transmission zeros between lower as in Fig. 5-6 and upper passband edges as well as provide wideband rejection in the stopband. The complete filter response using both techniques and the effect of stepped impedance resonator in the ring circuit is presented in Fig. 5-7.

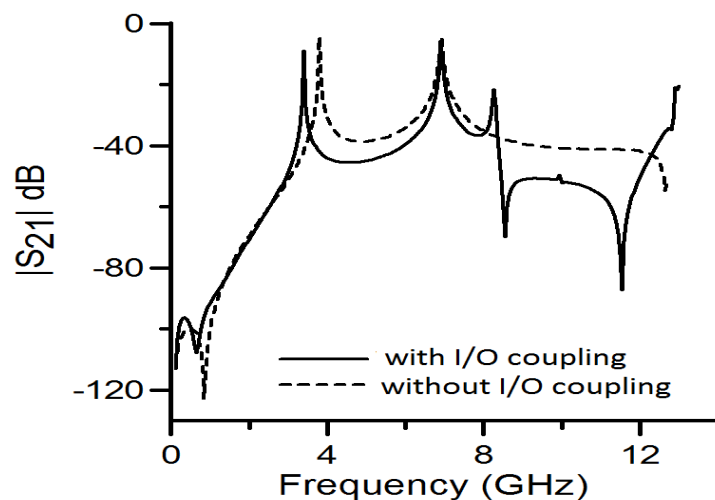
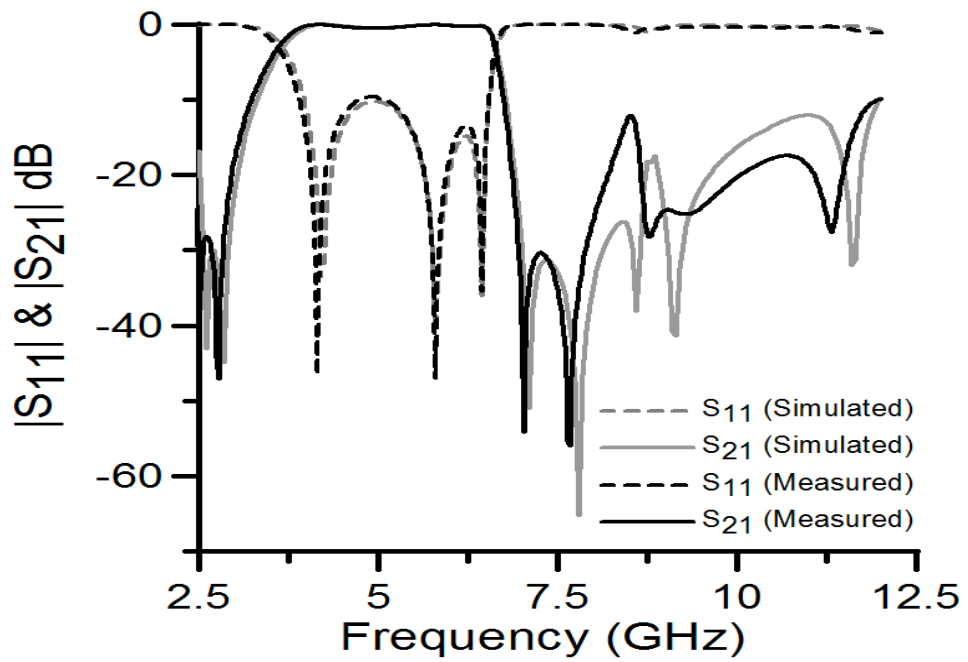
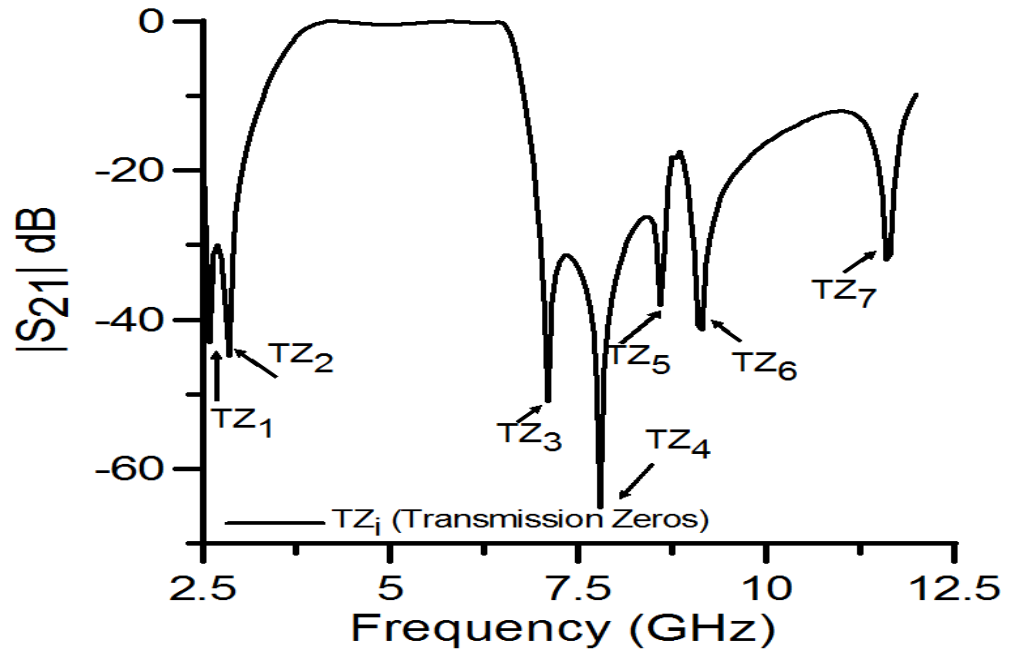
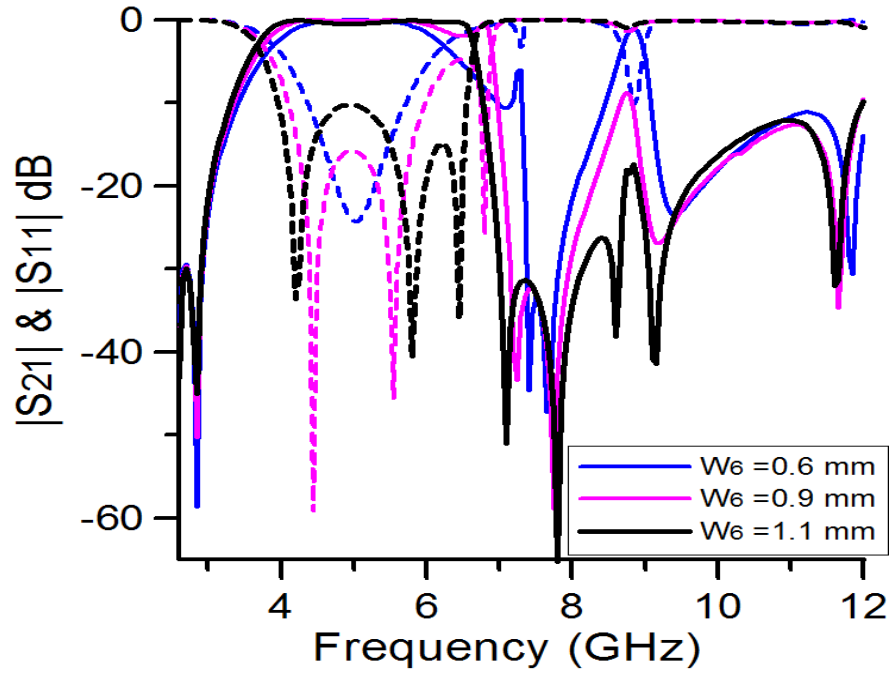


Fig. 5-6 Improved filter lower selectivity via I/O coupling.





(c)

Fig. 5-7 (a) Simulated  $|S_{21}|$ -parameter with lower and upper skirts, where transmission zeros  $TZ_1, TZ_2, TZ_6, TZ_7$  are created by I/O coupling and the transmission zeros  $TZ_3, TZ_4, TZ_5$  are by bandstop structure (b) Simulated and measured S-parameters of the proposed filter, (c) Effect in the main transmission line by varying width of the SIR resonator.

### 5.1.3 Filter with reconfigurable bandwidth

It is known that the frequency response of a filter is able to be reconfigured with the relocation of transmission zeros and poles with the filter structure. Practically, the zero/pole relocation can be realised with the traditionally microwave resonator loaded with varactor. To study the proposed filter resonance properties, a full-wave em simulator (*em* Sonnet™) is used and the relationship between the resonant frequencies and the central loading shorted stub  $L_7$  is shown in Fig. 5-6. As shown in Fig. 5-8(b), by changing  $L_7$  while keeping the other size of the resonator fixed, the fundamental even-mode resonant frequency can be adjusted, whereas the odd-mode resonant frequency keeps basically unchanged. Therefore, the proposed filter resonator can support two degenerate modes and this feature has been utilised to achieve bandwidth reconfigurability. A single varactor diode is inserted for this purpose as illustrated in Fig. 5-8(a).

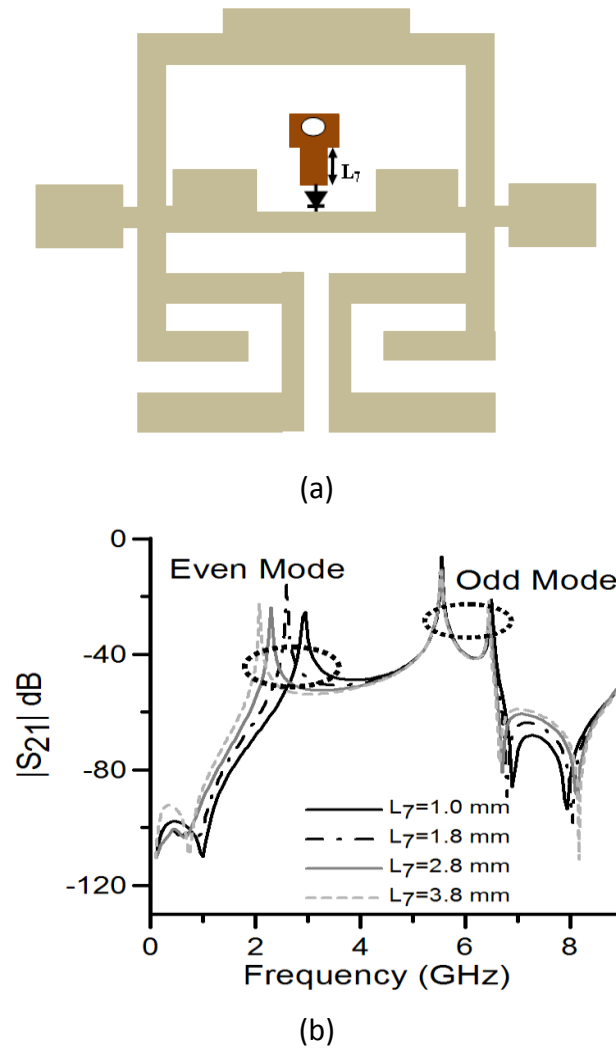


Fig. 5-8 (a) Filter layout with loading varactor diode, (b) Simulated  $|S_{21}|$  of the proposed resonator under weak coupling with varied  $L_7$ .

### 5.1.3.1 Experimental Results

To validate the circuit concept, the filter is designed and fabricated on Taconic RF35 substrate with  $\epsilon_r = 3.5$  and  $h = 0.76$  mm and tested with a single varactor diode (BP135-NXP) for tuning the FBW bandwidth. This filter is designed to have a 3-dB passband from 3.1–6.6 GHz with a mid-band frequency of 4.85 GHz. The overall filter dimension is approximately  $0.14\lambda_g \times 0.12\lambda_g$  (excluding the two feed lines), where  $\lambda_g$  is the microstrip guided wavelength on the substrate at centre frequency. In this experiment, the varactor bias voltage was varied from 0V to 30V, which varied capacitance from around 21 pF to approximately 2 pF [21]. In Fig. 5-9 and 5-10, the simulated and measured  $|S_{21}|$  and  $|S_{11}|$  under different reverse bias are demonstrated, respectively. As a result, the measured data are in excellent

agreement with the simulated data. Table II listed the 3 dB fractional bandwidth (FBW) and the maximum passband insertion loss (IL) at different bias for simulation and measurement. From the obtained results, the passband insertion loss is less than 1.1 dB and the return loss is greater than 12 dB. Most importantly, the FBW has a relatively high reconfigurability ranging from 53.8% (at 5.5 GHz) to 84.2% (at 5.1 GHz). Furthermore, the skirt selectivity remains almost unchanged, which is crucial to eliminate undesired interferences. The photograph of the proposed filter is shown in Fig. 5-11.

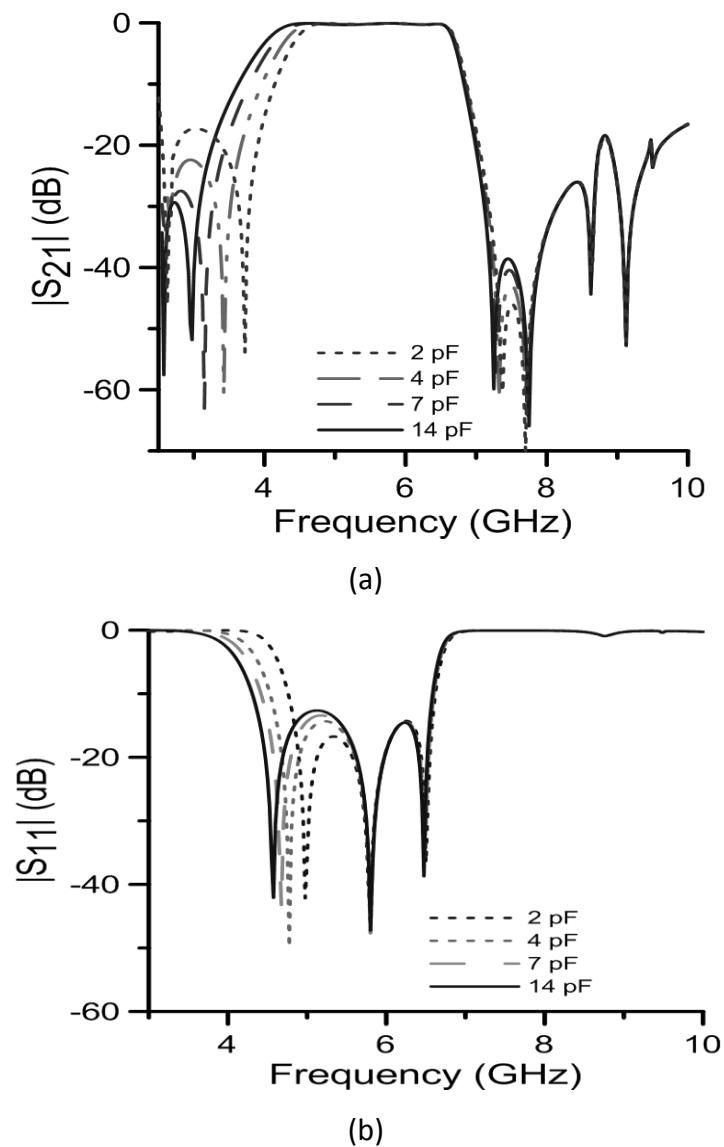
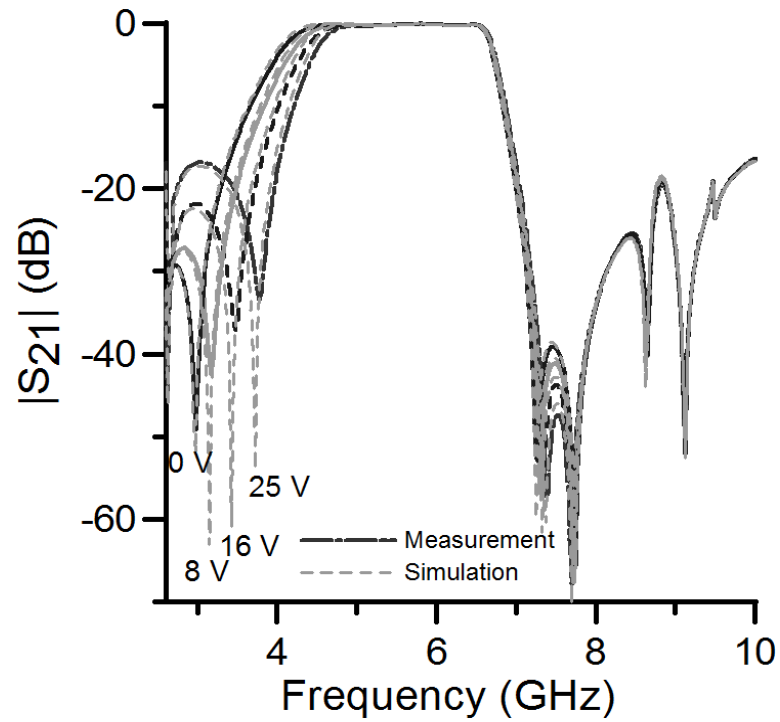
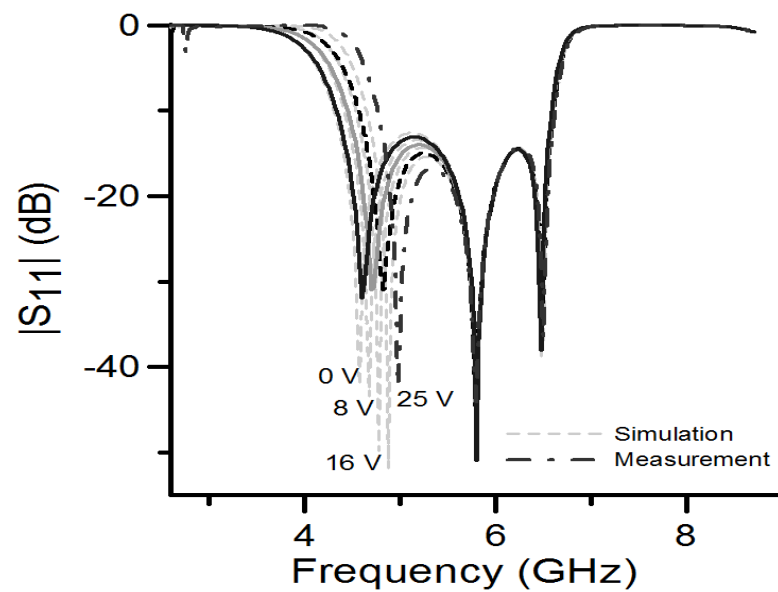


Fig. 5-9 (a) Simulated S-parameter ( $|S_{21}|$ ) of the proposed filter under different loading capacitance, (b) Simulated S-parameter ( $|S_{11}|$ ) of the proposed filter under different loading capacitance



(a)



(b)

Fig. 5-10 (a) Simulated and measured S-parameter ( $|S_{21}|$ ) of the proposed filter under different biasing voltages, (b) Simulated and measured S-parameter ( $|S_{11}|$ ) of the proposed filter under different biasing voltages.

**Table II** Filter Performances

Reverse Bias (V)	0	8	25
FBW (Simulated)	86.2%	74.4%	55.8%
FBW (Measured)	84.2%	72.3%	53.8%
IL (Simulated)	0.6 dB	0.7 dB	0.8 dB
IL (Measured)	0.9 dB	1.0 dB	1.1 dB



Fig. 5-11 Photograph of the proposed filter

### 5.1.3.2 Summary

A miniaturised sharp rejection microstrip bandpass filter based on dual-mode resonator with reconfigurable bandwidth for the lower UWB band (3.1-6.6 GHz) applications has been presented. Simulation based extraction allows the calculation of the complicated structure relatively quickly and thus greatly expediting the filter design process. A single varactor diode was used to reconfigure the fractional bandwidth of the filter. The demonstrated BPF has a relatively low insertion loss and a wider FBW tuning range with almost unchanged selectivity. In order to illustrate the accuracy of the design procedure, filter has been fabricated and tested. The proposed reconfigurable filter has shown good agreement (insertion loss difference  $\approx 0.3$  dB and FBW  $< 3\%$ ) between simulated and measured results. The obtained results indicate that the proposed reconfigurable filter is promising filter solution for modern UWB systems.

## 5.2 CPW-fed Reconfigurable Filter

This section describes the following issues:

- ❖ A new concept using DML (doubly metalized line) to achieve highly compactness.
- ❖ A simple and convenient approach to attain frequency reconfigurability.
- ❖ A method to create stop band attenuation in the lower band.

Hence, a new compact CPW fed reconfigurable UWB bandpass filter using DML (doubly metalized line) lines is presented. A cross section of doubly metalized line is viewed in Fig. 5-12. The CPW-fed third-order microstrip reconfigurable UWB bandpass filter is build on both sides of the substrate in which the ground metallization is placed on the top side for CPW in Fig. 5-13(a) and filter resonators are on the rear side as in Fig. 5-13(b).

The layout of the proposed filter in Fig. 5-13(c) is a third-order bandpass filter composed of a single  $\lambda_g/2$  wavelength resonator at 4 GHz, which is placed between a pair of  $\lambda_g/4$  wavelength resonators at 4 GHz. On the top layer, two ports 50 $\Omega$  CPW feeding lines are placed to feed the microstrip UWB filter. These feeding lines are capacitively coupled with filter resonators as in Fig. 5-13(d). In addition, from the analysis of the circuit, it has been observed that the structure has a stop-band attenuation at the upper stopband as shown in Fig. 5-14 (a). Therefore, a transmission zero is needed to achieve lower attenuation at the stop-band. This can be obtained by linking the CPW feeding lines with an inductive strip as in Fig. 5-13(a) and the corresponding response is shown in Fig. 5-14.

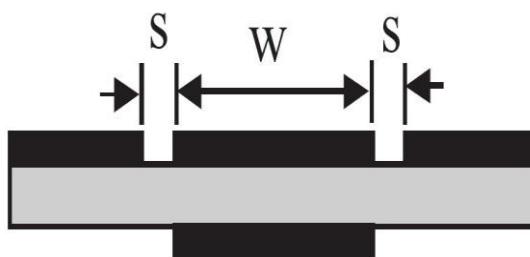
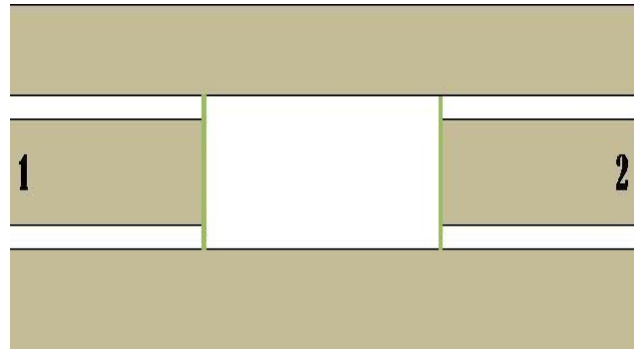
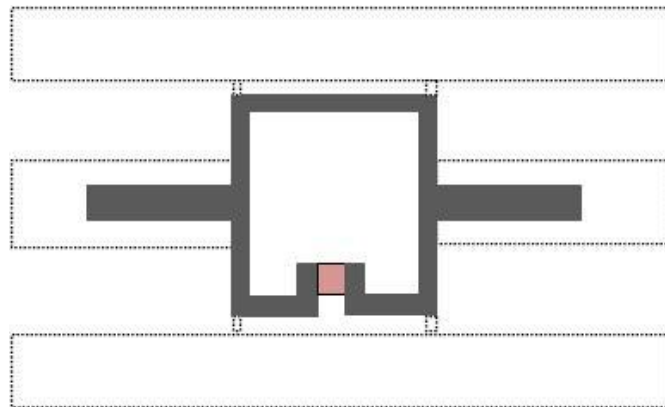


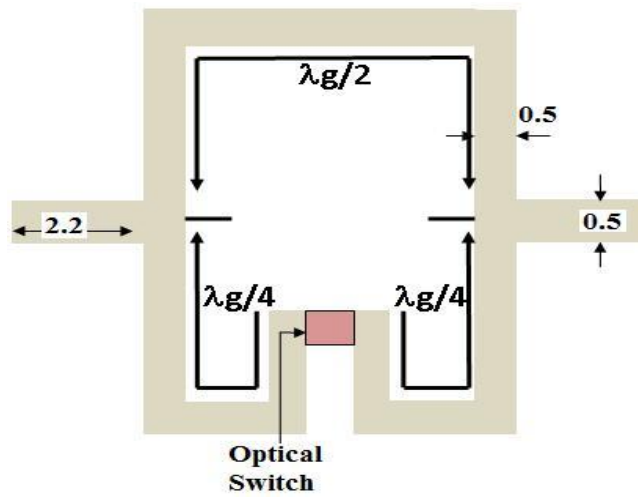
Fig. 5-12 Cross section of a doubly metalized line



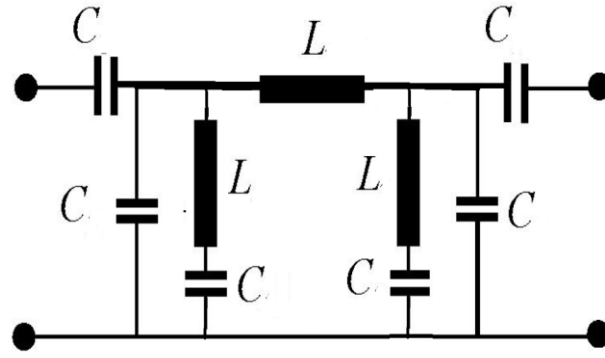
(a)



(b)

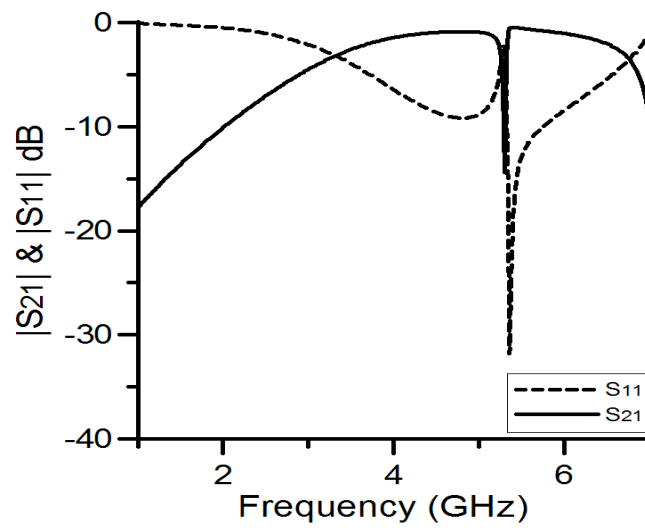


(c)

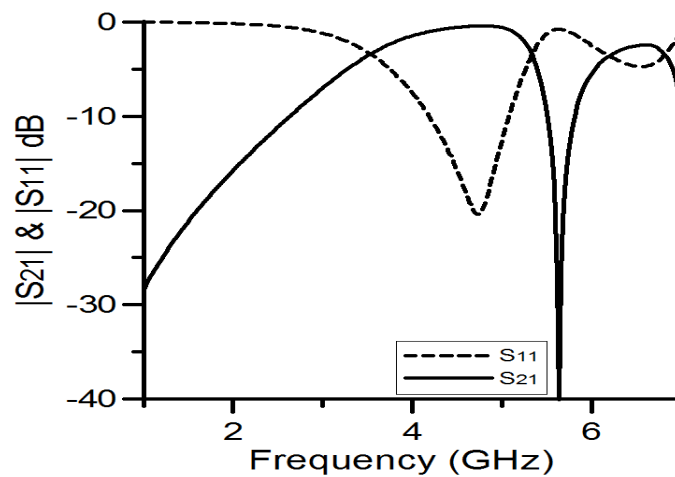


(d)

Figure 5-13 (a) Top side (CPW feeding lines), (b) Back side (filter resonators) layout of reconfigurable filter with CPW feeding lines, and (c) Layout of the proposed UWB bandpass filter with optical switch model (dimensions in mm), and (d) Equivalent circuit of the proposed filter.



(a)



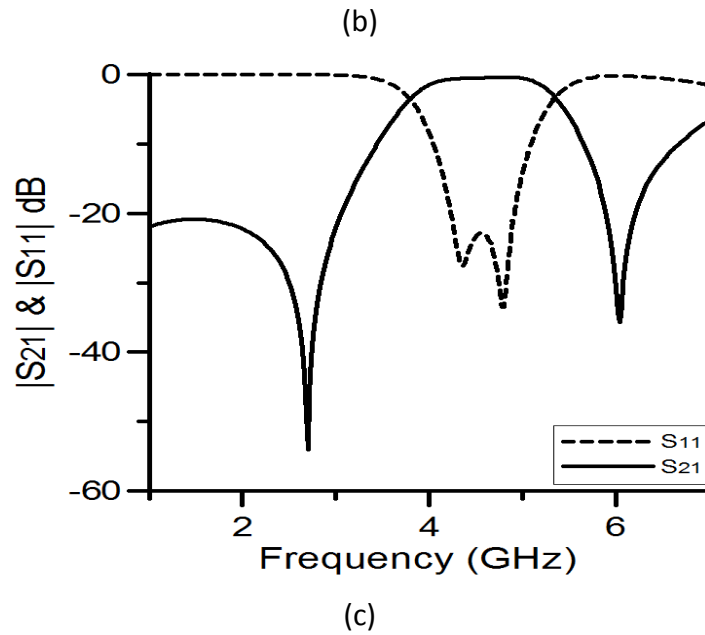
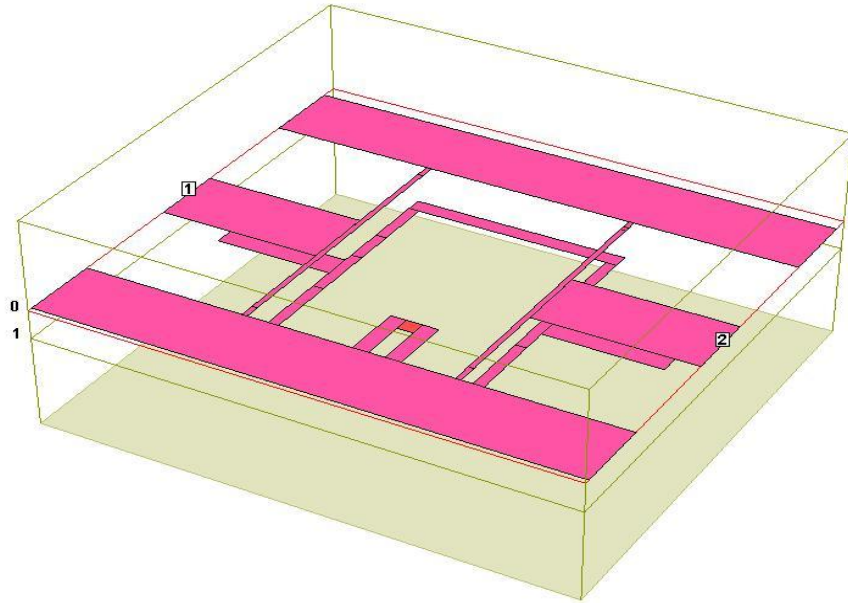


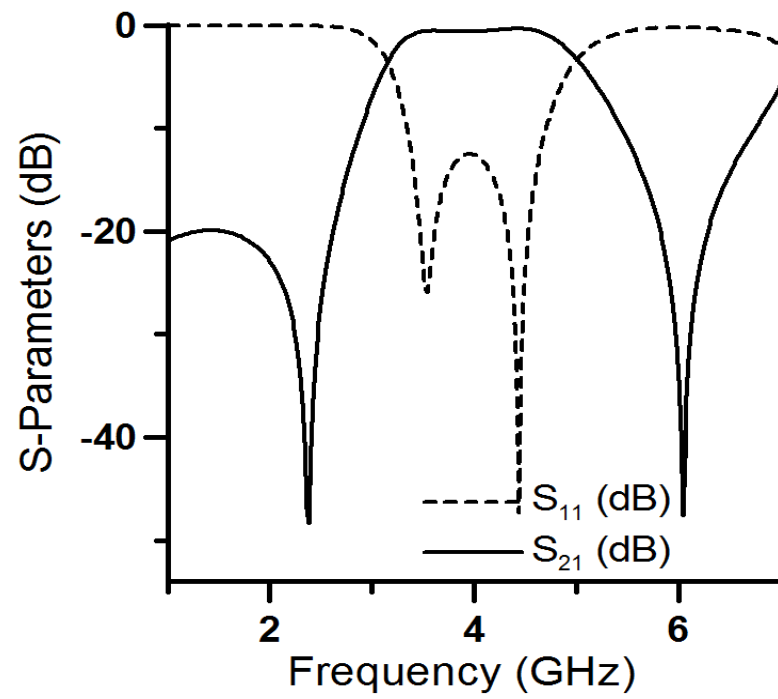
Fig. 5-14 Transmission response (a) no connection between CPW ports, (b) a single CPW port is connected through ground, and (c) both CPW ports are connected through ground.

This filter is designed to have a 3 dB passband from 3.1 GHz – 5.0 GHz with a mid-band frequency of 4 GHz. To achieve reconfigurability, an optical switch model in Fig. 5-13(c) is overlaid in between two  $\lambda_g/4$  resonators. The model is generated by Agilent ADS simulator at ON/OFF state using values from Table-I and the measured S-parameters are incorporated to EM Sonnet simulator through data file option. The switch has a conductivity of 35.2 mS/m in the dark state (OFF) and a conductivity of 150.4 S/m when optically activated (ON).

A third order reconfigurable band notch UWB bandpass filter is designed on both sides of the Rogers substrate (RO6010) with a thickness of 0.635 mm, relative dielectric constant of 10.8, and optimized by em sonnet<sup>TM</sup> simulator. The overall filter dimension in millimetres is 8.2 x 6.0 mm. Simulation results for the filter in the ON-state (200W) and OFF-state (0W) are shown in Fig. 5-15. The simulation results show that for bandpass filter the insertion loss is 0.4 dB and return loss is > 15 dB and for bandstop filter, the rejection level is > 40 dB and the insertion loss in the passband is 0.3 dB.



(a)



(b)

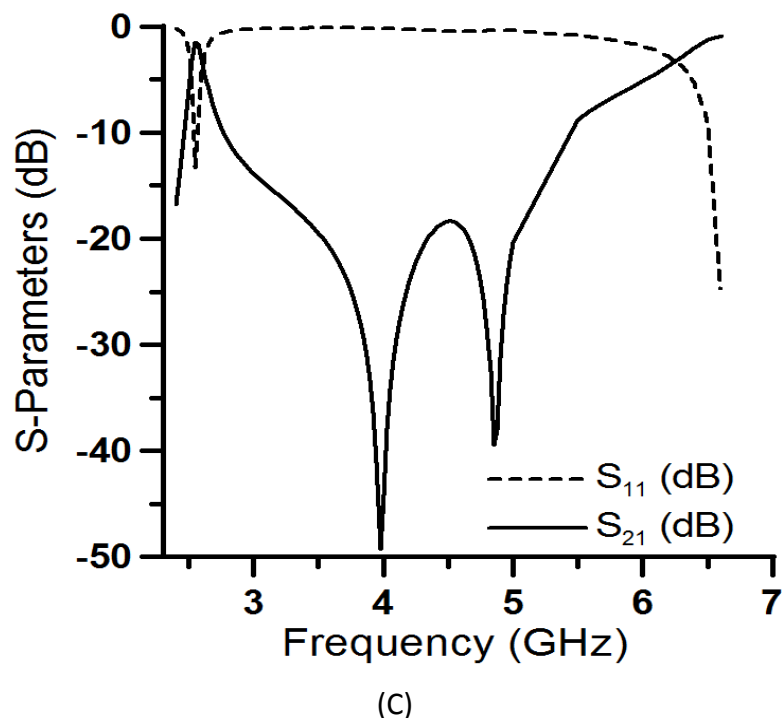


Fig. 5-15 (a) 3-D filter layout generated by EM sonnet software and transmission response of the reconfigurable filter with optical switch model in the (b) ON, and (c) OFF states

### 5.2.1 Summary

This section proposed a very compact reconfigurable filter for CPW and microstrip applications. The stub based filter is designed using doubly metalized technique and an innovative transmission zero creation method is shown without increasing the circuit complexity or the size of the filter. Also, to achieve reconfiguration, an optical switch model has been used in the ON state (200W) and in the OFF state (0W). The proposed filter example is highlighted the compactness achieved with these configurations especially in comparison to other research work. The design procedure is also relatively simple and inexpensive to fabricate compared to other popular multilayer approaches.

## 5.3 References

- [5-1] Lugo, C., Jr. & Papapolymerou, J. (2004). Electronic Switchable Bandpass Filter Using PIN Diodes for Wireless Low Cost System-on-a-package Applications, Proceedings of IEE Microwave Antennas and Propagation, Vol. 151, No. 6, pp. 497 – 502, Dec. 2004.
- [5-2] Lugo, C., Jr. & Papapolymerou, J. (2005). Single switch reconfigurable bandpass filter with variable bandwidth using a dual-mode triangular patch resonator, Proceedings of IEEE MTT-S International Microwave Symposium, pp. 779 – 782, Jun. 2005.
- [5-3] Li Zhu, Vijay Devabhaktuni, Chunyan Wang, Ming Yu, “Adjustable Bandwidth Filter Design Based on Interdigital Capacitors,” IEEE Microwave and Wireless Components Letters, vol. 18, pp. 16–18, Jan. 2008
- [5-4] H. Joshi, H. H. Sigmarsson, S. Moon, D. Peroulis, and W. J. Chappell, “High-Q fully reconfigurable tunable bandpass filters,” IEEE Trans. Microwave Theory Tech., Vol. 57, No. 12, pp. 3525-3533, Dec. 2009.
- [5-5] A. Miller and J.-S. Hong, “Wideband bandpass filter with reconfigurable bandwidth,” IEEE Microwave Wireless Compon. Lett., vol. 20, no. 1, pp. 28-30, Jan. 2010.
- [5-6] W. M. Fathelbab and M. B. Steer, “A reconfigurable bandpass filter for RF/microwave multifunctional systems,” IEEE Microwave Wireless Compon. Lett., vol. 53, no. 3, pp. 1111-1116, Mar. 2005.
- [5-7] H. Zhang and K. J. Chen, “Bandpass filters with reconfigurable transmission zeros using varactor-tuned tapped stubs,” IEEE Microwave Wireless Compon. Lett., vol. 16, no. 5, pp. 249-251, May 2006.
- [5-8] M. Sanchez-Renedo et al., “Tunable combline filter with continuous control of center frequency and bandwidth,” IEEE Trans. Microwave Theory Tech., vol. 53, no. 1, pp. 191–199, Jan. 2005.

- [5-9] L. Zhu, S. Sun, and W. Menzel, "Ultra-wideband (UWB) bandpass filter using multiple-mode resonator," *IEEE Microw. Wireless Compon. Lett.*, vol. 15, no. 11, pp. 796–798, Nov. 2005.
- [5-10] J. Gao, L. Zhu, W. Menzel, and F. Bögelsack, "Short-circuited CPW multiple-mode resonator for ultra-wideband (UWB) bandpass filter," *IEEE Microw. Wireless Compon. Lett.*, vol. 16, no. 3, pp. 104–106, Mar. 2006.
- [5-11] A. M. Abbosh, "Planar bandpass filters for ultra-wideband applications," *IEEE Trans. Microw. Theory Tech.*, vol. 55, no. 10, pp. 2262–2269, Oct. 2007.
- [5-12] H. Shaman and J. Hong, "A novel ultra-wideband (UWB) bandpass filter (BPF) with pairs of transmission zeroes," *IEEE Microw. Wireless Compon. Lett.*, vol. 17, no. 2, pp. 121–132, Feb. 2007.
- [5-13] X.H. Wu, Q.X. Chu, X.K. Tian, X. Quyang, "UWB Quintuple-mode, Bandpass filter with sharp roll-off and super-wide upper stopband", *IEEE Microwave Wireless Comp. Lett.*, pp. 661–663, Dec. 2011.
- [5-14] L. Zhu, S. Sun, and W. Menzel, "Ultra-wideband (UWB) bandpass filters using multiple-mode resonator", *IEEE Microwave Wireless. Compon. Letter*, vol. 15, pp. 796–798, Nov. 2005.
- [5-15] J. J. Burke and R.W. Jackson, "Surface-to-surface transition via electromagnetic coupling of microstrip and coplanar waveguide," *IEEE Trans. Microwave Theory Tech.*, vol. 37, pp. 519–525, Mar. 1989.
- [5-16] Zhu, L. and K. Wu, "Characterization of finite-ground CPW reactive series-connected elements for innovative design of uniplanar M(H) MICs," *IEEE Trans. Microwave Theory Tech.*, Vol. 50, No. 2, 549-557, Feb. 2002.

[5-17] L. Zhu, W. Menzel, "Broad-band microstrip-to-CPW transition via frequency dependent electromagnetic coupling," IEEE Transactions on Microwave Theory Tech., Vol. 52, No. 5, pp. 1517- 1521, May 2004.

[5-18] Balalem A., Machac J., Omar A., "Quasi-Lumped Filters on Doubly Metallized Planar Lines", IEEE Radio Electronika Conference, pp. 1-3, June 2007.

[5-19] M. F. Karim, A. Q. Liut, A. Alphones, and A. B. Yu," A Novel Reconfigurable Filter Using Periodic Structures", IEEE MTT-S, pp. 943-946, Jun. 2006.

[5-20] M.F. Karim, Y.X. Guo, Z.N. Chan and L.C. Ong, "Miniaturized reconfigurable and switchable filter from UWB to 2.4 GHz WLAN using PIN diodes", IEEE MTT-S, pp. 509-512, Jun. 2009.

[5-21] [http://www.nxp.com/documents/data\\_sheet/BP135.pdf](http://www.nxp.com/documents/data_sheet/BP135.pdf)

---

## 6.0 DUAL WIDEBAND BANDPASS FILTER WITH INDEPENDENTLY CONTROLLED FREQUENCY BANDWIDTH

---

Electronically switchable and reconfigurable microwave devices such as filters are in great demand for existing wireless communication systems, and this trend will continue for future systems. To meet the increasing requirement of modern multifunctional systems, bandpass filters should have multi-frequency response. Reconfigurable bandpass filters (BPFs) can be used to control the spectrum of proposed signals and support multiple information channels [1]-[2]. Recently, dual-band BPFs have drawn a lot of attention and this topic has been intensively researched [3]-[8]. Combination of a BPF filter and a bandstop filter in series [3], or two bandpass filters which have individual passband in parallel [4], can construct a dual-band filter. But this type of filters has drawbacks in relatively large filter size. The defected stepped impedance resonators [5] or meander open-loop resonators [6] are introduced in the dual-band filter design to reduce the filter size; while they have a relatively large number of resonators. Dual-band filters using the stepped impedance resonators [7]-[8], dual-mode resonators [9]-[10], or embedded resonators [11]-[12], which coupled each other have less resonators and compact size. However, the design procedure is very complicated because the coupling co-efficiencies of the resonators at two separate passbands are difficult to be fulfilled simultaneously.

Furthermore, much concentration has been given to electrical tunability as one of the diverse features of BPFs [13]-[16]. A tunable upper passband has been realised by using controllable even mode resonant frequencies [13], and harmonic suppressed tunable filters with two transmission zeros have been demonstrated [14]. In [17], a single-band switchable microstrip BPFs with dissimilar stepped impedance resonators (SIRs) and PIN diodes were reported to develop good selectivity and stopband rejection simultaneously. Also a

switchable dual-band BPFs with four states is proposed in [18], and dual-band BPFs with only one channel at a time [19].

Most of the aforementioned filters, the following issues are to be addressed:

- ❖ Analysis of the filter structure to shed light as to the design rules for higher order filters.
- ❖ A wide frequency range ratio of the dual passbands and filters with wide bandwidth.
- ❖ Independent control of switching dual frequency states without effecting other performance parameters pertaining to filters design.
- ❖ A continuing challenge in circuit size and complex fabrication procedure.

This chapter covered all the above issues using the extension of previous structure that was presented in chapter 5. The proposed dual band filter exhibits similar dual mode features and its fractional bandwidths can be tuned to a wide range by exploiting even mode characteristics as in chapter 5.

## 6.1 Characteristics of the Proposed Filter

This section discusses the following points:

- ❖ A comprehensive design approach using even-odd mode analysis as to highlight design steps.
- ❖ Methods to sharpen the out-of-band rejection skirts between dual passband edges.
- ❖ Miniaturisation techniques using a stepped impedance based ring resonator because a ring resonator owns the advantages of compact size and high quality (Q) factor; also the resonant frequencies of the ring resonator can be adjusted by using stepped impedance topology with a variable impedance ratio.

Hence, the proposed dual-wideband bandpass filter is designed at the centre frequencies at 4.9 GHz and 9.6 GHz and is excited via ports 1 and 2, where  $Z_0=50 \Omega$ . Fig. 6-1 depicts the schematic layout of the type of UWB filter, which consists of the proposed novel dual-mode ring resonator and a pair of I/O feeders. The proposed ring resonator is composed of a

stepped impedance based resonators and a centrally loaded inductive short-circuited stub; the resonator has a length of  $2(l_1+l_2+l_3+l_4)$  and characteristic admittance  $Y_i$ , electrical length  $\theta_i = \beta L_i$ , while the short-circuited stub, acting as a perturbation, has a length of  $l_5 < \lambda_{g \text{ even}}/4$ . Since the ring resonator is symmetrical to the A-A' plane, the odd-even mode can be adopted to characterize it. In order to maintain the symmetry of the circuit, the stub is divided into two parts with the same characteristic admittance  $2Y_5$ .

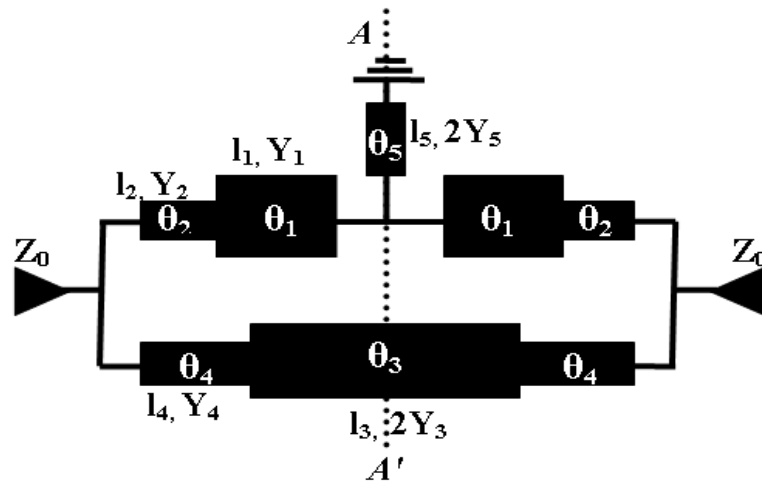


Fig. 6-1 Schematic layout of the proposed filter

For odd-mode excitation, there is a voltage null or short-circuited which is considered as a electric wall along the symmetry lane, the resulting input admittance for odd-mode can be expressed as

$$Y_{inodd} = Y_{upper,o} + Y_{lower,o} \quad (6.1)$$

$$Y_{upper,o} = Y_1 \frac{j(Y_2 \tan \theta_2 + Y_1 \tan \theta_1)}{Y_1 - Y_2 \tan \theta_1 \theta_2} \quad (6.2)$$

$$Y_{lower,o} = Y_3 \frac{j(Y_4 \tan \theta_4 + Y_3 \tan \theta_3)}{Y_3 - Y_4 \tan \theta_3 \theta_4} \quad (6.3)$$

According to the resonance condition  $Y_{in odd} = 0$ , there must be

$$Y_1 - Y_2 \tan \theta_1 \theta_2 = 0 \quad (6.4)$$

$$Y_3 - Y_4 \tan \theta_3 \theta_4 = 0 \quad (6.5)$$

From the formula (6.4) and (6.5), the total electrical lengths of  $\theta_{odd}$  can be deduced as

$$\theta_{odd} = \theta_{upper,o} + \theta_{lower,o} \quad (6.6)$$

$$\theta_{upper,o} = \theta_1 + \theta_2 = \arctan\left(\frac{R_{z1}}{\tan\theta_2}\right) + \theta_2 \quad (6.7)$$

$$\theta_{lower,o} = \theta_3 + \theta_4 = \arctan\left(\frac{R_{z2}}{\tan\theta_4}\right) + \theta_4 \quad (6.8)$$

where  $R_{z1} = Y_2/Y_1$  and  $R_{z2} = Y_4/Y_3$  are the impedance ratios in (6.7) and (6.8). Using (6.7), the relationship between the normalized total electrical length  $\theta_{odd}$  and  $\theta_2 = \pi - c/4f_{odd}\sqrt{\epsilon_{eff}}$  is plotted in Fig. 6-2, which shows that compact size may be obtained by having an appropriate and small impedance ratio  $R_z$ .

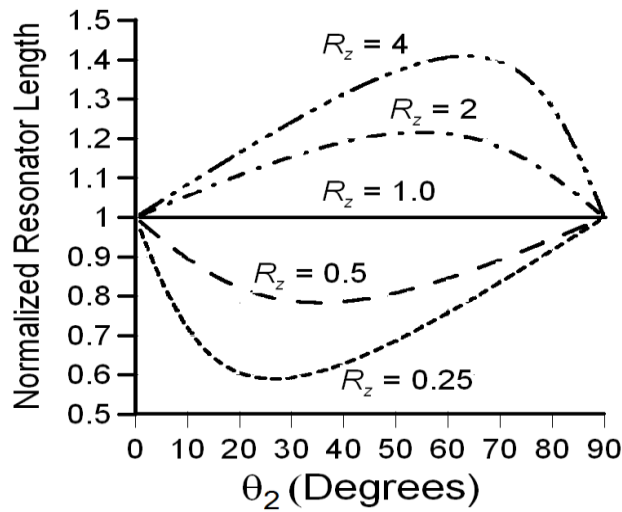


Fig. 6-2 The normalised resonator length against  $\theta_2$  for various impedance ratios  $R_z$  to visualize the effect of the stepped impedance on the length of the resonator.

The even-mode circuit is achieved by adding a magnetic wall along the symmetrical plane, therefore the even-mode input admittance can be deduced as

$$Y_{ineven} = Y_{upper,e} + Y_{lower,e} \quad (6.9)$$

$$Y_{upper,e} = jY_1 \tan\theta_1 + jY_2 \frac{Y_5 - 2Y_2 \tan\theta_2 \tan\theta_5}{Y_5 \tan\theta_2 + 2Y_2 \tan\theta_5} \quad (6.10)$$

$$Y_{lower,e} = jY_3 \left\{ \frac{2(Y_3 \tan \theta_3 + Y_4 \tan \theta_4)(Y_3 - Y_4 \tan \theta_3 \theta_4)}{Y_3(1 - \tan^2 \theta_3)(1 - \tan^2 \theta_4) - 2Y_4 \tan \theta_3 \theta_4 - 2Y_3 \tan \theta_3 \theta_4} \right\} \quad (6.11)$$

According to the resonance condition  $Y_{in\ even} = 0$ , there must be

$$Y_5 \tan \theta_2 + 2Y_2 \tan \theta_5 = 0 \quad (6.12)$$

$$Y_3(1 - \tan^2 \theta_3)(1 - \tan^2 \theta_4) - 2Y_4 \tan \theta_3 \theta_4 - 2Y_3 \tan \theta_3 \theta_4 = 0 \quad (6.13)$$

According to the formulas (6.12) and (6.13), the specific effect of the length  $l_5$  is investigated and the resonant-mode frequencies with varied  $l_5$ . As shown in Fig. 6-3, by changing the stub length  $l_5$  while keeping the other lengths are fixed, the fundamental even-mode resonant frequency can be shifted within a wide range, whereas the fundamental resonant frequency is preserved.

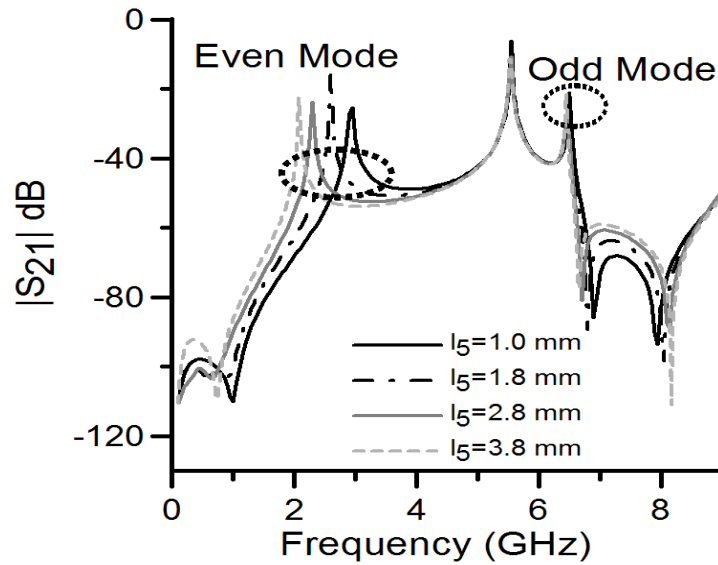


Fig. 6-3 Simulated values of the degenerate modes' frequencies against the length of  $l_5$  when  $(l_1 + l_2 + l_3 + l_4)$  are fixed

By solving the equations (6.4)-(6.5) and (6.12)-(6.13), the fundamental resonant frequency can be determined as follows:

$$f_{odd} = \frac{c}{4(l_1 + l_2 + l_3 + l_4)\sqrt{\epsilon_{eff}}}$$

$$f_{even} = \frac{c}{4(l_1 + l_2 + l_3 + l_4 + 2l_5)\sqrt{\epsilon_{eff}}} \quad (6.14)$$

where  $\beta L_i = \theta_i$  ( $i=1,2,3,4,5$ ) and  $\beta$  is the propagation constant.

In order to produce transmission zeros at desired frequencies to improve filter selectivity, two techniques have been adopted, firstly, to sharpen the first passband band out-of-band rejection skirt, the shunt stubs  $2(l_6)$  are stretched as illustrates in Fig. 6-4 , i.e., from  $\lambda_g/4$  to  $2\lambda_g/4$  which turns the section from short to open-circuited stub which contributes two attenuation poles on each side of the passband. The electrical length  $\lambda_g/2$  have been calculated at a centre frequency of 4.9 GHz. Various design approaches for selectivity improvement have been discussed in [20], from which one appropriate half-wavelength open-circuited stubs topology has been chosen to design the proposed stub characteristics admittances denoted by  $Y_{ia}$ ,  $Y_{ib}$ . The design equations for determining these characteristic admittances are given by,

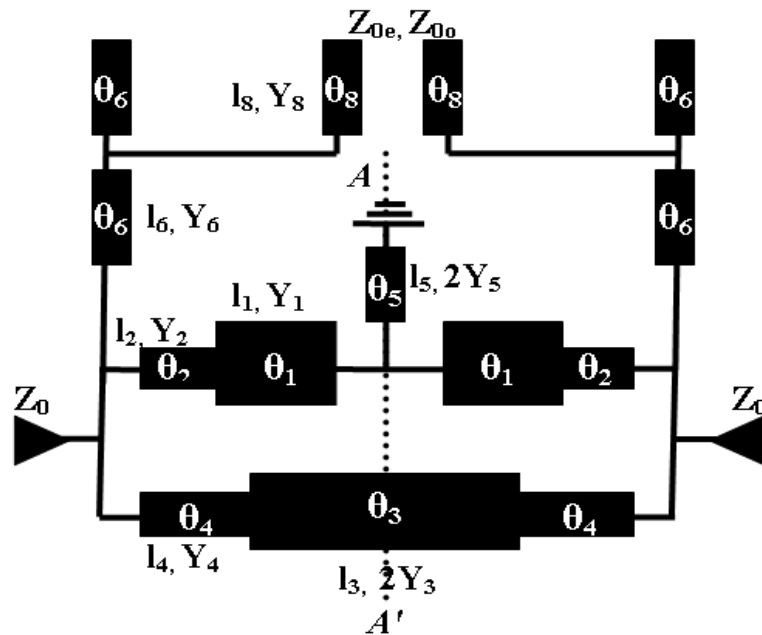


Fig. 6-4 Schematic layout with open stubs and source-load coupling

A shunt  $\lambda_g/2$ , open-circuited stub having an inner  $\lambda_g/4$  portion with a characteristic admittance can be written from [20]

$$Y_{ia} = \frac{Y_i(\alpha_i \tan^2 \theta_6 - 1)}{(\alpha_i + 1) \tan^2 \theta_6} \quad (6.15)$$

where  $Y_i$  is described in [20] and  $\theta$  has been defined by,

$$\theta_6 = \frac{\pi}{2} \left( 1 - \frac{FBW}{2} \right) \quad (6.16)$$

and an outer  $\lambda_g/4$  portion characteristic admittance can be defined by

$$Y_{ib} = \alpha_i Y_{ba} \quad (6.17)$$

where the parameter  $\alpha_i$  is given by,

$$\alpha_i = \cot^2 \left( \frac{\pi f_{zi}}{2 f_0} \right) \quad \text{for } f_{zi} < f_1 \quad (6.18)$$

where  $f_1$  is the low band-edge frequency of the passband, and  $f_{zi}$  is a frequency at which the shunt open-circuited stub presents a short circuit to the main transmission line and causes a transmission zero.

Furthermore, secondly, a cross coupling between the I/O feedlines has been introduced by placing a section of U-shaped ( $l_g$ ) transmission line to improve the selectivity of the second passband as shown in Fig. 6-4 on the two shunt open-circuited stub  $\theta_g$ . For the case where there is no capacitive coupling between two extensions means the gap is large, the transmission zero simply occurs at the frequency where  $\theta_g = 90^\circ$ . However, when there is a coupling between the two sections, the transmission zero will split. The even-mode zero condition is still  $\theta_g = 90^\circ$  and the odd-mode zero condition may be approximately summarised as

$$\tan \theta_{g_{odd}} = \frac{1}{4 \pi f_{zero} C_0 Z_g} \quad (6.19)$$

where  $C_0$  is the capacitance associated with the gap. To realise zero in lower stopband, the line length  $\theta_g$  keeps slight longer. For our discussion, we may define a source-load coupling as

$$k = \frac{Z_{0e} - Z_{0o}}{Z_{0e} + Z_{0o}} \quad (6.20)$$

## 6.2 Dual Band Inverter

Dual band filters require dual band resonators to create two different passbands and a separate coupling structure or inverter between resonators is needed to establish the bandwidth for each band. This arrangement increases the circuit size and combines additional networks. To overcome this issue, a single dual band inverter comprises of two open stubs is proposed, which can be easily merged with adjacent resonators to reduce the

circuit size and provided coupling supports to both passband without any adjustments. The design procedure of dual band inverter is then follow the classical synthesis rules.

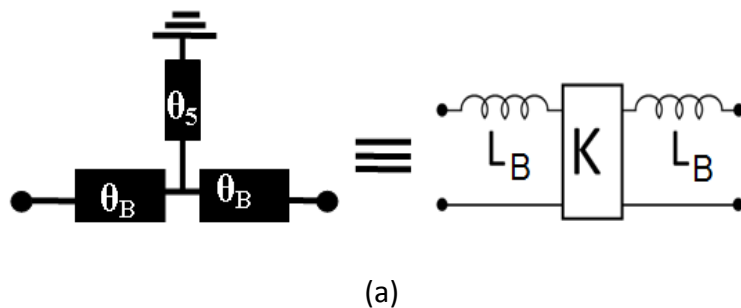
Therefore, a simple quarter-wavelength transmission line or inductively loaded short-circuited stub is used as a inverter. To investigate further, the ABCD parameters, given by (6.21), of the mid-section of the resonator, illustrated in Fig. 6-5(a), may be equated to that of its lumped equivalent network from where it is possible to define the model parameters  $K$  and  $L_B$  as (6.22) and (6.23). Since the model assumes frequency invariance of its parameters, an exact match may only be expected at the centre frequency of the resonator.

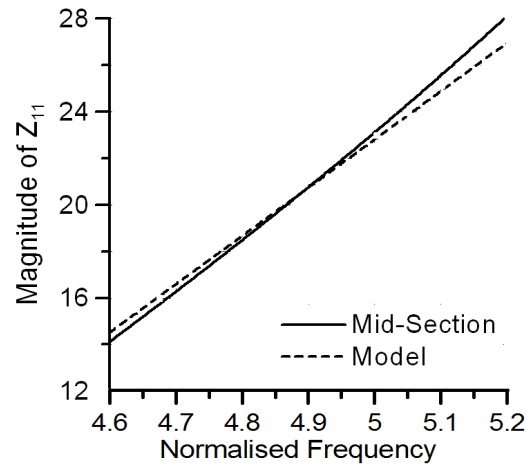
The ABCD matrix of the impedance inverter as shown in Fig. 6-5(a) is obtained as

$$\begin{aligned} \begin{bmatrix} A & B \\ C & D \end{bmatrix} &= \begin{bmatrix} \cos(\theta_B) & jZ_B \sin\theta_B \\ j\frac{\sin\theta_B}{Z_B} & \cos\theta_B \end{bmatrix} \begin{bmatrix} 1 & 0 \\ -\frac{j \cot\theta_5}{Z_5} & 1 \end{bmatrix} \begin{bmatrix} \cos(\theta_B) & jZ_B \sin\theta_B \\ j\frac{\sin\theta_B}{Z_B} & \cos\theta_B \end{bmatrix} \\ &= \begin{bmatrix} \cos(2\theta_B) + \frac{Z_B}{2Z_5} \sin(2\theta_B) \cot(\theta_5) & j(Z_B \sin(2\theta_B) + \frac{[Z_B \sin(\theta_B)]^2}{Z_5} \cot(\theta_5)) \\ j\left(\frac{\sin(2\theta_B)}{Z_B} - \frac{\cos^2(\theta_B) \cot(\theta_5)}{Z_5}\right) & \cos(2\theta_B) + \frac{Z_B}{2Z_5} \sin(2\theta_B) \cot(\theta_5) \end{bmatrix} \end{aligned} \quad (6.21)$$

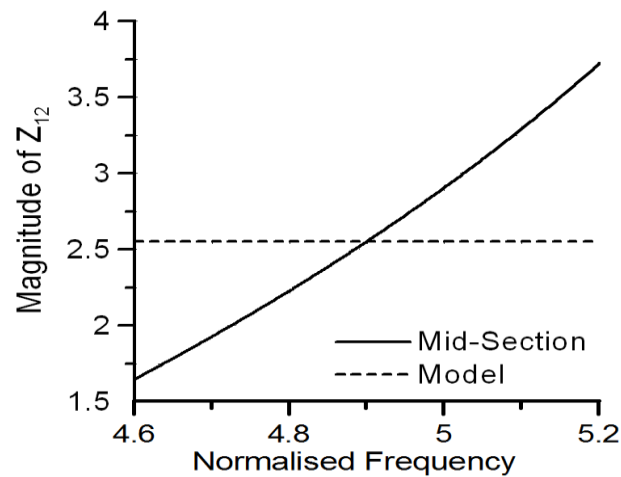
$$K = \frac{1}{jC}; \quad (6.22)$$

$$L_B = \frac{KA}{\omega_0}; \quad (6.23)$$





(b)



(c)

Fig. 6-5 (a) Model of resonator mid-section and equivalent lumped element circuit of direct-coupled dual-mode resonator, (b) Comparison of driving point impedance of direct coupled dual-mode resonator mid-section and that of equivalent circuit (c) transfer impedance of direct coupled dual-mode resonator mid-section and that of equivalent circuit.

Fig. 6-5(b)-(c) plot the impedance parameters where  $Z_B = Z_5 = 80\Omega$ ,  $\theta_B = 21^\circ$ ,  $\theta_5 = 14.8^\circ$ . The corresponding model parameters were calculated to be  $L_B = 2.98$  nH and  $K = 2.32$  at the centre frequency. There is a reasonably good agreement in the driving point impedances over a wide frequency range from which it may be deduced that the frequency dependence of  $L_B$  is fairly small. The relatively strong frequency dependence of the transfer impedance, which is equivalent to the inverter impedance,  $K$ , is clearly evident.

However, it is understood from the investigation that the aforementioned inverter only suitable for single band filter designs. In order to transmission line act as a dual-band inverter, additional open stub can be attached to both ends of the transmission line, as shown in Fig. 6-6. The proposed dual-band impedance inverter as in Fig. 6-6 consists of open stub and a transmission line loaded with short-circuited stub which acts as K-inverter. The corresponding electrical lengths which are defined at frequency  $f_{lower}$  can be summarised as follows:

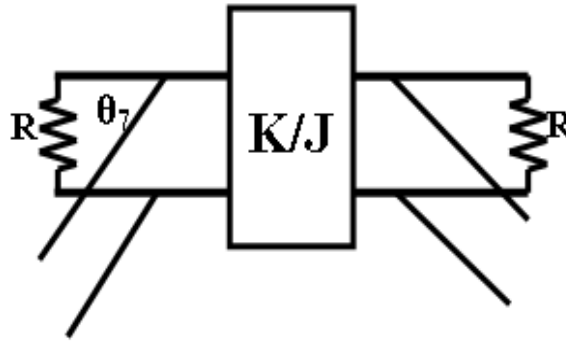


Fig. 6-6 Dual-band resonator with open-circuited stub

The total ABCD matrix of the proposed impedance inverter as shown in Fig. 6-6 is obtained as

$$A = D = \cos(2\theta_B) + \frac{Z_B}{2Z_5} \sin(2\theta_B) \cot(\theta_5) \quad (6.24)$$

$$B = \cos(2\theta_B) + \frac{Z_B}{2Z_5} \sin(2\theta_B) \cot(\theta_5) \cdot \frac{j \tan \theta_{ia}}{Z_{ia}} + j \left( \frac{\sin(2\theta_B)}{Z_B} - \frac{\cos^2(\theta_B) \cot(\theta_5)}{Z_5} \right) \quad (6.25)$$

$$C = j(Z_B \sin(2\theta_B) + \frac{[Z_B \sin(\theta_B)]^2}{Z_5} \cot(\theta_5)) \quad (6.26)$$

The ABCD matrix of the idle impedance inverter can be deduced as

$$\begin{bmatrix} A & B \\ C & D \end{bmatrix} = \begin{bmatrix} 0 & jK \\ 1/jK & 0 \end{bmatrix} \quad (6.27)$$

For dual-band admittance, the same value of  $K$  and phase shift  $90^\circ$  should be given and evaluated at two operating frequencies ( $f_{\text{lower}}$  and  $f_{\text{upper}}$ ). The simultaneous equations for solving the parameters of dual-band inverter are written by equating ABCD parameters of (6.24)-(6.26) and (6.27) to satisfy two frequency bands,

$$\cos(2a\theta_B) + \frac{Z_B}{2Z_5} \sin(2a\theta_B) \cot(a\theta_5) = 0 \quad (6.28)$$

$$\cos(2a\theta_B) + \frac{Z_B}{2Z_5} \sin(2a\theta_B) \cot(a\theta_5) \cdot \frac{\tan a\theta_7}{Z_7} + \left( \frac{\sin(2a\theta_B)}{Z_B} - \frac{\cos^2(a\theta_B) \cot(a\theta_5)}{Z_5} \right) = K \quad (6.29)$$

$$(Z_B \sin(2a\theta_B) + \frac{[Z_B \sin(a\theta_B)]^2}{Z_5} \cot(a\theta_5)) = \frac{1}{K} \quad (6.30)$$

where  $a$  is the frequency ratio ( $f_{\text{upper}}/f_{\text{lower}}$ ) between two frequency bands.

The slope parameter can be deduced as

$$x_i = R_i \frac{g_0 g_1}{\Delta_i} \quad (6.31)$$

where  $\Delta_i$  is the relative bandwidth and  $R_i$  is the termination resistance. By solving the equations (6.28)-(6.30) and (6.31), the solutions can be found for the dual-band impedance inverter as well as the electrical length and characteristic impedance of the open stubs along with the inverter.

## 6.3 Design Procedure of the Reconfigurable Dual Wideband BPF

The design procedure in section 6.1 and 6.2 is then apply to reconfigurable dual-band filter in section 6.3. The proposed ring resonator generate two signal paths where the lower path consists of a ring resonator and two open shunt stubs  $2(l_6)$  as in Fig. 6-1(a), and the upper path is composed of  $2(l_1 + l_7)$ , while the short-circuited stub and  $l_1$  section is common to both passband paths.

For the given filter specifications, the general design procedure can be summarised as follows:

- a) According to the given centre frequency and bandwidth, determine the total length  $2(l_1 + l_2 + l_3 + l_4)$  of the ring resonator by (6.6). Tune the length  $l_5$  of the short-circuited stub to meet the desired bandwidth from Fig. 6-3.
- b) After determining the impedance ratio  $R_z$ , the electrical length of SIRs can be derived from Fig. 6-2.
- c) Use the equations (6.15)-(6.16), to determine the characteristics impedance and the electrical length of the open stub  $2(l_6)$  in order to obtain transmission zeros between first passband edges.
- d) By using the formula (6.28), the electrical length of the resonator ( $l_7$ ) can be derived and the impedance ratio between  $l_1$  and  $l_7$  is determined from Fig. 6-2.
- e) Solution can be found for the dual-band inverter from the equation (6.29)-(6.30) and (6.31).
- f) To improve selectivity between second passband edges, the proposed source-load coupling line length  $l_8$  can be derived by (6.19) and the coupling value from (6.20).

### 6.3.1 Reconfigurable Lower Passband

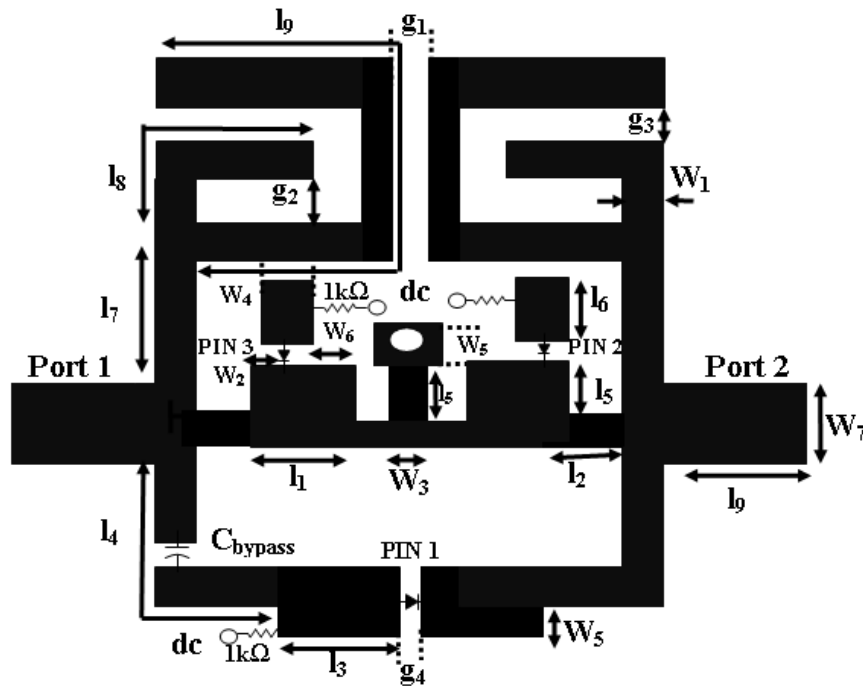
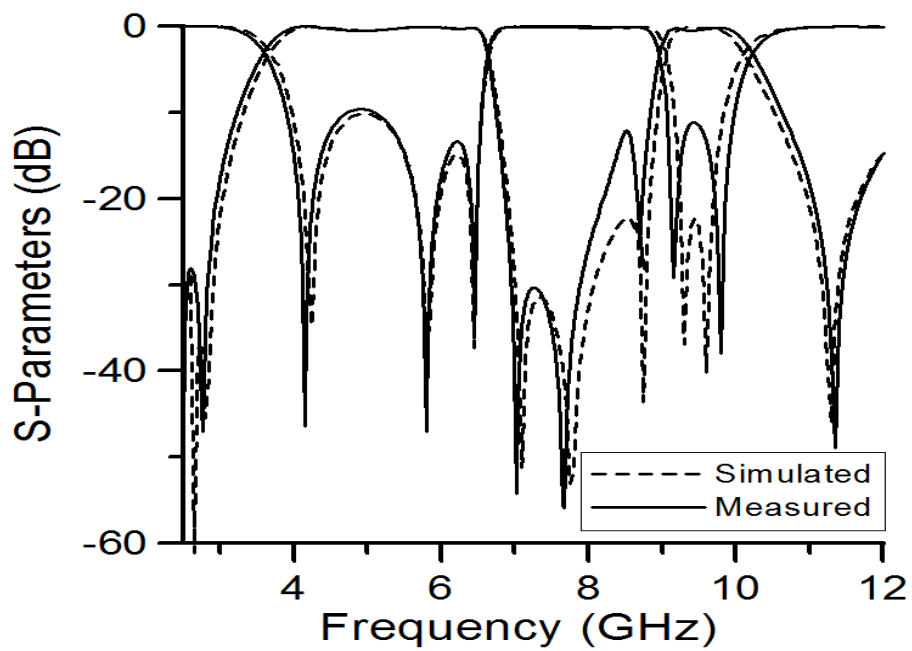


Fig. 6-7 Layout of the proposed dual-wideband bandpass filter with a reconfigurable frequency states [ $l_1=1.5$ ,  $l_2=1.5$ ,  $l_3=2.1$ ,  $l_4=3.6$ ,  $l_5=2.8$ ,  $l_6=6.4$ ,  $l_7=2.3$ ,  $l_8=2.9$ ,  $l_9=5$ ,  $l_{10}=0.1$ ,  $W_1=0.9$ ,  $W_2=1.4$ ,  $W_3=0.4$ ,  $W_4=1.0$ ,  $W_5=1.1$ ,  $W_6=0.5$ ,  $W_7=1.6$ ,  $g_1=0.4$ ,  $g_2=0.6$ ,  $g_3=0.5$ ,  $g_4=0.5$ , and via diameter = 0.7,  $C_{bypass}=33$  pF (Unit:mm)]

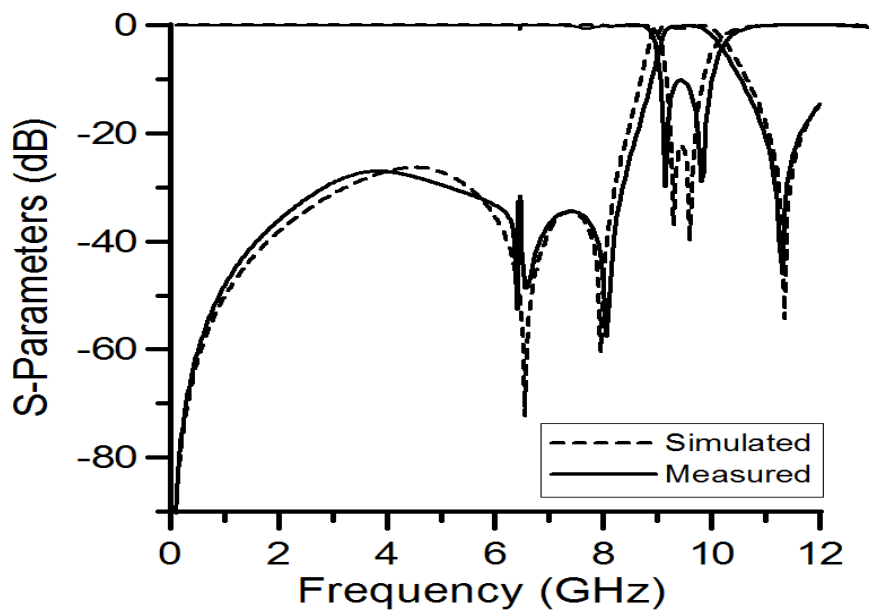
In this section, a novel structure to implement dual-wideband behaviour is proposed, where two signal paths are created within the same filter ring resonator to achieve independently switched frequency states of both passbands. One path delivers only the signals at the upper passband and the other path transfers the signals at the lower passband frequency. By turning the PIN diodes state on and off, frequency can be reconfigured into four states.

The schematic layout of the final filter is presented in Fig. 6-7. The proposed lower passband was designed to operate between frequencies from 3.2 GHz to 6.6 GHz with centre frequency 4.9 GHz and the fractional bandwidth 70%. To realize reconfigurability, a PIN diode PIN1 is placed between the gap of  $l_4$  as shown in Fig. 6-7. A bypass capacitor  $C_{bypass}$  is used to avoid a short circuit for the dc bias applied to the pin diode. In the forward bias or on state, the pin diode behaves like a small resistance so that the section  $l_4$  creates a path ( $l_1 + l_2 + l_3 + l_4$ ) to propagate the transmission signal; thus generating a passband with 4.9 GHz

centre frequency as illustrated in Fig 6-8(a). Also passband location can be controlled by varying the section  $l_5$  position as illustrated in Fig. 6-3. This state corresponds to the lower passband "ON". Conversely, in the zero bias or off state, the pathway is broken and the structure  $l_3 + l_4$  acts as an open-circuited stub and creates a transmission zero at around 6.7 GHz which helps to suppress the lower passband during "OFF" time as shown in Fig. 6-8(b). This response corresponds to the channel "OFF".



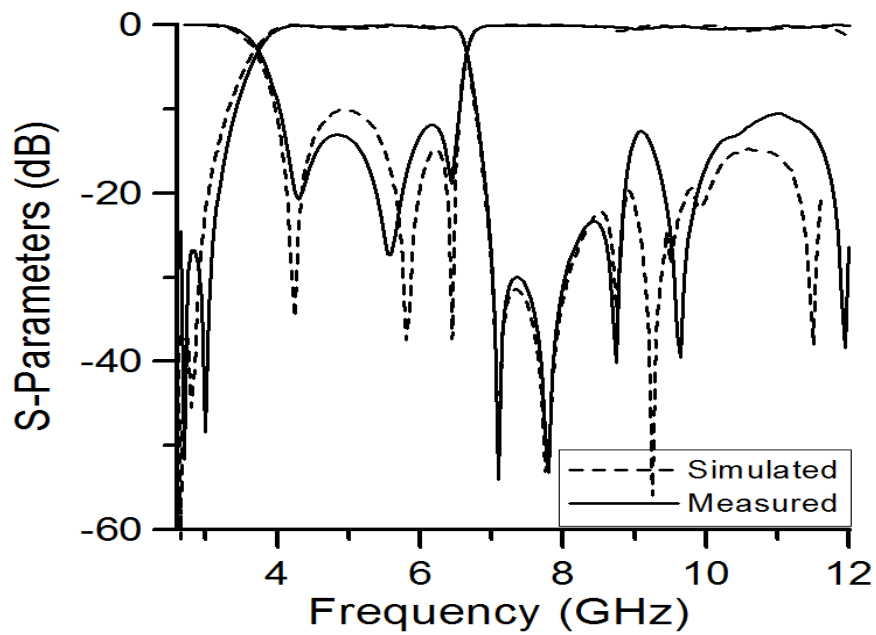
(a)



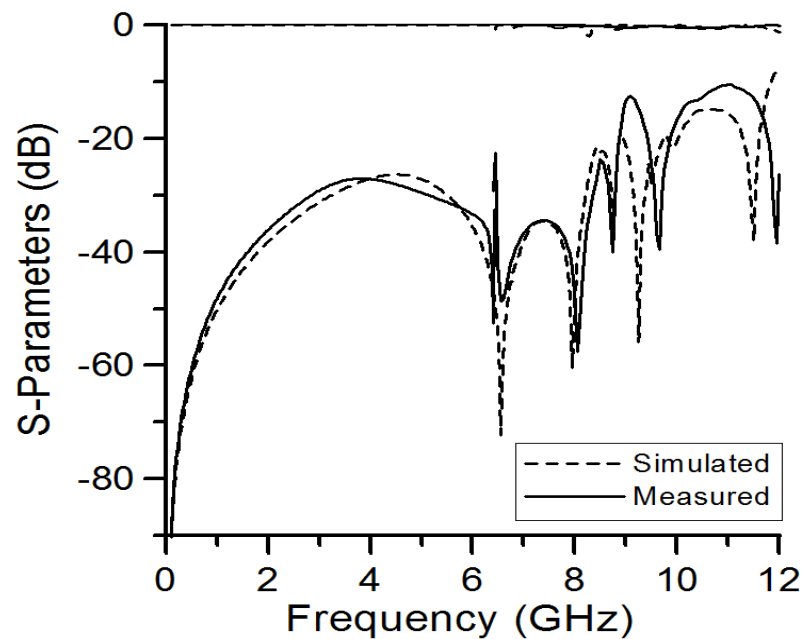
(b)

Fig. 6-8 Simulated and measured response of the fabricated filter with the pin switch (a) Both Channels are on with at centre frequency at 4.9 and 9.6 GHz in the PIN1 ON state and PIN2 ON state [STATE-1], (b) One Channels is on at centre frequency at 9.6 and one is off at 4.9 GHz in the PIN1 OFF state and PIN2 ON state [STATE-2]

### 6.3.2 Reconfigurable Upper Passband



(a)



(b)

Fig. 6-9 Simulated and measured response of the fabricated filter with the pin switch (a) One Channels is on at centre frequency at 4.9 and one is off at 9.6 GHz in the PIN1 ON state and PIN2 OFF state [STATE-3], (b) Both Channels are off with at centre frequency at 4.9 and 9.6 GHz in the PIN1 OFF state and PIN2 OFF state [STATE-4].

The proposed upper passband was designed to operate between frequencies from 8.9 GHz to 10.3 GHz with centre frequency 9.6 GHz and the fractional bandwidth 14.5%. The proposed section consists of  $2(l_5 + l_6)$  and it has been found from (6.28) that the specific length is required to generate the upper passband. The stepped impedance based resonator is used to achieve the compactness. To realize the switchability, PIN2 and PIN3 diode is placed between the gap of  $l_5$  and  $l_6$  as shown above in Fig. 6-7, which control the line length for upper passband without effecting the lower passband. The design procedure of (d)-(e) have been used to calculate the proposed structure and the parameter details are:  $\theta_7 = 20.29^\circ$ ,  $\theta_8 = 89.1^\circ$ ,  $Z_7 = 62.04\Omega$ ,  $Z_8 = 68\Omega$  with  $R_2 > 1$ , the coupling co-efficient  $k$  is 0.053 under  $Z_{0e} = 85.2\Omega$ ,  $Z_{0o} = 68.2\Omega$  and the calculated slope parameter of the open resonator is 0.0471 mhos.

The filter is designed and fabricated on Taconic RF35 substrate with  $\epsilon_r = 3.5$  and  $h = 0.76$  mm. This dual-wideband band filter is designed to have a 3-dB passband from 3.2–6.6 GHz with a mid-band frequency of 4.9 GHz and 8.9–10.3 GHz at 9.6 GHz mid-band frequency. The overall filter dimension is approximately  $0.14\lambda_g \times 0.12\lambda_g$  (excluding the two 50  $\Omega$  feed lines), where  $\lambda_g$  is the microstrip guided wavelength on the substrate at centre frequency. The filter is optimised by EM Sonnet software and the corresponding measurements are taken with Agilent vector network analyzer E38361A. In this experiment, the PIN diode (NXP BAP65-02) used in this experiment has a capacitance of 0.8 pF, a parasitic inductance 0.7 nH, and a low resistance of 0.9  $\Omega$  [21]. To turn on the diodes, the external dc voltage is 3V, and the current is 1mA. The dc blocking capacitance is 33 pF and the resistor 1k $\Omega$  is used for biasing.

In Fig. 6-8 and 6-9, the simulated and measured  $|S_{21}|$  and  $|S_{11}|$  under the PIN diode ON and OFF states are demonstrated, respectively. It can be seen that the proposed filter can operate at 4.9 GHz and 9.6 GHz, and the measured FBWs are 68% in the lower passband and

13% in the upper passband. Table I listed the insertion loss (IL) at different states, while the measured return loss is greater than 12 dB in most cases. Furthermore, the skirt selectivity remains almost unchanged, which is crucial to eliminate undesired interferences. The photograph of the proposed filter is shown in Fig. 6-10. The small discrepancies between the simulated and measured responses may be attributed to the various fabrication errors involved. The design procedure especially the circuit model is simulated by employing a MATLAB software, which allowed all of the filter parameters to be determined relatively quickly given the prototype element values.

**Table I** Insertion loss for various states of the proposed BPF

4.9 GHz/9.6 GHz	4.9 GHz ON	4.9 GHz OFF
9.6 GHz ON	1.2 dB/ 1.1 dB	28 dB/ 1.1 dB
9.6 GHz OFF	1.2 dB/ 16.5 dB	19 dB/ 15 dB

**Table II** Comparison of various Reconfigurable BPFs

Ref.	No. of Zeros	Isolation ratio between passbands ( $f_2/f_1$ )	Frequency response & Switch	Size (mm)
[22]	Two	2	Four-state & 04	60.84 × 75.45 ( $\epsilon_r$ : 3.55)
[23]	None	2.4	Four-state & 02	78 × 5.7 ( $\epsilon_r$ : 3.38)
[24]	One	1.94	Two-state & 02	30 × 30 ( $\epsilon_r$ : 2.65)
This work	Six	1.96	Four-state & 03	8.5 × 7.1 ( $\epsilon_r$ : 3.5)

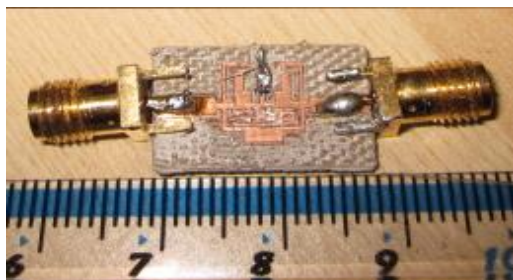


Fig. 6-10 Photograph of the fabricated filter

### 6.3.3 Summary

This section presented a novel, compact, and highly selective reconfigurable bandpass filter (BPF) with four-state frequency responses, where dual-band bandpass and single bandpass characteristics can be conveniently switched by turning PIN diodes on and off. The proposed design uses stepped impedance resonator (SIR) for realization of bandpass filter (BPF) and employs a short-circuited stub to obtain dual-mode performance and control passband bandwidths. Simple filter design techniques are derived using conventional synthesis method and the methods of generating transmission zeros are discussed to improve passband selectivity. A dual-band inverter is adopted which can be merged with adjacent resonators without increasing circuit size. To illustrate the concept, filter samples are designed, fabricated and measured. Measurements on a fabricated reconfigurable filter confirm the accuracy of the design procedure. Measured responses show good agreement with simulation. The proposed filter is able to achieve significant size reduction (8.5 mm × 7.1 mm excluding the feeding ports) as compared to the conventional dual-band filters and bandpass filters with switchable bandwidth.

## 6.4 References

- [6-1] Wong, P.W., and Hunter, I.C., "Electronically reconfigurable microwave bandpass filter", IEEE Trans. Microw. Theory Tech., vol. 57, no. 12, pp. 3070–3079, Dec. 2009.
- [6-2] Tu, W.-H., "Swiathable microstrip bandpass filters with reconfigurable onstate frequency responses", IEEE Microw. Wirel. Compon. Lett., vol. 20, no. 4, pp. 208–210, May 2010.
- [6-3] Tsai, L. C., Hsue, C. W., "Dual-band bandpass filters using equallength coupled-serial-shunted lines and Z-transform technique," IEEE Trans. Microw. Theory Tech., vol. 52, no. 4, pp. 1111 -1117, Apr. 2004
- [6-4] Miyake, H., Kitazawa, S., Ishizakt, T., Yanada, T., Nagatomi, Y, "A miniaturized monolithic dual band filter using ceramic lamination technique for dual mode portable telephones", IEEE MTT-S International Symposium Digest., pp.789-792, Jun. 1997.
- [6-5] Wu, B., Liang, C.H., Qin, P.Y., Li, Q, "Compact dual-band filter using defected stepped impedance resonator," IEEE Microw. Wireless Compon. Lett., vol. 18, no. 10, pp. 674-676, Oct. 2008
- [6-6] Weng, M. H., Huang, C. Y., Wu, H. W., Shu, K., Su, Y. K., "Compact dual-band bandpass filter with enhanced feed coupling structures", Microw. Optical Technol. Lett., vol. 49, no. 1, pp. 171–173, Nov. 2007.
- [6-7] Chu, Q.X., Chen, F.C., "A compact dual-band bandpass filter using meandering stepped impedance resonators," IEEE Microw. Wireless Compon. Lett, vol. 18, no. 5, pp. 320-3220, May 2008.
- [6-8] Chang, Y.C., Kao, C.H., Weng, M.H., Yang, R.Y. , "Design of the compact dual-band bandpass filter with high isolation for GPS/WLAN applications," IEEE Microw. Wireless Compon. Lett., vol. 19, no. 12, pp. 780-782, Dec. 2009.

- [6-9] Zhou, M.Q., Tang, X.H., Xiao, F., "Compact dual band bandpass filter using novel E-type resonators with controllable bandwidths," *IEEE Microw. Wireless Compon. Lett.*, vol. 18, no. 12, pp. 779-781, Dec. 2008.
- [6-10] Zhang, X.Y., Shi, J., Chen, J. X., Xue, Q., "Dual-band bandpass filter design using a novel feed scheme," *IEEE Microw. Wireless Compon. Lett.*, vol. 19, no. 6, pp. 350-352, Jun. 2009.
- [6-11] Chen, C. Y., Hsu, C. Y., Chuang, H. R., "Design of miniature planar dual-band filter using dual-feeding structures and embedded resonators," *IEEE Microw. Wireless Compon. Lett.*, vol. 16, no. 12, pp. 669-671, Dec. 2006.
- [6-12] Luo, X., Qian, H. Z., Ma, J. G., Ma, K. X., Yeo, K. S. , "Compact dual-band bandpass filters using novel embedded spiral resonator (ESR)," *IEEE Microw. Wireless Compon. Lett.*, vol. 20, no. 8, pp. 435-437, Aug. 2010.
- [6-13] X. Y. Zhang and Q. Xue, "Novel centrally loaded resonators and their applications to bandpass filters," *IEEE Trans. Microw. Theory Tech.*, vol. 56, no. 4, pp. 913–921, Apr. 2008.
- [6-14] X. Y. Zhang and Q. Xue, "High-selectivity tunable bandpass filters with harmonic suppression," *IEEE Trans. Microw. Theory Tech.*, vol. 58, no. 4, pp. 964–969, Apr. 2010.
- [6-15] Y.-S. Lin, P.-Y. Chang, and Y.-S. Hsieh, "Compact electronically switchable parallel-coupled microstrip bandpass filter with wide stopband," *IEEE Microw. Wireless Compon. Lett.*, vol. 18, no. 4, pp. 254–256, Apr. 2008.
- [6-16] J. Lee and K. Sarabandi, "An analytic design method for microstrip tunable filters," *IEEE Trans. Microw. Theory Tech.*, vol. 56, no. 7, pp.1699–1706, Jul. 2008.
- [6-17] S. F. Chao, C. H. Wu, Z. M. Tsai, H. Wang, and C. H. Chen, "Electronically switchable bandpass filters using loaded stepped-impedance resonators," *IEEE Trans. Microw. Theory Tech.*, vol. 54, no. 12, pp. 4193–4201, Dec. 2006.

[6-18] Dai G.L., Xia M.Y., "Design of compact dual-band switchable bandpass filter", *Electron. Lett.*, vol. 45, no. 10, pp. 506–507, May 2009.

[6-19] Mahe F., Tanne G., Rius E., Et AL., "Electronically switchable dual-band microstrip interdigital bandpass filter for multi standard communication applications," *European Microwave Conf.*, pp. 1-4, Oct. 2000.

[6-20] J.-S. Hong and M. J. Lancaster, *Microstrip Filters for RF/Microwave Applications*, 1st ed. New York: Wiley, Ch. 5–6, 2001.

[6-21] [http://www.nxp.com/documents/data\\_sheet/BAP65-02.pdf](http://www.nxp.com/documents/data_sheet/BAP65-02.pdf) (2013)

[6-22] Pu-Hua Deng and Jyun-Hao Jheng, "A Switched Reconfigurable High-Isolation Dual-Band Bandpass Filter," *IEEE Microw. Wireless Compon. Lett.*, VOL. 21, NO. 2, pp. 71-73, Feb. 2011.

[6-23] W.-H. Tu, "Design of switchable dual-band bandpass filters with four states", *IET Microw. Antennas Propag.*, Vol. 4, Iss. 12, pp. 2234–2239, Mar. 2010.

[6-24] B. Lui, F. Wei and X. Shi., "Switchable bandpass filter with two-state frequency responses", *Electronics Lett.*, Vol. 47, No. 1, pp. 506–507, Jan. 2011.

---

## 7.0 CONCLUSIONS AND FUTURE WORK

---

Planar filters are extensively employed in various wireless and radar applications. The increasing growth and commercial interest in communication sectors escalate significantly the demand for low cost, compact size and high performance multifunctional filters as filters play a key role in confined signals. An overview of reconfigurable filters using different techniques was discussed in the earlier section where it was apparent that there was a need to develop reconfigurable wideband filters with frequency and bandwidth control. The basic aim of this research report is the development of miniaturised reconfigurable filters for UWB applications. The investigation focuses on several key challenges pertaining to microwave filters such as compactness, selectivity, in-band rejection, stopband rejection with deep attenuation, and switchability with the proposal of a novel compact stub-type resonator configuration.

In this dissertation, the miniaturised square ring shape close and open loop resonators were analysed and equivalent circuits for their behaviour were proposed. A convenient design procedure was discussed in order to congregate deeper insight into the relationship between the physical and electrical parameters. Application of these resonators in filter design was implemented in four stages. Firstly, for ultra-wideband filters application, the proposed structure was modelled where the bandwidth can be controlled through the grounded shunt stubs impedance. An open-circuited stub was placed in the symmetry plane of the resonator in order to achieve bandstop characteristics and the feasibility of an optical switch as an alternate of common PIN diodes had been observed. The development of a complete filter design procedure include lowpass prototype networks to the realization of distributed filter parameters, was also explained.

Secondly, in order to increase the filter selectivity, an effective design procedure to generate a pair of transmission zeros between passband edges was introduced and a section was built

within the proposed filter resonator through which wide stopband can be attained by suppressing the second harmonic. Next, implementation of reconfigurable notched rejection band in the propose filter passband was investigated. Hence, several novel design techniques to create single and multiple notched bands in the miniaturised UWB filter using square ring shape structure were suggested.

Thirdly, a novel highly compact planar dual-mode resonator configuration for UWB applications was developed. With the aid of dual mode feature, bandwidth reconfiguring technique was demonstrated and an analysis of the dual-mode structure was presented in order to prove the existence of two unique modes of resonance. Also, a comprehensive design technique to create multiple transmission zeros in the lower and upper stopband was developed. Later, a unique coplanar waveguide (CPW) fed reconfigurable filter circuit was constructed as a substitute of direct coupled feeding line and discussions were supplemented with experimental results.

Finally, the investigation extended to constructing a novel structure in order to implement dual wideband behaviour by using a single ring resonator. A detail analysis with design procedure was outlined and a solution was presented for controlling frequency bandwidths independently according to the application interest. Simulation and experimental results were presented to validate the arguments.

## 7.1 Research Contributions

The contributions of the research are summarised as follows:

1. A novel compact reconfigurable filters using ring-shape stub types resonator is presented for UWB applications. The proposed resonator is extensively analysed to extract the design parameters and characterized reconfiguring behaviour by employing an open-circuited section leading to a gap, which is overlaid with switches. An electromagnetic interference free optical switch performances have been shown as a candidate for future generation. Also, a technique is developed to eliminate the unwanted frequency via

externally coupled T-shape structure and a solution is provided to minimise the circuit area by embedding the proposed structure into inner circuit area.

2. A new highly selective filter with multifunctional capabilities is demonstrated for future wireless communication sectors. A technique is introduced by which pairs of transmission zeros can be generated between passband edges and a harmonic suppression method is produced without enlarging the circuit size. Also, a novel approach is proposed for in-band rejection along with several other single and multi-notched band techniques using the proposed resonator have been investigated to find an optimum solutions.

3. A novel highly compact dual-mode ring resonator configuration is explored for the design of planar RF and microwave bandpass filters. The structure based on stepped impedance resonator (SIR) is characterised and the existence of two unique modes of resonance is substantiated. A design approach using dual mode feature is constructed for microwave bandpass filter with bandwidth reconfigurability. The presented approach is attained relatively wide tuning range with low in-band insertion loss and without effecting the filter selectivity while the fractional bandwidth varies. Furthermore, a very compact ring shape resonator employing CPW-fed technology has been shown as a substitute of conventional direct feeding structure.

4. A novel super compact prototype is designed to implement the dual band characteristics using single ring resonator. A comprehensive filter design procedure is outlined to expedite the development process. A dual band inverter is superimposed within the resonator without effecting the filter response and an innovative independently controlled frequency bandwidth approach is presented.

## 7.2 Future Work

A lot of the sections in this research report contributes rise to further work. Even though many features of this resonator were examined within the given time frame, still several

interesting issues have not been solved and can be the basis for future investigations. These are outlined in the following:

- In this report stub-type resonators were employed in design of wideband bandwidth bandpass filters. The stub bandpass filter characteristic depend on the characteristic admittance and impedance of the shunt stubs and connecting line. Hence, it may be a challenge in realising a filter with narrow bandwidth due to its unrealistically low stub admittance requirement.
- The thesis focused on the development of bandpass filters where the input and output couplings where exclusively achieved through direct inductively coupled lines. But, investigations on orthogonal or parallel feed coupling of the resonator may be performed to assess the practicability of employing these resonators in wideband filter design. Also, the proposed design procedures and equivalent circuits are approximated mostly for wideband structure. A simplified transmission line structures can be extrapolated instead be used.
- In the proposed ring resonator, the dual mode characteristic is realised through the grounded middle stub and the bandwidth reconfigurability has been observed by varying the coupling coefficient induced by shorted stub. However, this coupling variation is only applicable to wideband filters design. As a result, a new inverter coupling scheme could be introduced to obtain narrow and broad bandwidth according to applications interest.
- The proposed filter structure are constructed mostly with single layer, which incorporates restriction in miniaturisation as the size of a distributed filter is directly proportional its operating wavelength. To achieve further compactness, multi-layer design configurations would be a good choice. However, multi-layer structure has different inter-resonator coupling mechanisms so that the relation must be conceived prior to dealing with that.
- The materials used in the filter design presented in this dissertation are Rogers 5880 and Taconic RF-35, which are considered as a lossy material. Therefore, filter performances can be further improved by utilising expensive less loss materials.